Contents

Bulletin KRASEC. Phys. & Math. Sci, 2014, vol. , no. 2, pp. 3-12. ISSN 2313-0156

MSC 35M10

ABOUT A METHOD OF RESEARCH OF THE NON-LOCAL PROBLEM FOR THE LOADED MIXED TYPE EQUATION IN DOUBLE-CONNECTED DOMAIN

O.Kh. Abdullayev

National University of Uzbekistan by Mirzo Ulugbeka, 100174, Uzbekistan, Tashkent c., VUZ gorodok st.
E-mail: obidjon.mth@gmail.com

In the present paper an existence and uniqueness of solution of the non-local boundary value problem for the loaded elliptic-hyperbolic type equation on the third order in double-connected domain was investigated. The uniqueness of solution was proved by the extremum principle for the mixed type equations, and existence was proved by the method of integral equations.

Key words: loaded equation, elliptic-hyperbolic type, double-connected domain, an extremum principle, existence of solution, uniqueness of solution, method of integral equations

Introduction

We shall notice that with intensive research on problem of optimal control of the agroeconomical system, regulating the level of ground waters and soil moisture, it has become necessary to investigate a new class of equations called "LOADED EQUATIONS". Such equations were investigated in first in the works by N.N. Nazarov and N.Kochin, but they didn't use the term "LOADED EQUATIONS". For the first time, the most general definition of the LOADED EQUATIONS was given and various loaded equations were classified in detail by A.M. Nakhushev [1].

Let's notice that non-local problems for the loaded elliptic-hyperbolic type equations in double-connected domains have not been investigated. In the given paper, uniqueness of solution of the non-local boundary value problem for the loaded elliptic-hyperbolic type equation in double-connected domain was proved, and the method of the solvability of the investigated problem was presented.

Abdullayev Odidjon Khayrullaevich – Ph.D. (Phys. & Math.) Associate Professor Dept. of Differential equations of the National University of Uzbekistan named after Ulugbek, Uzbekistan.

The statement of the Problem

Let's consider the equation

$$u_{xx}+sgn(xy)u_{yy}+\Re(x,y)=0 \tag{1}$$

in double-connected domain of Ω, bounded with to(two) lines:

$$\sigma_1:\ x^2+y^2=1\ ;\quad \sigma_2:\ x^2+y^2=q^2;\ atx>0,y>0;$$

$$\sigma_1^*:\ x^2+y^2=1\ ;\quad \sigma_2^*:\ x^2+y^2=q^2,\ atx<0,y<0;$$

and characteristics:

$$A_jA_j^*:x-y=(-1)^{j+1};\quad B_jB_j^*:x-y=(-1)^{j-1}\cdot q,\ \ (j=1,2)$$

at $x\cdot y<0$, of the equations (1), where $A_1(1;0)$, $A_2(0;1)$, $A_1^*(0;-1)$, $A_2^*(-1;0)$, $B_1(q;0)$, $B_2(0;q)$, $B_1^*(0;-q)$, $B_2^*(-q;0)$, $0<q<1$, $(j\ =\ 1,2)$.

$$\Re(x,y)=\frac{1-sgn(xy)}{2}\cdot[\lambda_1\cdot\Re_1(x,y)+\lambda_2\cdot\Re_2(x,y)],\quad \lambda_1,\lambda_2=const>0;$$

$$\Re_1(x,y)=\frac{1+sgn(xy+x^2)}{2}u(x,0),\quad \Re_2(x,y)=\frac{1+sgn(xy+y^2)}{2}u(0,y).$$

Let's enter designations:

$$E_j\left(\frac{q-(-1)^j}{2};\frac{q+(-1)^j}{2}\right),E_j^*\left(\frac{(-1)^{j-1}-q}{2};\frac{(-1)^j-q}{2}\right),$$

$$C_j\left((-1)^{j-1}\frac{q}{2};(-1)^j\frac{q}{2}\right),\ \Omega_0=\Omega\cap(x>0)\cap(y>0),\Omega_0^*=\Omega\cap(x<0)\cap(y<0),$$

$$\Delta_1=\Omega\cap(x+y>q)\cap(y<0);\Delta_1^*=\Omega\cap(x+y<-q)\cap(y<0),$$

$$\Delta_2=\Omega\cap(x+y>q)\cap(x<0),\ \Delta_2^*=\Omega\cap(x+y<-q)\cap(y>0),$$

$$D_1=\Omega\cap(-q<x+y<q)\cap(y<0),\quad D_2=\Omega\cap(-q<x+y<q)\cap(y>0),$$

$$D_0=\Omega_0\cup\Delta_1\cup\Delta_2,\quad D_0^*=\Omega_0^*\cup\Delta_1^*\cup\Delta_2^*,$$

$$I_j=\{t:\ 0<t<q\};\quad I_{2+j}=\left\{t:0<(-1)^{j-1}t<1\right\},$$

where $t=\begin{cases} x\ at\ \ j=1,\\ y\ at\ \ j=2.\end{cases}$

Let's designate, through $\theta_1\left(\frac{x+1}{2};\frac{x-1}{2}\right)$, $\theta_2\left(\frac{y-1}{2};\frac{y+1}{2}\right)$ points of intersections of characteristics of the equation (1) with leaving points $(x,0)\in A_1B_1$ and $(0,y)\in A_2B_2$ with characteristics $A_1A_1^*$ and $A_2A_2^*$, accordingly.

In the domain of Ω the following problem is investigated

Task. ***(Problem A.)*** *To find function $u(x,y)$ with following properties:*

1) $u(x,y) \in C(\bar{\Omega})$;

2) $u(x,y)$ is the regular solution of the equation (1) in the domain of $\Omega \backslash (xy = 0) \backslash (x+y = \pm q)$, besides, $u_y \in C(A_1B_1 \cup A_2^*B_2^*)$, $u_x \in C(A_2B_2 \cup A_1^*B_1^*)$ at that $u_x(0,t)$, $u_y(t,0)$ can tend infinity of an order of less unit at $t \to \pm q$, and finite at $t \to \pm 1$;

3) $u(x,y)$ satisfies gluing conditions on lines of changing type:

$$u_y(x,-0) = u_y(x,+0), \text{ in regular intervals on } (x,0) \in A_1B_1 \cup A_2^*B_2^*,$$

$$u_x(-0,y) = u_x(+0,y), \text{ in regular intervals on } (0,y) \in A_1^*B_1^* \cup A_2B_2,$$

4) $u(x,y)$ satisfies to boundary conditions:

$$u(x,y)\big|_{\sigma_j} = \phi_j(x,y); \ \ (x,y) \in \overline{\sigma_j}, \tag{2}$$

$$u(x,y)\Big|_{\sigma_j^*} = \phi_j^*(x,y); \ \ (x,y) \in \overline{\sigma_j^*}, \tag{3}$$

$$\frac{d}{dx}u(\theta_1(x)) = a_1(x)u_y(x;0) + b_1(x), \quad q < x < 1, \tag{4}$$

$$\frac{d}{dy}u(\theta_2(y)) = a_2(y)u_x(0;y) + b_2(y), \quad q < y < 1, \tag{5}$$

$$u(x,y)\Big|_{B_jB_j^*} = g_j(t), \ \ t \in \overline{I_j}, \tag{6}$$

where $\phi_j(x,y)$, $\phi_j^*(x,y)$, $g_j(t), a_j(t), b_j(t)$, $(j = 1,2)$ is given function, at that:

$$\left.\begin{array}{l} g_j\left(\frac{q}{2}\right) = g_j^*\left(\frac{q}{2}\right), \ \phi_2(q,0) = g_1(q), \ \phi_2(0,q) = g_2(q), \\ \phi_2^*(0,-q) = g_1(-q), \ \phi_2^*(-q,0) = g_2(-q), \end{array}\right\} \tag{7}$$

$$\phi_j(x,y) = (xy)^{\gamma}\overline{\phi_j}(x,y); \ \overline{\phi_j}(x,y) \in C\left(\overline{\sigma_j}\right), \ 2 < \gamma < 3 \tag{8}$$

$$\phi_j^*(x,y) = (xy)^{\gamma}\overline{\phi_j^*}(x,y); \ \overline{\phi_j^*}(x,y) \in C\left(\overline{\sigma_j^*}\right), \ 2 < \gamma < 3, \tag{9}$$

$$g_j(t) \in C\left(\overline{I_j}\right) \cap C^2\left(I_j\right), \tag{10}$$

$$a_j(t), \ b_j(t) \in C[q,1] \cap C^2(p,q); \tag{11}$$

Theorem. *If conditions (7) - 11) and*

$$a_1(x) > \frac{1}{2}, \quad a_2(y) > \frac{1}{2} \quad ; \tag{12}$$

*are satisfied, then the solution of the **Problem A** exists and it is unique.*

Proof. Note, that the solution the equation (1) in hyperbolic domains looks like:

$$u(x,y) = f_1(x+y) + f_2(y-x) + \lambda_2 \int_q^y (y-t)z(0,t)dt, aty > 0,\ x < 0; \tag{13}$$

$$u(x,y) = f_1(x+y) + f_2(x-y) + \lambda \int_y^{-q} (t-y)z(0,t)dt, atx > 0,\ y < 0; \tag{14}$$

Owing to (13) we will receive, that the solution of Cauchy problem of the equation (1) satisfies conditions $u(0,y) = \tau_2(y)$ and $u_x(0,y) = \nu_2(y)$ in the domain of Δ_2, looks like:

$$u(x,y) = \frac{\tau_2(x+y) + \tau_2(y-x)}{2} + \frac{1}{2}\int_{y-x}^{y+x} \nu_2(t)dt - \frac{\lambda}{2}\int_q^{y+x} (x+y-t)\tau_2(t)dt -$$

$$-\frac{\lambda}{2}\int_q^{y-x} (y-x-t)\tau_2(t)dt + \lambda\int_q^y (y-t)\tau_2(t)dt. \tag{15}$$

From here, by virtue, (5) we will receive a functional relation between $\tau_2(y)$ and $\nu_2(y)$ from the domain of Δ_2 on the piece A_2B_2:

$$\frac{1}{2}\tau_2'(y) + \frac{1}{2}\nu_2(y) - \lambda_2\int_q^y \tau_2(t)dt + \frac{\lambda_2}{2}\int_q^{\frac{y+1}{2}} \tau_2(t)dt = \nu_2(y)a_2(y) + b_2(y),$$

i.e.,

$$(2a_2(y) - 1)\,\nu_2(y) = \tau_2'(y) + \lambda_2\int_q^{\frac{y+1}{2}} \tau_2(t)dt + 2\lambda_2\int_q^y \tau_2(t)dt - b_2(y). \tag{16}$$

Confirm, that a functional relation between $\tau_1(x)$ and $\nu_1(x)$we will obtain by the same method, from the solution of Cauchy problem for the equation (1) satisfying to conditions $u(x,0) = \tau_1(x)$; $u_y(x,0) = \nu_1(x)$ in the domain of Δ_1, and with the account of conditions (4), which presented on the form:

$$(2a_1(x) - 1)\,\nu_1(x) = \tau_1'(x) + \lambda_1\int_q^{\frac{x+1}{2}} \tau_1(t)dt + 2\lambda_1\int_q^y \tau_1(t)dt - b_1(x). \tag{17}$$

□

The uniqueness of solution of the Problem A

It is known that, if the homogeneous problem has only trivial solution than a solution of the accordingly non-uniform problem is unique, therefore, we need to prove that the homogeneous problem has only trivial solution.

Let $b_1(y) \equiv b_2(x) \equiv 0$ then, from (16) and (17), accordingly, we will receive:

$$(2a_2(y)-1)\,\nu_2(y) = \tau_2'(y) + \lambda_2 \int_q^{\frac{y+1}{2}} \tau_2(t)dt + 2\lambda_2 \int_q^{y} \tau_2(t)dt, \tag{18}$$

and

$$(2a_1(x)-1)\,\nu_1(x) = \tau_1'(x) + \lambda_1 \int_q^{\frac{x+1}{2}} \tau_1(t)dt + 2\lambda_1 \int_q^{x} \tau_1(t)dt. \tag{19}$$

Lemma 1. *If $b_1(y) \equiv b_2(x) \equiv 0$ and satisfied conditions (12) that solution $u(x,y)$ of the equation (1) reaches the positive maximum, and the negative minimum in closed domain of $\overline{D_0}$ only on $\overline{\sigma_1}$ and $\overline{\sigma_2}$.*

Proof. According to the extremum principle for the hyperbolic [2] and elliptic equations [3], the solution $u(x,y)$ of the equation (1) can reach the positive maximum and the negative minimum in closed domain of $\overline{D_0}$ only on $A_2B_2 \cup A_1B_1$ and $\overline{\sigma_1} \cup \overline{\sigma_2}$. We need to prove, that the solution $u(x,y)$ of the equation (1) can't reach the positive maximum and the negative minimum in $A_2B_2 \cup A_1B_1$.

Let the function $u(x,y)$ $(u(0,y) = \tau_2(y))$ reach the positive maximum (the negative minimum) on some point of$y_0 \in A_2B_2$, then from (18) and based on (12) we will receive

$$\nu_2(y_0) = \frac{\lambda_2}{2a_2(y_0)-1}\left[\int_q^{\frac{y_0+1}{2}} \tau_2(t)dt + 2\int_q^{y_0} \tau_2(t)dt\right] > 0 \quad (\nu_2(y_0) < 0).$$

Therefore, in the view of to the gluing condition, we have $\nu_2^+(y_0) > 0 \quad \left(\nu_2^+(y_0) < 0\right)$, and it contradicts the known Zareba-Zero principle [3], according to which in a point of a positive maximum (a negative minimum) should be $\nu_2(y_0) < 0 \quad (\nu_2(y_0) > 0)$. Thus, $u(x,y)$ does not reach the positive maximum (the negative minimum) on the point of $y_0 \in A_2B_2$.

Owing to (19) and (12), it is similarly proved that the function $u(x,y)$ does not reach the positive maximum and the negative minimum in the interval of A_1B_1.

The Lemma 1 is proved. □

As $\tau_2(y)$ does not reach the positive maximum and the negative minimum in the interval of A_2B_2 then, $\tau_2(y) = const$ in the interval of A_2B_2. Further by virtue $u(x,y) \in C(\bar{\Omega})$, we will receive $\tau_2(1) = \phi_1(0,1) \equiv 0$, $\tau_2(q) = \phi_2(0,q) \equiv 0$ at the $\phi_j(x,y) \equiv 0$. From here, as $\tau_2(y) \in C\left(\overline{A_2B_2}\right)$ we will conclude that, $\tau_2(y) \equiv 0$ in $\overline{A_2B_2}$. Therefore, if $b_2(y) \equiv 0$ and $a_2(y) > \frac{1}{2}$, then from (18) we will get $\nu_2(y) \equiv 0$. Also, by the same method, we can get $\tau_1(x) \equiv 0$ in $\overline{A_1B_1}$ and $\nu_1(x) \equiv 0$.

Hence, owing to uniqueness of solution of the Cauchy problem for the equation (1), we will have $u(x,y) \equiv 0$ in domains $\overline{\Delta_1}$ and $\overline{\Delta_2}$.

Consequently, in the view of the **Lemma 1**, at $\phi_1(x,y) \equiv \phi_2(x,y) \equiv 0$ we will deduce, that $u(x,y) \equiv 0$ in closed domain of $\overline{\Omega_0}$. Thus, $u(x,y) \equiv 0$ in $\overline{D_0}$.

Further, owing to condition 7 and considering the uniqueness of solution of the Gaursat problem at$g_j(t) \equiv 0$, $t \in \overline{I_j}$ we will receive $u(x,y) \equiv 0$ in $\overline{D_j}$ $(j = 1,2)$.

Takes place:

Lemma 2. *The solution $u(x,y)$ of the equation (1) reach the positive maximum and the negative minimum in closed domain $\overline{D_0^*}$ only on $A_2^*B_2^* \cup A_1^*B_1^*$, $\overline{\sigma_1^*}$ and $\overline{\sigma_2^*}$. (* ***Lemma 2 will be proved similarly as Lemma 1)***

On the basis of **Lemma 2**, on account of 3 at $\phi_j^*(x,y) \equiv 0$, we will receive $u(x,y) \equiv 0$ in the domain of $\overline{D_0^*}$. Thus, the solution of homogeneous **Problem A** is identically equal to zero in the domain of Ω. (***The uniqueness of solution of the*** **Problem A** ***is proved*****.)**

The existence of solution of the problem I

It's known, that the solution $u(x,y)$ of the Nyman problem (**Problem N**) [2] satisfying conditions:

1) $u(x,y) \in C(\overline{D_0}) \cap C^2(D_0 \backslash xy = 0) \cap C^1(D_0)$ is the solution of the equation (1);
2) $u_y \in C(A_1B_1)$, $u_x \in C(A_2B_2)$, at that $u_x(0,t), u_y(t,0)$ can tend to infinity of an order of less unit at $t \to q$, and finite at $t \to 1$;
3) satisfies to boundary conditions (2) (j=1,2) and $u_x(0,y) = \nu_2(y)$, $u_y(x,0) = \nu_1(x)$ is exists and is unique and represented in the form [2]

$$u(x,y) = \int\limits_{\sigma_1} \phi_1(\xi,\eta) \frac{\partial}{\partial n} G(\xi,\eta;x,y) dS - \int\limits_{\sigma_2} \phi_2(\xi,\eta) \frac{\partial}{\partial n} G(\xi,\eta;x,y) dS + \\ + \int\limits_q^1 \nu_1^+(t) G(t,0;x,y) dt + \int\limits_q^1 \nu_2^+(t) G(0,t;x,y) dt, \tag{20}$$

where $G(\xi,\eta;x,y)$ is Green's function of the problem N for the Laplase equation in the domain of Ω_0, which looks like:

$$G(\xi,\eta;x,y) = \frac{1}{2\pi} \ln \left| \frac{\theta_1\left(\frac{\ln v + \ln \overline{\mu}}{2\pi i r}\right) \theta_1\left(\frac{\ln \overline{v} + \ln \overline{\mu}}{2\pi i r}\right) \theta_1\left(\frac{\ln(-v) + \ln \overline{\mu}}{2\pi i r}\right) \theta_1\left(\frac{\ln(-\overline{v}) + \ln \overline{\mu}}{2\pi i r}\right)}{\theta_1\left(\frac{\ln v - \ln \mu}{2\pi i r}\right) \theta_1\left(\frac{\ln \overline{v} - \ln \mu}{2\pi i r}\right) \theta_1\left(\frac{\ln(-v) - \ln \mu}{2\pi i r}\right) \theta_1\left(\frac{\ln(-\overline{v}) - \ln \mu}{2\pi i r}\right)} \right|, \tag{21}$$

where $v = \xi + i\eta$, $\overline{v} = \xi - i\eta$, $\mu = x + iy$, $\overline{\mu} = x - iy$, $r = \frac{1}{\pi i} \ln q$, $i^2 = -1$, $\theta_1(\xi) = \theta_1\left(\xi \left| -\frac{1}{r}\right.\right)$ is theta function.

From (20) $y = 0$ and$x = 0$, we will get functional relations between $\tau_2^+(y)$, $\nu_2^+(y)$ and $\tau_1^+(x)$, $\nu_1^+(x)$, respectively, on the pieces A_2B_2 and A_1B_1 getting from the domain Ω_0:

$$\tau_1^+(x) = \sum_{k=1}^{2} (-1)^{k-1} \int\limits_{\sigma_k} \phi_k(\xi,\eta) \frac{\partial}{\partial n} G(\xi,\eta;x,0) dS + \int\limits_q^1 \nu_1^+(t) G(t,0;x,0) dt + \\ + \int\limits_q^1 \nu_2^+(t) G(0,t;x,0) dt. \tag{22}$$

$$\tau_2^+(y) = \sum_{k=1}^{2} (-1)^{k-1} \int\limits_{\sigma_k} \phi_k(\xi,\eta) \frac{\partial}{\partial n} G(\xi,\eta;0,y) dS + \int\limits_q^1 \nu_1^+(t) G(t,0;0,y) dt +$$

$$+\int_q^1 \nu_2^+(t)G(0,t;0,y)dt, \tag{23}$$

After differentiating equalities (22) by x and (23) by y, we obtain

$$\tau_1'^+(x) = \int_q^1 \nu_1^+(t)\frac{\partial G(t,0;x,0)}{\partial x}dt + \int_q^1 \nu_2^+(t)\frac{\partial G(0,t;x,0)}{\partial x}dt + F_1'(x), \tag{24}$$

where $F_1(x) = \sum\limits_{k=1}^{2}(-1)^{k-1}\int\limits_{\sigma_k}\varphi_k(\xi,\eta)\frac{\partial}{\partial n}G(\xi,\eta;x,0)dS$, and

$$\tau_2'^+(y) = \int_q^1 \nu_1^+(t)\frac{\partial G(t,0;0,y)}{\partial y}dt + \int_q^1 \nu_2^+(t)\frac{\partial G(0,t;0,y)}{\partial y}dt + F_2'(y), \tag{25}$$

where $F_2(y) = \sum\limits_{k=1}^{2}(-1)^{k-1}\int\limits_{\sigma_k}\phi_k(\xi,\eta)\frac{\partial}{\partial n}G(\xi,\eta;0,y)dS$.

Further, the equations (16) and (17) we will rewrite in the form:

$$\tau_j'(t) + \lambda_j\int_q^{\frac{t+1}{2}} K(t,z)\tau_j'(z)dz = \tilde{F}_j(t), \tag{26}$$

where

$$\tilde{F}_j(t) = (2a_j(t)-1)\nu_j(t) + b_j(t) + \lambda_j\tau_j(q)\left(\frac{5t+1}{2} - 3q\right), \tag{27}$$

$$K(t,z) = \begin{cases} \frac{5y+1}{2} - 3z, & q \le z \le t; \\ \frac{t+1}{2} - z, & t \le z \le \frac{t+1}{2}, \end{cases} \qquad t = \begin{cases} x \text{ at } j=1, \\ y \text{ at } j=2. \end{cases} \tag{28}$$

Note that we will search the function $\nu_j(t)$ from the class of $C^2(q,1)$, which can tend to infinity of an order of less unit at $t \to q$, and finite at $t \to 1$. From here and owing to account (11), we will decide $\tilde{F}_j(t) \in C^2(q,1)$ and that $\tilde{F}_j(t)$ can tend to infinity of an order of less unit at $t \to q$, and finite at $t \to 1$.

Hence, by virtue

$$\left|K_j(t,z)\right| \le const,$$

we will conclude that the equations (26) are the Volterra integral equations of the second kind which unequivocally solved by the method of consecutive approach [2] and its solution is represented in the form:

$$\tau_j'(t) = \lambda_j\int_q^{\frac{t+1}{2}} R_j(t,z,\lambda_j)\tilde{F}_j(z)dz + \tilde{F}_j(t), \tag{29}$$

where $R_j(t,z,\lambda_j)$ are resolves of the kernels $K_j(t,z)$, and that

$$\left|R_j(t,z,\lambda_j)\right| \le const, (j=1,2). \tag{30}$$

Further, having excluded $\tau_j'(t)$ from the relations (24) and (29), we will receive system of the integral equations

$$\begin{cases} (2a_1(x)-1)\nu_1(x)+\lambda_1\int\limits_q^{\frac{x+1}{2}}\tilde{R}_1(x,z,\lambda_1)\nu_1(z)dz-\int\limits_q^1\nu_1^+(t)\frac{\partial G(t,0;x,0)}{\partial x}dt=\Phi_1(x) \\ (2a_2(y)-1)\nu_2(y)+\lambda_2\int\limits_q^{\frac{y+1}{2}}\tilde{R}_2(y,z,\lambda_2)\nu_2(z)dz-\int\limits_q^1\nu_2^+(t)\frac{\partial G(0,t;0,y)}{\partial y}dt=\Phi_2(y) \end{cases} \tag{31}$$

where

$$\Phi_1(x)=\int\limits_q^1\nu_2^+(t)\frac{\partial G(0,t;x,0)}{\partial x}dt-\lambda_1\int\limits_q^{\frac{x+1}{2}}R_1(x,z,\lambda_1)\tilde{b}_1(z)dz-\tilde{b}_1(x)+F_1'(x), \tag{32}$$

$$\tilde{b}_1(x)=b_1(x)+\frac{\lambda_1\phi_2(q,0)}{2}(5x-6q+1);$$

$$\Phi_2(y)=\int\limits_q^1\nu_1^+(t)\frac{\partial G(t,0;0,y)}{\partial y}dt-\lambda_2\int\limits_q^{\frac{y+1}{2}}R_2(y,z,\lambda_2)\tilde{b}_2(z)dz-\tilde{b}_2(y)+F_2'(y), \tag{33}$$

$$\tilde{b}_2(y)=b_2(y)+\frac{\lambda_2\phi_2(0,q)}{2}(5y-6q+1).$$

$$G(t,0;x,0)=G(0,t;0,x)=K_1(x,t),$$

$$K_1(x,t)=\frac{1}{\pi}\left[\frac{\ln t\ln x}{\ln q}+K_1^*(x,t)+K_1^*(x,-t)\right] \tag{34}$$

$$G(t,0;0,x)=G(0,t;x,0)=K_2^{(}x,t)=K_1^{(}x,-it), \tag{35}$$

$$K_1^*(x,t)=\ln\left|\frac{1-tx}{t-x}\right|+\sum_{n=1}^{\infty}\left(\ln\left|\frac{1-q^{2n}tx}{t-q^{2n}x}\right|+\ln\left|\frac{1-q^{-2n}tx}{t-q^{-2n}x}\right|\right). \tag{36}$$

Further, after some simplifications, from (31)-(36) we can get the system of singularity integral equation concerning $\nu_1(x)$ and $\nu_2(y)$ which represented on(in) the form [2]

$$\begin{cases} \nu_1^{(}x)=\int\limits_q^1\nu_1(t)A_1(x,t)dt+\tilde{\Phi}_1(x) \\ \nu_2^{(}x)=\int\limits_q^1\nu_2(t)A_2(x,t)dt+\tilde{\Phi}_2(x) \end{cases}; \tag{37}$$

where $\tilde{\Phi}_j(x)=\frac{\Phi_j(x)}{2a_j(x)-1}$;

$$A_j(x,t)=\begin{cases} \lambda_j\frac{\tilde{R}_j(x,z,\lambda_j)}{2a_j(x)-1}-\frac{\bar{K}_1(x,t)}{2a_j(x)-1}, & q\le z\le\frac{x+1}{2}; \\ \frac{\bar{K}_1(x,z)}{2a_j(x)-1}, & \frac{x+1}{2}\le z\le 1, \end{cases} \tag{38}$$

$$\bar{K}_1(x,t)=\frac{2\ln|t|}{x\ln q}+K(x,t)+K(x,-t), \tag{39}$$

$$K(x,t)=\frac{1}{\pi}\left[\frac{1}{t-x}-\frac{t}{1-tx}+\sum_{n=1}^{\infty}\left(\frac{q^{2n}}{t-q^{2n}x}-\frac{q^{2n}t}{1-q^{2n}tx}-\frac{q^{-2n}t}{1-q^{-2n}tx}+\frac{q^{-2n}}{t-q^{2n}x}\right)\right]. \quad (40)$$

Further, we will investigate the function $\Phi_1(x)$:

$$\Phi_1(x)=\int_q^1 \nu_2^+(t)\bar{K}_1(x,it)dt-\lambda_1\int_q^{\frac{x+1}{2}} R_1(x,z,\lambda_1)\tilde{b}_1(z)dz-\tilde{b}_1(x)+$$

$$+\int_{\sigma_1}\phi_1(\xi,\eta)\frac{\partial}{\partial x}\left(\frac{\partial G(\xi,\eta;x,0)}{\partial\xi}\right)d\eta-\int_{\sigma_1}\phi_1(\xi,\eta)\frac{\partial}{\partial x}\left(\frac{\partial G(\xi,\eta;x,0)}{\partial\eta}\right)d\xi+$$

$$-\int_{\sigma_2}\phi_2(\xi,\eta)\frac{\partial}{\partial x}\left(\frac{\partial G(\xi,\eta;x,0)}{\partial\xi}\right)d\eta+\int_{\sigma_2}\phi_2(\xi,\eta)\frac{\partial}{\partial x}\left(\frac{\partial G(\xi,\eta;x,0)}{\partial\eta}\right)d\xi=$$

$$=\int_q^1 \nu_2^+(t)\bar{K}_1(x,it)dt-2\int_0^1\phi_1(\xi,\eta)\frac{\xi}{\sqrt{1-\xi^2}}\frac{\partial}{\partial x}\left(\frac{\partial G(\xi,\eta;x,0)}{\partial\xi}\right)d\xi-$$

$$-\int_0^1\phi_1(\xi,\eta)\frac{\partial}{\partial\xi}\left(\frac{\partial G(\xi,\eta;x,0)}{\partial\eta}\right)d\xi+2\int_0^q\phi_2(\xi,\eta)\frac{\xi}{\sqrt{q^2-\xi^2}}\frac{\partial}{\partial x}\left(\frac{\partial G(\xi,\eta;x,0)}{\partial\xi}\right)d\xi+$$

$$+\int_0^q\phi_2(\xi,\eta)\frac{\partial}{\partial x}\left(\frac{\partial G(\xi,\eta;x,0)}{\partial\eta}\right)d\xi+\beta(x)=$$

$$=\alpha_1(x)+\alpha_2(x)+\alpha_3(x)+\alpha_4(x)+\alpha_5(x)+\beta(x)$$

where $\beta(x)=-\lambda_1\int_q^{\frac{x+1}{2}} R_1(x,z,\lambda_1)\tilde{b}_1(z)dz-\tilde{b}_1(x)$.

Owing to account (9), (11), (21), (30), (39) and (40), we will get (***see*** [2]):

$$|\beta(x)|\le const,\quad |\alpha_1(x)|\le const,\quad |\alpha_2(x)|\le const,\quad |\alpha_3(x)|\le const,$$

$$|\alpha_4(x)|\le (x-q)^{\gamma-3}const,\quad |\alpha_5(x)|\le (x-q)^{\gamma-3}const,\quad (2<\gamma<3). \quad (41)$$

Hence, by virtue (12) and (41), we will conclude that $\tilde{\Phi}_1(x)\in C^2(q,1)$, and $\tilde{\Phi}_1(x)$ can tend to infinity an order of less one at $x\to q$, and at $x\to 1$ it is limited.

It is similarly proved, that $\tilde{\Phi}_2(y)\in C^2(q,1)$, and $\Phi_2(y)$ can tend to infinity an order of less one at $y\to q$, and at $y\to 1$ it is limited.

Thus, the system of integral equation (37) is reduced to the Fredholm integral equations of the second kind, by the known method Karleman-Vekua [4], just as in works [2], [3].

Note, that unique solvability of the Fredholm integral equations of the second kind follows from the uniqueness of solution of the **Problem A** and from the theory integral equations.

Solving the system of integral equations (37), we will found $\nu_1(x)$ and $\nu_2(y)$ [2], further owing to account (24) and $\tau_1(q) = \phi_2(q,0)$, $\tau_2(q) = \phi_2(0,q)$ from (29) we will find $\tau_j(t)$ (j=1,2).

Hence, after having found $\tau_1(x)$ and $\nu_1(x)$, $\tau_2(y)$ and $\nu_2(y)$, the solution of the **Problem A** can be restored in the domain of Ω_0 as the solution of the **Problem N** (20), and in domains Δ_j (j=1,2) as the solution of the Cauchy problem. The solution of the **Problem A** in domains of D_j(j=1,2) can be restored as a solution of the Gaursat problem with conditions (6) and $u(x,y)\big|_{B_jE_j} = h_j(t)$, where $h_j(t)$ (j=1,2) are traces of solution of the Cauchy problems in domains Δ_j (j=1,2), on the line $x+y=q$, and reciprocally in domains Δ_j^* (j=1,2) as the solution of the Cauchy-Gaursat problem with conditions $u_y(x,0) = \nu_1^*(x)$; $u_x(0,y) = \nu_2^*(y)$, $-1 < x,y < -q$ and $u(x,y)\Big|_{B_j^*E_j^*} = h_j^*(t)$, where $h_j^*(t)$ (j=1,2) are traces of solution of the Gaursat problems in domains D_j (j=1,2). And finally the solution of the **Problem A** can be restored in the domain of Ω_0^* as the solution of the problem N, similarly as (20). The **Theorem** is proved.

References

1. Nakhushev A.M. *Nagruzhennye uravneniya i ih prilozheniya* [The loaded equations and their applications]. Moscow, Nauka Publ., 2012. 232 p.
2. Abdullaev O.Kh. *Kraevaya zadacha dlya nagruzhennogo uravneniya 'elliptiko-giperbolicheskogo tipa v dvusvyaznoj oblasti* [Boundary value problem for a loaded equation elliptic-hyperbolic type in double connected domain]. *Vestnik KRAUNC. Fiziko-matematicheskie nauki – Bulletin of the Kamchatka Regional Association «Education-Scientific Center». Physical & Mathematical Sciences*, 2014, vol. 8, no. 2, pp. 33-48.
3. Bitsadze A.V. Differential equations of Mixed type. New York, Pergamon Press, 1964. 160 p.
4. Ìuskheleshvili N.I. *Singulyarnye integral'nye uravneniya* [Singularity integral equations]. Moscow, Nauka Publ., 1968. 512 p.

Original article submitted: 10.12.2014

Bulletin KRASEC. Phys. & Math. Sci, 2014, vol. , no. 2, pp. 13-17. ISSN 2313-0156

MSC 34L40

CERTAIN PROPERTIES OF FRACTIONAL INTEGRO-DIFFERENTIATION OPERATOR OF FUNCTIONS IN OTHER FEATURES

A.S. Nishonboev

Fergana State University, 150100, Uzbekistan, Fergana c., Murabbiylar st., 19
E-mail: azizbek.nishoboev@mail.ru

Prove an important lemma for the operator of fractional integro-differentiation of functions of other functions.

Key words: Gaussian function, the function Meyer, Mellin transform

Assume the notations:

$$D^{l}_{a,g(x)}\phi(x)=\begin{cases}\frac{1}{\Gamma(-l)}\int\limits_{a}^{x}[g(x)-g(t)]^{-l-1}\phi(t)g'(t)dt, & l<0\\ \phi(x), & l=0\\ \frac{d^{n+1}}{d[g(x)]^{n+1}}D^{l-(n+1)}_{0g(x)}\phi(x), & l>0\end{cases} \tag{1}$$

$$F_{0,g(x)}\left[\begin{array}{cc} a & b\\ e & x\end{array}\right]\phi(x)=\begin{cases}\frac{1}{\Gamma(-l)}\int\limits_{a}^{x}[g(x)-g(t)]^{-l-1}F(a,b,c;\frac{g(x)-g(t)}{g(x)})\phi(t)g(t)'dt, l<0\\ \phi(x), l=0\\ \left[g(x)\right]^{b}\frac{d^{n+1}}{d[g(x)]^{n+1}}[g(x)]^{-b}F_{0,g(x)}\left[\begin{array}{cc} a+b+1, & b\\ l-n-1, & x\end{array}\right]\phi(x), l>0\end{cases} \tag{2}$$

were a, b and l are any real numbers, n is the integer part of l; $\Gamma(x)$ – gamma-function; $F[\ldots]$ is the Gaussian hypergeometric function [1].

Lemma 1. *Let $\varphi(x)\in L(0,1)$, $l_1+l_3<0$, $l_3<0$. Than almost everywhere at (0,1), the following relation holds*

$$D^{l_1}_{0x^2}D^{l_3}_{0x}\phi(x)=2^{l_3}\cdot x^{l_3+1}F_{0x^2}\left[\begin{array}{cc} -\frac{1+l_3}{2}, & -l_1-\frac{l_3}{2}\\ -l_1-l_3, & x\end{array}\right]\frac{\phi(x)}{x}. \tag{3}$$

Here l_1, l_3 – are the given real numbers;

Proof. Consider the case when $l_1<0$, $l_3<0$. Due to the definition (1) we have

$$D^{l_1}_{0x^2}D^{l_2}_{0x}\phi(x)=\frac{x^{-l_1}}{\Gamma(-l_1)\Gamma(-l_3)}\int\limits_{0}^{x}(x^2-t^2)^{-l_1-1}dt^2\int\limits_{0}^{t}(t-y)^{-l_3-1}\phi(y)dy. \tag{4}$$

Nishonboev Azizbek Solizhonovich – Lecturer, of Dep. Mathematical Analysis and Differential Equations, Fergana State University, Republic of Uzbekistan.

After some transformations from (4), we obtain

$$I = D_{0x^2}^{l_1} D_{0x}^{l_3} \phi\left(\sqrt{x}\right) = \frac{x^{-l_1}}{\Gamma(-l_1)\Gamma(-l_3)} \int_0^x (x-t)^{-l_1-1} dt \int_0^t (\sqrt{t}-\sqrt{y})^{-l_3-1} \phi\left(\sqrt{y}\right) d\sqrt{y}. \quad (5)$$

Changing the integration order, from (5) we find

$$I = \int_0^x \phi(y) d\sqrt{y} \int_y^x (x-t)^{-l_1-1} (\sqrt{t}-\sqrt{y})^{-l_3-1} dt, \quad (6)$$

Changing $t = xz$ from (6) we obtain

$$I = \frac{x^{-l_1}}{\Gamma(-l_1)\Gamma(-l_3)} \int_0^x (\sqrt{y})^{-l_3-1} \phi(y) K(\sigma) d\sqrt{y}, \quad (7)$$

where

$$K(\sigma) = \int_0^\infty K_1\left(\sqrt{\sigma z}\right) K_2(z)\, dz, \quad (8)$$

$$K_1(z) = (z-1)_+^{-l_3-1}, \quad K_2(z) = (1-z)_+^{-l_1-1}, \quad (9)$$

$$\sigma = \frac{x}{y}, \quad z_+^l = \begin{cases} 0, & z \le 0 \\ z^l, & z > 0 \end{cases}.$$

To calculate the integral (8), Mellin transform is used a [1]

$$f*(s) = M\{f(x); s\} = \int_0^\infty f(x) x^{s-1} dx. \quad (10)$$

Then, considering the relation [3]

$$M\left\{ x^{\delta_1} \int_0^\infty \xi^{\delta_2} g_1(x\xi)\, g_2(\xi)\, d\xi; s \right\} = g_1^*(s+\delta_1)\, g_2^*(1-\delta_1+\delta_2-s), \quad (11)$$

we obtain

$$M\{K(\sigma); s\} = K^*(s) K_1^*(s) K_2^*(1-s). \quad (12)$$

Further, in virtue of the formula [3]

$$M\left\{ (x-1)_+^{c-1}; s \right\} = \Gamma(c)\Gamma\left[\begin{matrix} 1-c-s \\ 1-s \end{matrix} \right], \quad \mathrm{Re}c > 0, \quad \mathrm{Re}s < 1 - \mathrm{Re}c. \quad (13)$$

$$M\{f(x^p)\} = \frac{1}{p} f*\left(\frac{s}{p}\right), \quad p \neq 0, \quad (14)$$

$$M\left\{ (1-x)_+^{c-1}; s \right\} = \Gamma(c)\Gamma\left[\begin{matrix} s \\ s+c \end{matrix} \right], \quad \mathrm{Re}c > 0, \quad \mathrm{Re}s > 0 \quad (15)$$

find

$$K_1*(s)=2\Gamma(-l_3)\Gamma\left[\begin{array}{c}1+l_3-2s\\1-2s\end{array}\right],\quad \mathrm{Re}l_3<0,\quad 2\mathrm{Re}s<1+l_3, \tag{16}$$

and

$$K_2*(s)=\Gamma(-l_1)\Gamma\left[\begin{array}{c}s\\s-l_1\end{array}\right],\quad \mathrm{Re}l_1<0,\quad \mathrm{Re}s>0, \tag{17}$$

Substituting (16), (17) into (12) we obtain

$$K*(s)=2\Gamma(-l_1)\Gamma(-l_3)\Gamma\left[\begin{array}{cc}1+l_3-2s & 1-s\\1-2s & 1-l_1-s\end{array}\right], \tag{18}$$

$$\mathrm{Re}l_1<0,\quad \mathrm{Re}l_3<0,\quad 2\mathrm{Re}s<1+l_3,\quad \mathrm{Re}s<1.$$

Hence, applying the formula [2]

$$\Gamma(2a)=2^{2a-1}\sqrt{\pi}\Gamma(a)\Gamma(a+1/2), \tag{19}$$

from (18) we have

$$K*(s)=2^{l_3+1}\Gamma(-l_1)\Gamma(-l_3)\Gamma\left[\begin{array}{cc}\frac{1+l_3}{2}-s & \frac{2+l_3}{2}-s\\1-l_1-s & \frac{1}{2}-s\end{array}\right], \tag{20}$$

$$\mathrm{Re}l_1<0,\quad \mathrm{Re}l_3<0,\quad 2\mathrm{Re}s<1+l_3,\quad 2\mathrm{Re}s<2+l_3.$$

In virtue of the formula [3]

$$M\left\{(x-1)_+^{c-1}F(a,b,c;1-x);s\right\}=\Gamma(c)\Gamma\left[\begin{array}{cc}1+a-c-\gamma-s, & 1+b-c-s\\1-s, & 1+a+b-c-s\end{array}\right], \tag{21}$$

$$\mathrm{Re}c>0,\ \mathrm{Re}s<1+\mathrm{Re}(a-c),1+\mathrm{Re}(b-c).$$

$$M\{x^pf(x);s\}=f*(s+p), \tag{22}$$

$$F(a,b,c;z)=(1-z)^{-a}F(a,c-b,c;\frac{z}{z-1}), \tag{23}$$

from (20) we obtain

$$K(\sigma)=\frac{2^{l_3+1}\Gamma(-l_1)\Gamma(-l_3)}{\Gamma(-l_1-l_3)}x^{l_1+\frac{1+l_3}{2}}y^{\frac{l_3+1}{2}}(x-y)_+^{-l_1-l_3-1}\times \tag{24}$$

$$\times F(-\frac{1+l_3}{2},-l_1-\frac{l_3}{2},-l_1-l_3;\frac{x-y}{x}).$$

Substituting (24) into (7) and after some transforms we obtain the equality (3).

The similar proof is for the case when $0<l_1<-l_3$. □

Lemma 2. *If the conditions:*

$$1)\varphi(x)\in L(0,1),2)l_1+l_3<0,l_3<0,l_2>-l_1,$$

hold, almost everywhere at (0.1) the following formula is valid

$$D_{0x^2}^{l_1}\left(x^2\right)^{l_2}D_{0x}^{l_3}\phi(x)=\frac{\left(x^2\right)^{l_2-l_1}}{2^{l_3}}\int_0^x y^{-l_3-1}G_{33}^{30}\left(\frac{y^2}{x^2}\left|\begin{array}{c}1+l_2-l_1,\ 1,\ \frac{1}{2}\\ \frac{3+l_3}{2},\ \frac{2+l_3}{2},\ 1+l_2\end{array}\right.\right)\phi(y)\,dy. \tag{25}$$

Proof. To prove it, consider the case when $l_1 < 0$, $l_3 < 0$.
Then due to the definition (1) we have

$$D_{0x^2}^{l_1}\left(x^2\right)^{l_2} D_{0x}^{l_3}\phi(x) = \frac{1}{\Gamma(-l_1)\Gamma(-l_3)} \int_0^x (x^2-t^2)^{-l_1-1}(t^2)^{l_2} dt^2 \int_0^t (t-y)^{-l_3-1}\phi(y)\,dy. \quad (26)$$

After some transforms from (26) we find

$$I = D_{0x}^{l_1} x^{l_2} D_{0\sqrt{x}}^{l_3}\phi(\sqrt{x}) = \quad (27)$$

$$= \frac{1}{\Gamma(-l_1)\Gamma(-l_3)} \int_0^x (x-t)^{-l_1-1} t^{l_2} dt \int_0^t (\sqrt{t}-\sqrt{y})^{-l_3-1}\phi(\sqrt{y})\,d\sqrt{y}.$$

Changing the integration order, we obtain

$$I = \frac{1}{\Gamma(-l_1)\Gamma(-l_3)} \int_0^x \phi(\sqrt{y})\,d\sqrt{y} \int_y^t (x-t)^{-l_1-1} t^{l_2} (\sqrt{t}-\sqrt{y})^{-l_3-1} dt. \quad (28)$$

Assuming $t = xz$, from (28) we find

$$I = \frac{1}{\Gamma(-l_1)\Gamma(-l_3)} \int_0^x y^{-l_1-l_2-\frac{l_3+1}{2}} Q(\sigma) d\sqrt{y}. \quad (29)$$

where

$$Q(\sigma) = \sigma^{l_2-l_3} \int_0^\infty z^{l_2} f_1(\sqrt{\sigma z}) f_2(z) dz, \quad (30)$$

$$f_1(z) = (z-1)_+^{-l_3-1}; \quad f_2(z) = (1-z)_+^{-l_1-1}, \quad (31)$$

$$\sigma = \frac{x}{y}; \quad z_+^l = \begin{cases} 0, & z \le 0 \\ z^l, & z > 0 \end{cases}.$$

Applying the formula (11) from (30) we obtain

$$M\{Q(\sigma); s\} = f_1*(s) f_2*(1+l_2-s), \quad (32)$$

Further, in virtue of the formula (13), (14), (15) we find

$$f_1*(s) = 2\Gamma(-l_3)\Gamma\left[\begin{array}{c} 1+l_3-2s \\ 1-2s \end{array}\right], \quad \mathrm{Re} l_3 < 0, \quad 2\mathrm{Re} s < 1+l_3, \quad (33)$$

$$f_2*(s) = \Gamma(-l_1)\Gamma\left[\begin{array}{c} s \\ s-l_1 \end{array}\right], \quad \mathrm{Re} l_1 < 0, \quad \mathrm{Re} s > 0, \quad (34)$$

Substituting (33), (34) into (32), we obtain

$$Q*(s) = 2\Gamma(-l_1)\Gamma(-l_3)\Gamma\left[\begin{array}{cc} 1+l_3-2s & 1+l_2-s \\ 1-2s & 1+l_2-l_1-s \end{array}\right], \quad (35)$$

$$\mathrm{Re}l_1 < 0, \quad \mathrm{Re}l_3 < 0, \quad 2\mathrm{Re}s < 1 + l_3, \quad \mathrm{Re}s < 1 + l_2.$$

On the basis of the formula (19) (35), we have

$$Q*(s) = 2^{l_3+1}\Gamma(-l_1)\Gamma(-l_3)\Gamma\left[\begin{array}{ccc} \frac{1+l_3}{2} - s & \frac{2+l_3}{2} - s & 1 + l_3 - s \\ \frac{1}{2} - s & 1 - s & 1 + l_3 - l_1 - s \end{array}\right], \tag{36}$$

$$\mathrm{Re}l_1 < 0, \quad \mathrm{Re}l_3 < 0, \quad 2\mathrm{Re}s < 1 + l_3, \quad 2\mathrm{Re}s < 2 + l_3, \quad \mathrm{Re}s < 1 + l_2.$$

In virtue of the formula [2]

$$M\left\{G_{p'q'}^{m'n'}\left(z\left|\begin{array}{c} a_1, a_2, \ldots a_{p'} \\ b_1, b_2, \ldots b_{q'} \end{array}\right.\right); s\right\} =$$

$$= \Gamma\left[\begin{array}{c} s + b_1, s + b_2, \ldots s + b_{m'}, 1 - a_1 - s, 1 - a_2 - s, \ldots 1 - a_{n'} - s \\ s + a_{n'+1}, s + a_{n'+2}, \ldots s + a_{p'}, 1 - b_{m'+1} - s, 1 - b_{m'2} - s, \ldots 1 - b_{q'} - s \end{array}\right] \tag{37}$$

$$- \min_{1 \le k' \le m'} Reb_{k'} < Res < 1 - \max_{1 \le j \le n'} Rea_j, \quad p' = q' \ge 1, \quad m' + n' = p', \quad \sum_{j=1}^{n'} (a_j - b_j) > 0$$

from (35) we obtain

$$Q(\sigma) = 2^{l_3} \frac{1}{\Gamma(-l_1)\Gamma(-l_3)} G_{33}^{30}\left(\frac{y}{x}\left|\begin{array}{ccc} -\frac{1+l_3}{2}, & -\frac{l_1}{2}, & -l_2 \\ l_1 - l_2, & 0, & -\frac{1}{2} \end{array}\right.\right). \tag{38}$$

Substituting (35) into (29) and after some transforms, we obtain the equality (25). □

References

1. Bateman H., Erdelyi A. *Tables of integral transforms, Vol. 2.* New York-Toronto-London, McGRAW-HILL, 1954. (Russ. ed.: Bejtman H., 'Erdeji A. *Tablicy integral'nyh preobrazovanij. Kn. 2: Preobrazovaniya Besselya. Integraly ot special'nyh funkcij.* Moscow, Nauka Publ., 1970. 325 p.).
2. Marichev O.N. *Metod vychislenie integralov ot special'nyh funkcij* [The method for computing integrals of special functions]. Minsk, Nauka i tehnika Publ., 1978. 312 p.
3. Samko S.G., Kilbas A.A., Marichev O.N. *Integraly i proizvodnye drobnogo poryadka i nekotorye ih prilozheniya* [Integrals and derivatives of fractional order, and some applications]. Minsk, Nauka i tehnika Publ., 1987. 688 p.

Original article submitted: 20.10.2014

Bulletin KRASEC. Phys. & Math. Sci, 2014, vol. , no. 2, pp. 18-22. ISSN 2313-0156

MSC 35C05

ON ONE PROBLE FOR HIGHER-ORDER EQUATION

A.V. Yuldasheva

National University of Uzbekistan by Mirzo Ulugbeka, 100174, Uzbekistan, Tashkent c., VUZ gorodok st.

E-mail: yuasv86@mail.ru

In this paper not well posed problem for the even-order equation is studied. The stability of the problem is restored by additional conditions and conditions to domain.

Key words: partial differential equations of higher order, not well posed problem, method of separation of variables, simple continued fractions.

Problem definition

The present paper considers for the equation

$$\frac{\partial^{2k}u}{\partial x^{2k}} - \frac{\partial^2 u}{\partial t^2} = 0, \quad k = 2n+1,\ n \in N, \tag{1}$$

in the domain $D = \{(x,t) : 0 \le x \le \pi, 0 \le t \le 2\pi\}$ a problem with the following conditions:

$$\frac{\partial^{2m}u}{\partial x^{2m}}(0,t) = \frac{\partial^{2m}u}{\partial x^{2m}}(\pi,t) = 0, \quad m = 0,1,...,k-1, \quad 0 \le t \le 2\pi, \tag{2}$$

$$u(\alpha\pi,t) = f(t), \quad 0 \le t \le 2\pi, \tag{3}$$

where α is some constant from $(0,1)$ and $f(t)-$ is the given quite smooth function.

We shall show that if $\alpha$is an irrational number, then the theorem of solution uniqueness of the problem (1), (2), (3) is valid in the class $u \in C^{2k,2}_{x,t}(D)$.

Note that this problem is ill-posed, since a small change in the function $f(t)$ under the norm $C^s(s \in N)$ may cause arbitrary large change of the solution u under the norm L_2.

This problem may be regularized by a side condition, for example, by a priori estimate

$$\int_0^{\pi}\int_0^{2\pi}\left(\frac{\partial^k u}{\partial x^k}\right)^2 dtdx \le E^2, \quad 0 \le t \le 2\pi, \tag{4}$$

where E is the defined constant.

Yuldasheva Asal Victorovna – Ph.D. (Phys. & Math.), Lecturer of the Dep. Differential Equations and Mathematical Physics, of the National University of Uzbekistan, Tashkent.

The problem well-posedness

Assume that there is some function $u \in C_{x,t}^{2k,2}(D)$ which satisfies the conditions (1), (2), (3), then u may be presented in the form of a series

$$u(x,t) = \sum_{n=1}^{\infty} \sin nx \left(a_n \cos n^k t + b_n \sin n^k t \right), \tag{5}$$

and it follows from this representation that the function $f(t)$ should have the form

$$f(t) = \sum_{n=1}^{\infty} \sin n\alpha\pi \left(a_n \cos n^k t + b_n \sin n^k t \right). \tag{6}$$

Theorem 1. *If α is a irrational number, the problem (1), (2), (3) does not have more than one solution of $u \in C_{x,t}^{2k,2}(D)$.*

Proof. Indeed, if in (6) $f \equiv 0$, than $a_n = b_n = 0$. Consequently, и $u \equiv 0$. □

Remark. If α is a rational number, there is no uniqueness.

For example, let q be some natural number, then the function $u(x,t) = \sin qx \cos q^k t$ satisfies (1), (2) and

$$u(\frac{\pi}{q}, t) = 0, \quad 0 \le t \le 2\pi.$$

Defination. We shall indicate that the irrational number α have the order Ω, if Ω is the upper boundary of the numbers ω, satisfying the inequality

$$\left| \alpha - \frac{p}{q} \right| \frac{1}{q^{1+\omega}} \quad ,$$

for any $\frac{p}{q} \in Q$. It is known that almost all the numbers α have the order $\Omega = 1$ [3, **?**].

The next statement is associated with the question on the solution stability depending on α and f. Here is an example.

Theorem 2. *Let α be an irrational number. Then there is a sequence 2π of periodic functions $f_n \in C^{\infty}(R)$, uniformly vanishing, and it is such $u_n \in C_{x,t}^{2k,2}(D)$, satisfying (1), (2) and*

$$u_n(\alpha\pi, t) = f_n(t), \tag{7}$$

the following relation holds

$$\lim_{\to\infty} \|u_n\|_{L_2(D)} = +\infty. \tag{8}$$

Proof. Let

$$f_n(t) = \frac{1}{\sqrt{n^k}} \sin n^k t,$$

then

$$u_n(x,t) = \left(\sqrt{n^k} \sin n\alpha\pi \right)^{-1} \sin n^k t \sin nx.$$

It is known that [2] there is a sequence of such integers p_n, q_n that

$$\lim_{n\to\infty} q_n = +\infty, \quad \left| \alpha - \frac{p_n}{q_n} \right| < \frac{1}{q_n^2}$$

and then the theorem statement appears from the following estimation

$$|\sin q_n \alpha\pi| = |\sin(q_n\alpha - p_n)\pi| < \frac{\pi}{q_n}.$$

Note, that for any given integer s there is such an irrational number α (for example, of the order $s+2$) that the solution

$$u_n(x,t) = n^{-1-s}(\sin n\alpha\pi)^{-1}\sin n^k t\cdot\sin nx$$

of the problem (1), (2) and $u_n(\alpha\pi,t) = n^{-1-s}\sin n^k t$ satisfies the following estimation

$$\lim_{n\to\infty}\|u_n\|_{L_2(D)} = +\infty \quad \lim_{n\to\infty}\|f_n\|_{C^s(D)} = 0,$$

from which it is clear that the problem is ill-posed. □

Further we shall show that the problem is also unstable relative to α.

Theorem 3. *Let $p,q\in N, p<q$ and $\{\alpha_n\}$ be a sequence of irrational numbers converging to $\frac{p}{q}$. And let $u_n\in C^{2k,2}_{x,t}(D)$ be the solution of the problem (1), (2) and $u_n(\alpha\pi,t) = \sin q^k t$, then*

$$\lim_{\to\infty}\|u_n\|_{L_2(D)} = +\infty.$$

The solution is written in the form $u_n(x,t) = \frac{\sin q^k t\cdot\sin qx}{\sin q\alpha_n\pi}$, from which the theorem statement is obvious.

Thus, a side condition is required.

$$\int_0^{\pi}\int_0^{2\pi}\left(\frac{\partial^k u}{\partial x^k}\right)^2 dtdx \le E^2.$$

Problem with a bounded solution

Let α,ε,E be some positive constants, and $\alpha\in(0,1)$.

Let $f\in L_2(0,2\pi)$. The function class $u\in C^{2k,2}_{x,t}(D)$ satisfying (1), (2) and

$$\|u(\alpha\pi,\cdot) - f\|_{L_2(0,2\pi)} \le \varepsilon, \tag{9}$$

$$\left\|\frac{\partial^k u}{\partial x^k}\right\|_{L_2(D)} \le E. \tag{10}$$

is indicated by $\Gamma(\varepsilon,E)$. The condition (9) substitutes the condition (3), and the priori estimate (10) is required for the problem to be well-posed.

We introduce the following notations

$$\|u\|^2 = \sup_{x\in[0,\pi]}\int_0^{2\pi} u^2(x,t)dt, \tag{11}$$

$$\Delta(\varepsilon,E) = \sup_{v,w\in\Gamma(\varepsilon,E)}\|v-w\|. \tag{12}$$

Theorem 4. *Let α be a rational number, $\alpha = \frac{p}{q}, (p,q) = 1$ and*

$$q^2 \le 2\frac{E}{\varepsilon} \quad . \tag{13}$$

Then

$$\Delta(\varepsilon, E) \le 3\frac{E}{q^k}. \tag{14}$$

If $q = \left[\left(\frac{2E}{\varepsilon}\right)^{\frac{1}{k}}\right]$, *then*

$$\Delta(\varepsilon, E) \le 3\sqrt{E}\sqrt{\varepsilon}.$$

Proof. Let $v, w \in \Gamma(\varepsilon, E)$, then $u = v - w \in C_{x,t}^{2k,2}(D)$ satisfies (1), (2) and

$$\|u(\alpha\pi, \cdot)\|_{L_2(0,2\pi)} \le 2\varepsilon, \quad \left\|\frac{\partial^k u}{\partial x^k}\right\|_{L_2(D)} \le 2E. \tag{15}$$

Since u is represented as (5), the conditions (15) are rearranged as

$$\sum_{n=1}^{+\infty} (a_n^2 + b_n^2) \sin^2 n\frac{p}{q}\pi \le \frac{4\varepsilon^2}{\pi^2}, \tag{16}$$

$$\sum_{n=1}^{+\infty} n^{2k}(a_n^2 + b_n^2) \le \frac{8E^2}{\pi^2} \quad , \tag{17}$$

whence it follows

$$\sum_{n=1}^{+\infty} \left(\sin^2 n\frac{p}{q}\pi + n^{2k}\frac{\varepsilon^2}{E^2}\right)(a_n^2 + b_n^2) \le \frac{8\varepsilon^2}{\pi}. \tag{18}$$

From (5) we have

$$\|u\|^2 = \pi \max_{x\in[0,\pi]} \sum_{n=1}^{+\infty} (a_n^2 + b_n^2) \sin^2 nx \le \pi \sum_{n=1}^{+\infty} (a_n^2 + b_n^2).$$

It follows from (12)

$$\Delta^2(\varepsilon, E) \le \pi \sup\left\{\sum_{n=1}^{+\infty} (a_n^2 + b_n^2) : a_n, b_n\right\},$$

satisfying (18).

According to the Lagrange multiplier role we find

$$\Delta^2(\varepsilon, E) \le 8\varepsilon^2 \min(\sin^2 r\frac{p}{q}\pi + r^{2k}\frac{\varepsilon^2}{E^2})^{-1}, \quad r \in N. \tag{19}$$

From (13) we obtain

$$\sin^2 r\frac{p}{q}\pi + r^{2k}\frac{\varepsilon^2}{E^2} \ge \frac{\varepsilon^2}{E^2}q^{2k}, \quad 1 \le r \le q.$$

Substituting this estimation into (19) we obtain (14). The theorem has been proved. □

Assume that α is an irrational number expanded into a continued fraction

$$\alpha = \frac{1}{\alpha_1 + \frac{1}{\alpha_2 + \ldots}} \quad .$$

Theorem 5. *Let* $\alpha \in (0,1)$ *be an irrational number and* $\alpha_i \leq K_\alpha$, *then*

$$\Delta(\varepsilon, E) \leq 3\left(\frac{K_\alpha + 2}{2}\varepsilon E\right)^{\frac{1}{2}}. \tag{20}$$

Proof. To make sure that this estimation is valid, note that it follows from the theorem 4 that the estimation (19) is true for $\Delta(\varepsilon, E)$ then from the condition $\alpha_i \leq K_\alpha$ [3] we obtain

$$\sin^2 r\alpha\pi \geq \frac{27}{4(K_\alpha + 2)^2 r^2},\ r \geq 1.$$

Then

$$\min_{r \in N}\left\{\frac{27}{4(K_\alpha + 2)^2 r^2} + r^{2k}\frac{\varepsilon^2}{E^2}\right\} \geq \frac{\varepsilon}{E}\frac{\sqrt{27}}{(K_\alpha + 2)}.$$

Thus, the required estimation follows from the above

$$\Delta^2(\varepsilon, E) \leq 9\varepsilon E\left(\frac{K_\alpha + 2}{2}\right).$$

□

References

1. Frosali G. Papi. On the stability of the Dirichlet problem for the vibrating string equation. Ann. Scuola Norm. Sup. Pisa, 1979, vol. 6, pp. 719-728.

2. Yuldasheva A.V. Ob odnoj zadache dlya uravneniya vysokogo poryadka [A problem for the equation of high order]. *Doklady Akademii nauk Respubliki Uzbekistan – Reports of the Academy of Sciences of the Republic of Uzbekistan*, 2012, no. 5, pp. 11-14.

3. Hinchin A.Ya. *Cepnye drobi* [Continued fractions]. Leningrad, 1961. 112 p.

Original article submitted: 23.10.2014

Bulletin KRASEC. Phys. & Math. Sci, 2014, vol. , no. 2, pp. 23-26. ISSN 2313-0156

MATHEMATICS

MSC 18A32

FINITE GENERATED SUBGROUPS OF HYPERBOLIC GROUPS

A.P. Goryushkin

Vitus Bering Kamchatka State University, 683031, Petropavlovsk-Kamchatsky, Pogranichnaya st., 4, Russia

E-mail: as2021@mail.ru

It is proved that finite generated subgroups of infinite index of hyperbolic groups which are not quasi Abelian are complemented with a nontrivial free factor.

Key words: hyperbolic group, free product, free product with amalgamation, set of generators, index of a subgroup, normal subgroup

A subgroup H of a group G is called freely complemented if there is a nontrivial subgroup Q in G so that a subgroup generated by the subgroups H and Q is their free product: $gp(H,Q) = H * Q$. It is clear that the subgroups of a finite group or an Abelian group can not be freely complemented. The same applies to the subgroups of a quasi-Abelian group, for example, a infinite dihedral group. The aim of this paper is to show that in a hyperbolic group which is not quasi-abelian and which is given by the representation:

$$G =< a_1, b_1, \ldots, a_n,\ b_n,\ c_1, \ldots, c_t,\ d_1, \ldots, d_s; \tag{1}$$
$$c_1^{\gamma_1}, \ldots, c_t^{\gamma_t}, [a_1,\ b_1]\ \ldots\ [a_n, b_n] c_1\ \ldots\ c_t, d_1\ \ldots\ d_s >,$$

where $[a_i, b_i] = a_i^{-1} b_i^{-1} a_i b_i; n, s, t \geq 0; \gamma_i > 1$ – any finitely generated nontrivial subgroup of a infinite index is freely complemented.

Theorem. *Assume that G is a discrete group of orientation-preserving motions of the hyperbolic plane, G is not quasi-Abelian and G is not isomorphic to any group which has the representation:*

$$< a_1,\ b_1,\ \ldots,\ a_n,\ b_n;\ ([a_1,\ b_1]\ \ldots\ [a_n,\ b_n])^k\ > < a,\ b;\ a^n, b^m (ab)^k\ >,$$

where $k > 1$ and H is the finitely generated subgroup of G. Then G has a infinitely generated subgroup Q such that the subgroup generated by the subgroups H and Q is the free product of $H * Q$.

The proof is based on the following lemma of subgroups of a free product with amalgamation.

Lemma. *Let G be a free product of two groups A and B with an amalgamated subgroup U where one of the factors is a nontrivial free product, other than the*

Goryushkin Alexander Petrovich – Ph.D. (Phys. & Math.), Professor Dept. of Mathematics & Physics, Vitus Bering Kamchatka State University.

dihedral group, the subgroup U satisfies the maximum condition for subgroups and H is the finitely generated subgroup of a infinite index in G. Then G has an infinitely generated subgroup Q such that the subgroup generated by the subgroups H and Q is the free product of $H * Q$.

Proof. Let $G = A \underset{U}{*} B$ satisfy the condition of the theorem and H is the finitely generated subgroup of a infinite index in G. Subgroup U index in group A is infinite so if H is in conjunction of the subgroup U then H has an infinite index in group A. The finitely generated subgroup of an infinite index in a free product, other than the infinite dihedral group, has the property of free complementarity (see. [1]). Moreover, the complementary factor contains a free group of rank two and therefore we can consider it to be a free group of the countable rank from the beginning.

So, we can assume that H is not in conjugation of U. Moreover, the infinite decomposition in terms of double modulus $[G\colon (H, U)]$ follows from the infiniteness of the index $[G\colon H]$. It follows from the theorem 1.7 in [2] that the index $[A\colon (U, U)]$ is infinite.

Hereafter we shall use the notations from [3].

Let S be a set of elements of the group $A \underset{U}{*} B$, and the canonical form of the element s from S has the following form

$$s = s_{1(s)} g_{2(s)} \ \cdots \ g_{n(s)}.$$

We define the set $\bar{t}_X(S)$, depending on S and on $X (X = A$ or $X = B)$ according to the next rule:

$$\bar{t}_X(S) = \left\{ x \in X \ \middle| \ x \equiv g_{n(s)} \bmod (U, U) \, ; \, s \in S \setminus (A \cup B) \right\}.$$

For a suitable element g of G the set $\bar{t}_B(H^g)$ is empty and $\bar{t}_A(H^g) = \{ U a_0 U \}$, where a_0 is any reassigned fixed element of $A \setminus U$.

We can assume that the subgroup H already has this property, that is, the element gy is the identity element and the element a_0 of $A \setminus U$ is chosen so that the subgroup R which is the subgroup generated by U and the element a_0 has an infinite index in the subgroup A.

For each element d from $D = A \cap H$ and each element t from $\bar{t}_A(H)$ the product td belongs to the $\bar{t}_A(H)$ again which equals $U a_0 U$ by assumption.

In other words, every element d of D can be represented in the form

$$d = u_1 a_0^{-1} u_2 a_0 u_3,$$

where – u_1, u_2, u_3 are suitable elements of the amalgamated subgroup U.

Therefore D is contained in R. According to the theorem 1.8 from [3], there exists an infinite subgroup Q of A that $gp(R, Q) = R * Q$. Now we shall show that the subgroup $\bar{H}$ which is generated by subgroups H and Q is their free product $H * Q$. In order to do this, we need to prove that the element p of H which is the product of

$$p = p_1 p_2 \ \cdots \ p_n, \tag{2}$$

where $n \geq 1$ and p_i are non-identity elements selected alternatively from the subgroups Q и H, is not identity.

If all of the elements p_i from (1), which are included into H, are simultaneously the elements of A (that is they belong to the intersection D) then the element p belongs to

the free product of $Q * D$ and (2) is a normal form of the element p with respect to the decomposition of $Q * D$.

Therefore, we can assume that not all of p_i from the expansion (2) are the elements of A. Then, instead of (2) we consider other decomposition of p which can be obtained from (2) with some grouping factors p_i:

$$p = q_1 q_2 \ \dots \ q_k, \tag{3}$$

where $1 \leq k < n$,. Specifically, the element q_j is some p_i if $p_i \in H \setminus A$. Otherwise, q_j is the product

$$p \ = \ p_\alpha \ p_{\alpha+1} \ \dots \ p_\beta,$$

where $1 \leq \alpha < \beta \leq n$ and all the factors p_α, $p_{\alpha+1}$, ..., p_β belong to the factor A but the element $p_{\alpha-1}$ (in the case when $\alpha > 1$) and the element $p_{\beta+1}$ (in the case when $\beta < n$) do not belong to A.

Thus, in the expansion (3) the factors are selected by turns from $H \setminus A$ and the free product of $Q * R$. In this case, if q_j is the element of $Q * R$ then it is not included into the free factor R. It means that for each element r_1, r_2 from R the product of $r_1 q_{j_0} r_2$ does not belong to the subgroup R.

On the other hand, if $h \in H \setminus A$ and $h = h_1 h_2 \ \dots \ h_m$ is its canonical form then from $\bar{t}_A(H) \subseteq R$ we have that $h_m \in A$ implies $h_m \in R$ (and $h_1 \in A$ implies $h_1 \in R$)).

Hence, the canonical form of the element p has at least k syllables. But this means that the element p is not equal to unity and, thus, the subgroup H_2 is the free product of $H * Q$.

The lemma is proved.

We proceed now to the proof of the theorem.

If in the group with the representation (1) the parameter $s >$ then G is a free product of cyclic groups of the second order (and the infinite dihedral group is quasi-Abelian).

If $s > \ = 0$ then the representation (1) becomes a representation of the form

$$G = < a_1, \ b_1, \ \dots, \ a_n, \ b_n, \ c_1, \ \dots, \ c_t; c_1^{\gamma_1}, \dots, \ c_t^{\gamma_t}, [a_1, \ b_1] \ \dots \ [a_n, \ b_n] c_1 \dots_t >,$$

Now, if $n > 0$ and $t > 1$ then the group G can be represented as follows

$$G = gp(a_1, \ b_1, \ \dots, \ a_n, \ b_n) \underset{U}{*} gp(c_1, \ \dots, \ c_t),$$

where $U = gp([a_1, \ b_1] \ \dots \ [a_n, \ b_n]) = gp(c_t^{-1} c_{t-1}^{-1} \dots c_1^{-1})$.

The same is in the cases when $n > 1$ и $t = 0$ and when $n = 0$, $t > 3$.

In the latter case it may turn out that G is a free product of two dihedral groups with an amalgamated cyclic subgroup:

$$G = < c_1, \ c_2, \ c_3, \ c_4, \ c_1^2, c_2^2, c_3^2, c_4^2, \ c_1 c_2 c_3 c_4 > .$$

Then the group G is quasi-Abelian again. Generated by the element $c_1 c_2 (c_{13})^2$ the cyclic subgroup has the finite index in G indeed. If $s = n = 0$, $t \leq 2$, then the group G is finite. Thus, all hyperbolic groups, except for the cases with $s = 0, n > 0, t = 1$ or $s = 0, n = 0, t = 3$ in the representation (1), satisfy the conditions of the lemma. The theorem is proved. □

We should note that in the paper [4], the necessary and sufficient conditions for the existence of free complementarity for quasi-convex subgroups of an infinite index in a hyperbolic group were obtained by other methods.

References

1. Goryushkin A.P. O konechno porozhdennyh podgruppah svobodnogo proizvedeniya dvuh grupp s ob'edinennoj podgruppoj [About finitely generated subgroups of a free product of two groups with amalgamation]. *Uchenye zapiski Ivanovskogo pedagogicheskogo instituta– Scientific notes Ivanovo Pedagogical Institute*, 1972, no. 117, pp. 11–43.

2. Goryushkin A.P. *Gruppy, razlozhimye v svobodnoe proizvedenie (stroenie i primenenie)*[Groups decomposable into a free product (structure and application)]. Saarbryukken Pal. Acad. Publ., 2012. 142 p.

3. Goryushkin A.P. O podgruppah pochti amal'gamirovannogo proizvedeniya dvuh grupp s konechnoj ob'edinennoj podgruppoj [Subgroups almost amalgamated product of two groups with the ultimate amalgamation]. *Vestnik KRAUNC. Fiziko-matematicheskie nauki – Bulletin of the Kamchatka Regional Association «Education-Scientific Center». Physical & Mathematical Sciences*, 2012, vol. 4, no. 1, pp. 5–10.

4. Dudkin F.A., Sviridov K.S. Dopolnenie podgruppy giperbolicheskoj gruppy svobodnym mnozhitelem [Supplement subgroup of a hyperbolic group free multiplier]. *Algebra i logika – Algebra and Logic*, 2013, vol. 52, no. 3, pp. 332–351.

Original article submitted: 02.09.2014

Bulletin KRASEC. Phys. & Math. Sci, 2014, vol. , no. 2, pp. 27-33. ISSN 2313-0156

MATHEMATICAL MODELLING

MSC 35C05

MODELING INVERSIONS WITHIN LOW-MODE MODEL OF LARGE-SCALE DYNAMO

G.M. Vodinchar[1, 2], A.N. Godomskaya[1], O.V. Sheremetyeva[1, 2]

[1] Institute of Cosmophysical Researches and Radio Wave Propagation Far-Eastern Branch, Russian Academy of Sciences, 684034, Kamchatskiy Kray, Paratunka, Mirnaya st., 7, Russia

[2] Vitus Bering Kamchatka State University, 683031, Petropavlovsk-Kamchatsky, Pogranichnaya st., 4, Russia

E-mail: gvodinchar@ikir.ru, anna_antonenko@mail.ru, olga.v.sheremetyeva@gmail.com

In this paper we investigate the question of the possibility of inversions within the low-mode dynamo model. The conditions under which the possibility of more frequent reversal of the magnetic field in comparison with inversions in the velocity field of a viscous conducting magnetized fluid.

Key words: low-mode model, the Galerkin method, magnetic inversion

Introduction

The movement of incompressible viscous conductive magnetized fluid is considered in the coordinate system rotating with constant angular velocity Ω around Oz axis and placed in external force field with mass density $\mathbf{f}$. The fluid physical parameters are considered to be constant. Magnetohydrodynamic (MHD) equations include Navier-Stokes equation, induction equation for the magnetic field $\mathbf{B}$, continuity equation and solenoidal field $\mathbf{B}$:

$$\begin{cases} \dfrac{\partial \mathbf{v}}{\partial t} + (\mathbf{v}\nabla)\,\mathbf{v} + 2\Omega \times \mathbf{v} + \Omega \times (\Omega \times \mathbf{r}) = \nu \Delta \mathbf{v} - \dfrac{1}{\rho}\nabla P + \dfrac{1}{\rho\mu}(\nabla \times \mathbf{B}) \times \mathbf{B} + \mathbf{f}, \\ \dfrac{\partial \mathbf{B}}{\partial t} = \nabla \times (\mathbf{v} \times \mathbf{B}) + \nu_m \triangle \mathbf{B}, \\ \nabla \mathbf{v} = \nabla \mathbf{B} = 0, \end{cases} \tag{1}$$

Vodinchar Gleb Mikhailovich – Ph.D. (Phys. & Math.), Head of Lab. Modeling of physical processes, Institute of Cosmophysical Researches and Radio Wave Propagation FEB RAS, Associate Professor, Dept. Mathematics & Physics, Vitus Bering Kamchatka State University. *Godimskaya Anna Nikolaevna* – Postgraduate Student, Institute of Cosmophysical Researches and Radio Wave Propagation FEB RAS. *Sheremetyeva Olga Vladimirovna* – Ph.D. (Tech.), Researcher of Lab. Modeling of physical processes, Institute of Cosmophysical Researches and Radio Wave Propagation FEB RAS., Associate Professor, Dept. of Mathematics and Physics, Vitus Bering Kamchatka State University.

where $\mathbf{v}$ is the velocit, P is the pressure, $\mathbf{r}$ is the radius-vector, ρ is the density, ν is the cinematic viscosity, ν_m is the magnetic viscosity, μ is the magnetic permeability.

Since during the constant angular velocity Ω the centrifugal force acceleration can be presented in the form $\Omega \times (\Omega \times \mathbf{r}) = -\frac{1}{2}\nabla(\Omega \times \mathbf{r})^2$, then it may be joint with the pressure into one potential summand $\frac{1}{\rho}\nabla p'$, where the reduced pressure will be given by the following expression $p' = p + \frac{1}{2}\rho\nabla(\Omega \times \mathbf{r})^2$.

Let us introduce the following values of velocity U, linear dimensions of region L, time L/U, pressure ρU^2, magnetic induction $L\sqrt{\rho\mu}/U$. Then, in dimensionless variables the system (1) will have the form:

$$\begin{cases} \dfrac{\partial \mathbf{v}}{\partial t} + (\mathbf{v}\nabla)\mathbf{v} = \mathrm{R}^{-1}\Delta\mathbf{v} - \nabla p' - 2\varepsilon^{-1}(\mathbf{e}_z \times \mathbf{v}) + (\nabla \times \mathbf{B}) \times \mathbf{B} + \mathbf{f}, \\ \dfrac{\partial \mathbf{B}}{\partial t} = \nabla \times (\mathbf{v} \times \mathbf{B}) + \mathrm{R}_m^{-1} \triangle \mathbf{B}, \\ \nabla\mathbf{v} = \nabla\mathbf{B} = 0, \end{cases} \tag{2}$$

where the dimensionless parameters $R = UL/\nu$ is the Rynolds number, $\varepsilon = U/(\Omega L)$ is the Rossby number, $R_m = UL/\nu_m$ is the Rynolds magnetic number.

The system (2) must be supplemented by boundary conditions for the velocity and magnetic field. The type of boundary conditions is not significant for this paper, so they are not specified. These conditions are assumed to be linear and homogeneous.

One of the approaches to study the system (2) s the construction of Galerkin type few-mode approximations [1]. It should be noted that different versions of dynamo mechanism have the common fact that the source for the field $\mathbf{B}$ toroidal (poloidal) component is the interaction of the poloidal (toroidal) component of the same field with a liquid flow [5, 4]. Thus, it is assumed that the limit possible truncation, maintaining dynamo, is the case with three modes – hydrodynamic, toroidal magnetic, and poloidal magnetic ones.

Let us consider the problem of the choice of a single hydrodynamic mode. If the representation $\mathbf{v}(\mathbf{r},t) = u(t)\mathbf{v}_0(\mathbf{r})$ is used for velocity field and Galerkin approximation for the first equation is derived from the system (2), then the Coriolis approximation term is equal to zero

$$\varepsilon^{-1}u(t)\int (\mathbf{e}_z \times \mathbf{v_0})\,\mathbf{v_0}\,dV = 0.$$

Thus, information on fluid volume rotation vanishes from the obtained approximation. Owing to this fact, the authors think that the only way to keep the information on the rotation in a velocity single-mode approximation is to use one of the eigen modes of viscous rotating fluid free vibration as the mode. Than the information on the rotation will be included into the streamline form of the considered mode and imaginary component of its eigen value. The real part of this eigen value will determine the time of mode viscous dissipation.

For the chosen nondimensionalization technique such methods are determined from the solution of a spectral problem

$$\begin{aligned} &\Lambda\mathrm{R}^{-1}\mathbf{v} + \mathrm{R}^{-1}\Delta\mathbf{v} - \nabla p' - 2\varepsilon^{-1}(\mathbf{e}_z \times \mathbf{v}) = \mathbf{0}, \\ &\nabla\mathbf{v} = 0. \end{aligned} \tag{3}$$

This spectral problem must be closed by the same boundary conditions for the velocity as the system (2) is.

From the mathematical point of view, the summand $\nabla p'$ in this problem is the projector of the divergence field $2\varepsilon^{-1}(\mathbf{e}_z \times \mathbf{v})$ into solenoidal field space. It is also clear that the problem is a one-parametric one, and is determined by the ratio R/ε – the Coriolis number (Ekman reciprocal number).

As long as the spectrum of the problem (3) s complex, the eigen modes are also complex fields. Thus, in the construction of a few-mode approximation, there is a necessity to consider velocity complex modes and their complex amplitudes. We should also note that if the pare $(\Lambda_0, \mathbf{v}_0)$ is one of the problem (3)solutions, then the pair $(\Lambda_0^*, \mathbf{v}_0^*)$ will also be the solution for it. Hereafter the asterisk $(*)$ denotes complex conjugation. To present the magnetic field, real modes and their amplitudes are used. Thus, the following presentations of real fields are used in the problem (2):

$$\begin{aligned} \mathbf{v}(\mathbf{r},t) &= u(t)\mathbf{v}_0(\mathbf{r}) + u^*(t)\mathbf{v}_0^*(\mathbf{r}), \\ \mathbf{B}(\mathbf{r},t) &= B_1(t)\mathbf{b}_1(\mathbf{r}) + B_2(t)\mathbf{b}_2(\mathbf{r}), \end{aligned} \tag{4}$$

where $\mathbf{b}_1(\mathbf{r})$ and $\mathbf{b}_2(\mathbf{r})$ are some toroidal and poloidal magnetic modes, correspondingly.

Let us introduce a scalar product of complex vector fields by the formula

$$\langle \mathbf{p}, \mathbf{q} \rangle = \int_D \mathbf{p}\mathbf{q}^* dV,$$

where integration is made by region D volume. We shall further believe that all the considered modes are normalized in terms of the norm of this scalar product.

Galerkin approximation for the system (2), applying the expansion (4), has the form

$$\begin{cases} \dfrac{du}{dt} = C_{11}u^2 + C_{12}uu^* + C_{22}u^{*2} - \mathrm{R}^{-1}\Lambda_0 u + L_{11}B_1^2 + L_{12}B_1B_2 + L_{22}B_2^2 + F, \\ \dfrac{dB_1}{dt} = W_{11}uB_1 + W_{11}^*u^*B_1 + W_{12}uB_2 + W_{12}^*u^*B_2 - \mathrm{R}_m^{-1}\mu_1 B_1, \\ \dfrac{dB_2}{dt} = W_{21}uB_1 + W_{21}^*u^*B_1 + W_{22}uB_2 + W_{22}^*u^*B_2 - \mathrm{R}_m^{-1}\mu_2 B_2, \end{cases} \tag{5}$$

where C_{ij}, L_{ij}, F, W_{ij}, μ_i coefficients are generally complex numbers which are the following scalar products of vector fields:

$$\begin{aligned} C_{11} &= -\langle (\mathbf{v}_0\nabla)\mathbf{v}_0, \mathbf{v}_0 \rangle, \\ C_{12} &= -\langle (\mathbf{v}_0\nabla)\mathbf{v}_0^*, \mathbf{v}_0 \rangle - \langle (\mathbf{v}_0^*\nabla)\mathbf{v}_0, \mathbf{v}_0 \rangle, \\ C_{22} &= -\langle (\mathbf{v}_0^*\nabla)\mathbf{v}_0^*, \mathbf{v}_0 \rangle, \\ L_{11} &= \langle (\nabla \times \mathbf{b}_1)\mathbf{b}_1, \mathbf{v}_0 \rangle, \\ L_{12} &= \langle (\nabla \times \mathbf{b}_1)\mathbf{b}_2, \mathbf{v}_0 \rangle + \langle (\nabla \times \mathbf{b}_2)\mathbf{b}_1, \mathbf{v}_0 \rangle, \\ L_{22} &= \langle (\nabla \times \mathbf{b}_2)\mathbf{b}_2, \mathbf{v}_0 \rangle, \\ F &= \langle \mathbf{f}, \mathbf{v}_0 \rangle, \\ W_{ij} &= \langle \nabla \times (\mathbf{v}_0 \times \mathbf{b}_j), \mathbf{b}_i \rangle, \\ \mu_1 &= -\langle \Delta\mathbf{b}_T, \mathbf{b}_T \rangle > 0, \quad \mu_2 = -\langle \Delta\mathbf{b}_P, \mathbf{b}_P \rangle > 0, \end{aligned} \tag{6}$$

Developing the system (5) we considered [3], that toroidal and poloidal field spaces are invariant relatively the Laplace operator, toroidal and poloidal field orthogonality as well as Laplace operator positiveness.

The magnetic modes are assumed to ensure mutual generation of each other not generating themselves. Mathematically it means that coefficients $W_{ii} = 0$, and then the equation (5) take on the form:

$$\begin{cases} \dfrac{du}{dt} = C_{11}u^2 + C_{12}uu^* + C_{22}u^{*2} - \mathrm{R}^{-1}\Lambda_0 u + L_{11}B_1^2 + L_{12}B_1B_2 + L_{22}B_2^2 + F, \\ \dfrac{dB_1}{dt} = (W_{12}u + W_{12}^*u^*)B_2 - \mathrm{R}_m^{-1}\mu_1 B_1, \\ \dfrac{dB_2}{dt} = (W_{21}u + W_{21}^*u^*)B_1 - \mathrm{R}_m^{-1}\mu_2 B_2, \end{cases} \tag{7}$$

Investigation of MHD equation system in Galerkin type few-mode approximation for the presence of inversions

Inversion in any field under the consideration is expressed in corresponding mode sign change, and the problem on determination of the conditions and parameters, when magnetic field inversion takes place at the background of the absence of any inversions in the velocity field of a viscous incompressible fluid, is reduced to the selection of such coefficients in the system (7), that the mode $B_1(t)$ and $B_2(t)$ sign would change quite frequently at quite long time intervals of mode$u(t)$ and $u^*(t)$ constant sign.

To simplify the transformations in the course of the study, coefficient notation changes $\Lambda = \mathrm{R}^{-1}\Lambda_0$, $\mu_1 = \mathrm{R}_m^{-1}\mu_1$, $\mu_2 = \mathrm{R}_m^{-1}\mu_2$ are introduced into the system (7) and it is written as follows:

$$\begin{cases} \dfrac{du}{dt} = C_{11}u^2 + C_{12}uu^* + C_{22}u^{*2} - \Lambda u + L_{11}B_1^2 + L_{12}B_1B_2 + L_{22}B_2^2 + F, \\ \dfrac{dB_1}{dt} = (W_{12}u + W_{12}^*u^*)B_2 - \mu_1 B_1, \\ \dfrac{dB_2}{dt} = (W_{21}u + W_{21}^*u^*)B_1 - \mu_2 B_2, \end{cases} \tag{8}$$

Let us investigate the parameters of the obtained system (8), when magnetic field inversion is possible in the condition of relative constancy of velocity field.

Knowing the mode $u(t)$ and $u^*(t)$ vales from the differential equation system formed by the two last equations from (8), we determine the conditions when mode $B_1(t)$ and $B_2(t)$ sign change may occur, i.e. the magnetic field inversion:

$$\begin{cases} \dfrac{dB_1}{dt} = (W_{12}u + W_{12}^*u^*)B_2 - \mu_1 B_1, \\ \dfrac{dB_2}{dt} = (W_{21}u + W_{21}^*u^*)B_1 - \mu_2 B_2. \end{cases} \tag{9}$$

In the system (9) oscillations may appear only in the case when the solution has the following form

$$B_i(t) = \alpha_i e^{k_i t}, \; k_i \in \mathbb{C}, \tag{10}$$

where k_i is the complex root of the system (9) characteristic equation:

$$\begin{vmatrix} -\mu_1 - k & W_{12}u + W_{12}^* u^* \\ W_{21}u + W_{21}^* u^* & -\mu_2 - k \end{vmatrix} = 0$$

with negative discriminant

$$D = (\mu_2 - \mu_1)^2 + 16\Re(W_{12}u)\,\Re(W_{21}u) < 0 \tag{11}$$

where

$$\begin{aligned} u &= \Re(u) + i\Im(u), \\ u^* &= \Re(u) - i\Im(u), \\ W_{12} &= \Re(W_{12}) + i\Im(W_{12}), \\ W_{12}^* &= \Re(W_{12}) - i\Im(W_{12}), \\ W_{21} &= \Re(W_{21}) + i\Im(W_{21}), \\ W_{21}^* &= \Re(W_{21}) - i\Im(W_{21}). \end{aligned}$$

On the basis of the condition (11), the range of mode $u(t)$ values on a complex plane is the range limited by a hyperbolic type line with a symmetry center at the beginning of the coordinates. Generally, for any $u(t)$ value from the given range, mode $B_1(t)$ and $B_2(t)$ values may be randomly chosen that follows from the solution (10). Mode $B_1(t)$ and $B_2(t)$values are defined so that the equality $B(t) = \sqrt{B_1^2(t) + B_2^2(t)} = 1$ is satisfied which will allow us to study the mutual change of mode $B_1(t)$ and $B_2(t)$ values as well as the change of amplitude $B(t)$ value.

If the dissipative terms (Λu, $\mu_1 B_1$, $\mu_2 B_2$) and external influence (F) are not taken into the account in the system (8), the process of field mutual generation will be continuous(Fig. 1). Elimination only of external influence from the system (8) depending on parameter values of the equation will result in the process attenuation (Fig.2) or continuous process (Fig.3).

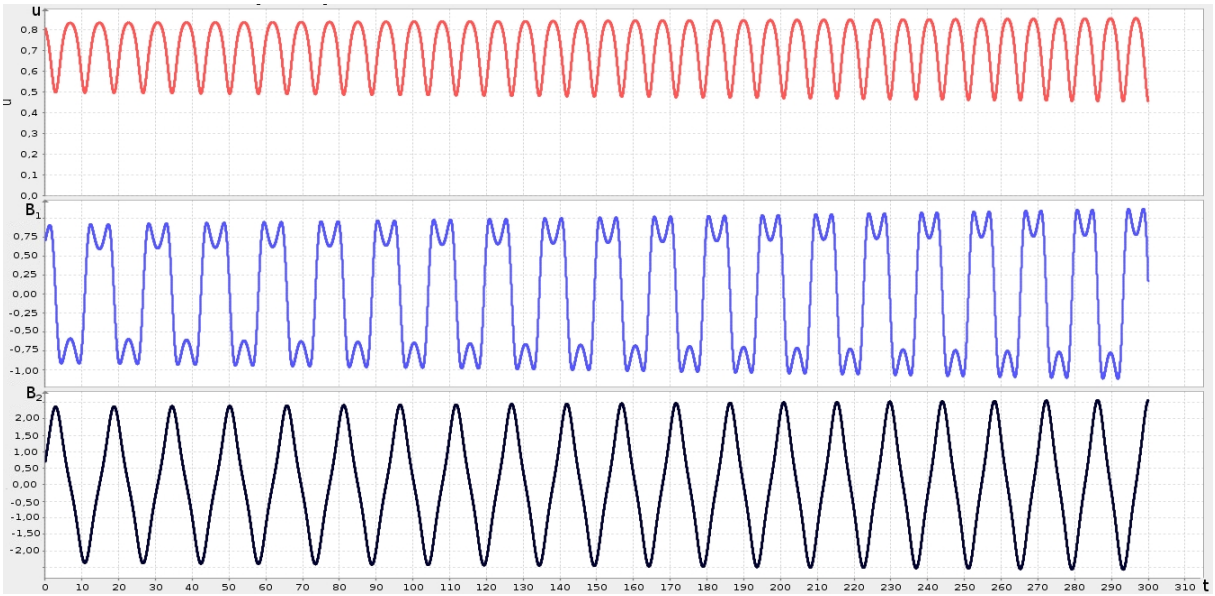

Fig. 1. Visualization of system (8) computational solution without dissipative terms and external influence ($\lambda = 10^{-3}$, $\mu = 4$).

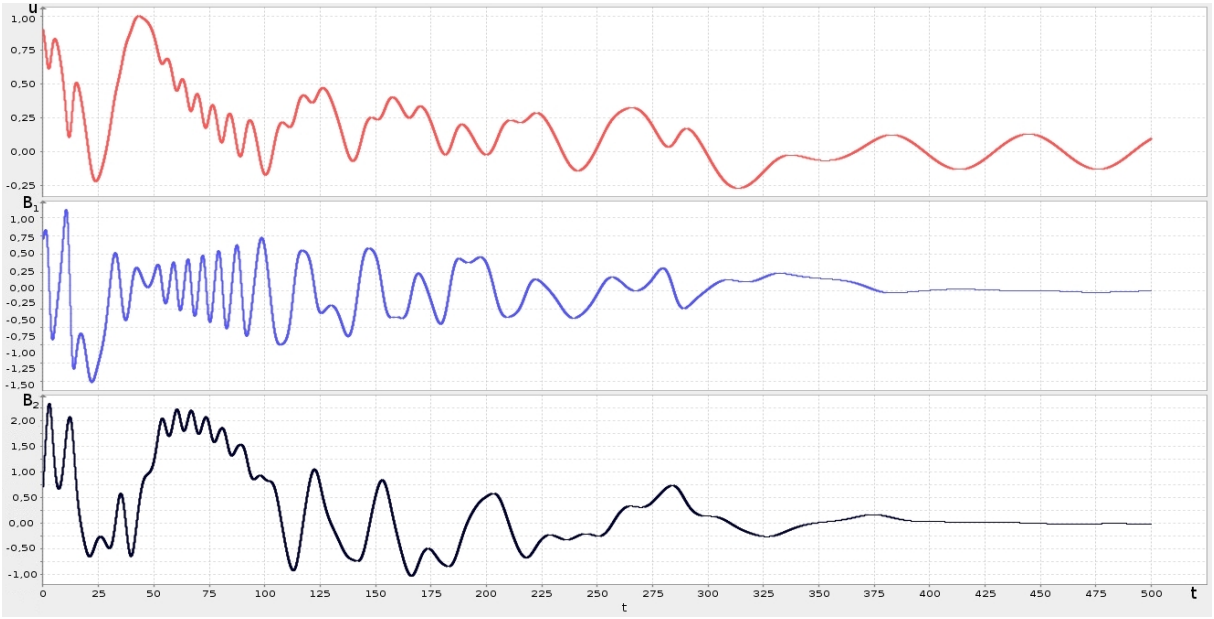

Fig. 2. Visualization of system (8) computational solution without external influence ($\lambda = 10^{-6}$, $\mu = 10^{-2}$).

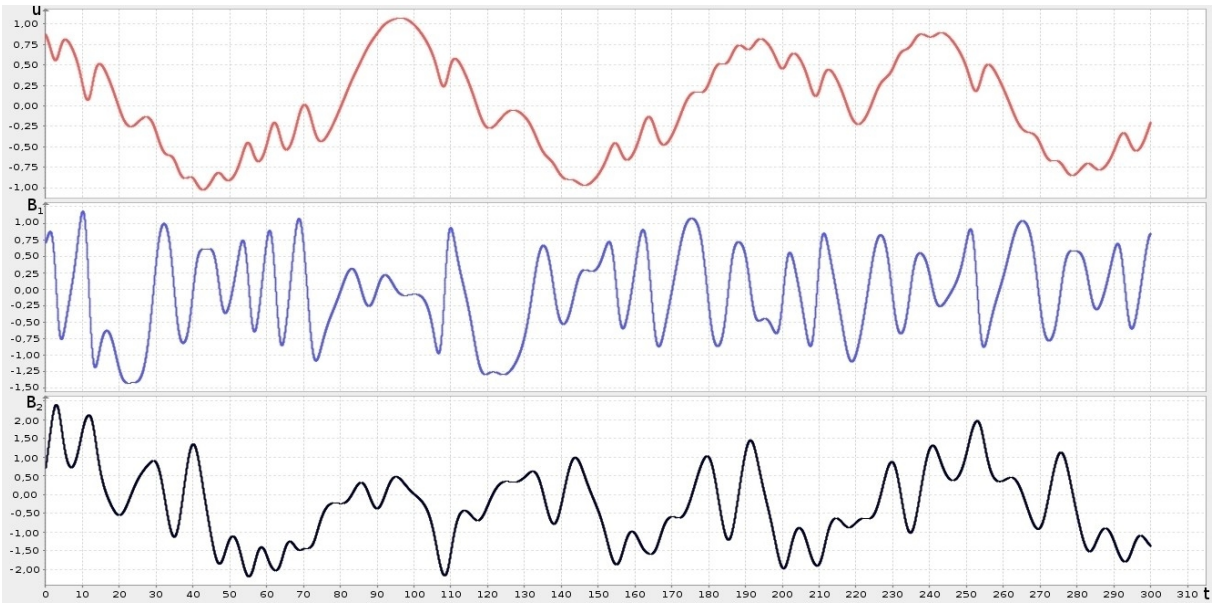

Fig. 3. Visualization of system (8) computational solution without external influence ($\lambda = 10^{-7}$, $\mu = 10^{-3}$).

Conclusions

Galerkin type MGD equation system in the few-mode approximation (8), where the external influence is not taken into the account for different parameter values, contains computational solutions with inversions both in magnetic field and in velocity field of a viscous fluid. There are cases of field attenuation and continuous mutual generation which indicates the adequacy of the description of the Earth core processes within the few-mode model.

References

1. Gledzer E.B., Dolzhanskij F.V., Obuhov A.M. *Sistemy gidrodinamicheskogo tipa i ih primenenie* [Systems of hydrodynamic type and their application]. Moscow, Nauka Publ., 1981. 368 p.

2. Grinspen H. *Teoriya vraschayuschihsya zhidkostej* [The theory of rotating fluids]. Leningrad, Gidrometeoizdat Publ., 1975. 304 p.

3. Chandrasekhar S. Hydrodynamics and Hydromagnetic Stability. Dover Publ. Inc., 1981. 654 p.

4. Krause, F. and Rädler, K.-H. Mean-filed magnetohydrodynamics and dynamo theory. Pergamon Press, 1980.

5. Zeldovich, Ya.B., Rusmaikin, A.A., and Sokoloff, D.D. Magnetic fields in astrophysics. The Fluid Mechanics of Astrophysics and Geophysics. New York, Gordon and Breach, 1983.

Original article submitted: 05.11.2014

Bulletin KRASEC. Phys. & Math. Sci, 2014, vol. , no. 2, pp. 34-38. ISSN 2313-0156

MSC 35C05

NUMERICAL ANALYSIS SOME OSCILLATION EQUATIONS WITH FRACTIONAL ORDER DERIVATIVES

R.I. Parovik[1, 2]

[1] Institute of Cosmophysical Researches and Radio Wave Propagation Far-Eastern Branch, Russian Academy of Sciences, 684034, Kamchatskiy Kray, Paratunka, Mirnaya st., 7, Russia

[2] Vitus Bering Kamchatka State University, 683031, Petropavlovsk-Kamchatsky, Pogranichnaya st., 4, Russia

E-mail: romanparovik@gmail.com

The paper presents a mathematical model of non-classical dynamic systems. A numerical method of difference schemes, depending on various parameters of the system were found numerical solutions of models. The phase trajectory.

Key words: operator Gerasimov-Caputo, numerical solution, finite difference scheme, the phase trajectories

Introduction

Construction of mathematical models, considering fractal properties of different environments, is of great theoretical and practical importance. For example, in a porous geological environment (geo-environment), its fractal dimension, which affects the process intensity, is interesting for the investigation due to the pore inhomogeneity and complicated topology. These processes are generally called non-local ones or the process with memory [1].

Non-local processes are described by mathematical modeling, by differential equations of fraction orders. Derivative fraction orders are closely associated with environment fractal dimension [2], and their functional dependence may be determined experimentally.

Environment fractal dimension may change depending on time and spatial value. Thus, fraction derivative order is, generally, some function on time and spatial value, and, consequently, it significantly complicates the equations describing non-local processes. Solutions of such equations are found by numerical methods which may be implemented in different computer software tools [3].

Parovik Roman Ivanovich – Ph.D. (Phys. & Math.), Dean of the Faculty Physics and Mathematics, Vitus Bering Kamchatka State University, Senior Researcher of Lab. Modeling of Physical Processes, Institute of Cosmophysical Researches and Radio Wave Propagation FEB RAS.

Definition of the problem

It is necessary to find the bias function $u(t)$ Investigation of oscillations in a fractal environment will be carried out according to the following equation of the variable fraction order:

$$\partial_{0t}^{\alpha(t)} u(\eta) + A(t)\,u(t) = 0,\ u(0) = u_0,\ u'(0) = 0, \quad 1 < \alpha(t) < 2, 0 < t < T, \tag{1}$$

where $\partial_{0t}^{\alpha(t)} u(\eta) = \dfrac{1}{\Gamma(2-\alpha(t))} \int\limits_0^t \dfrac{u''(\eta)\,d\eta}{(t-\eta)^{\alpha(t)-1}}$ is the Gerasimov-Caputo fraction order derivative, $A(t)$ is some function, u_0 is the known value.

The dynamic system (1) when $\alpha(t) = \alpha - const$ may have, for example, one of the following forms:

1) The equation (1) when $A(t) = \omega^{\alpha}$ transforms into the fractal oscillator equation [4] and in terms of Gerasimov-Caputo fractional differentiation operator [5].

2) In the case when in the equation (1), the relation $A(t) = a + b\cos(\omega t)$ is satisfied, we come to the equation of fractal parametric oscillator [6]-[7].

3) If (1) is put into the equation $A(t) = t$, we come to the equation of Airy fractal oscillations [8].

In a more general case, when $\alpha = \alpha(t)$, the equation (1) may be solved by the finite difference method. We introduce τ as a sample spacing, and $t_j = j\tau$, $j = 1,2,..,N$, $N\tau = T$, $u(j\tau) = u_k$. Then fraction order derivative in the equation (1) may be approximated as follows [3]

$$\partial_{0t}^{\alpha(t)} u(\eta) = \frac{\tau^{-\alpha_j}}{\Gamma(3-\alpha_j)} \sum_{k=0}^{j-1} \left[(k+1)^{2-\alpha_j} - k^{2-\alpha_j}\right] \left(u_{j-k+1} - 2u_{j-k} + u_{j-k-1}\right). \tag{2}$$

Substituting the formula (2) into the equation (1) and after some transformations we obtain a clear difference scheme:

$$u_{j+1} = \left[2 - A_j/B_j\right] u_j - u_{j-1} - \sum_{k=1}^{j-1} b_k \left(u_{j-k+1} - 2u_{j-k} + u_{j-k-1}\right), \tag{3}$$

where $b_k = (k+1)^{2-\alpha_j} - k^{2-\alpha_j}$, $B_j = \dfrac{\tau^{-\alpha_j}}{\Gamma(3-\alpha_j)}$, $u_1 = u_0$.

Numerical modeling

For simplicity, assume $u_0 = 1$. Consider some dynamic systems according to (1).

1.**Fractal oscillator.** Consider the case $\alpha(t) = \alpha - const$ and $A(t) = A - const$**.** On the basis of Maple system, simulations for (3) and solutions are constructed.

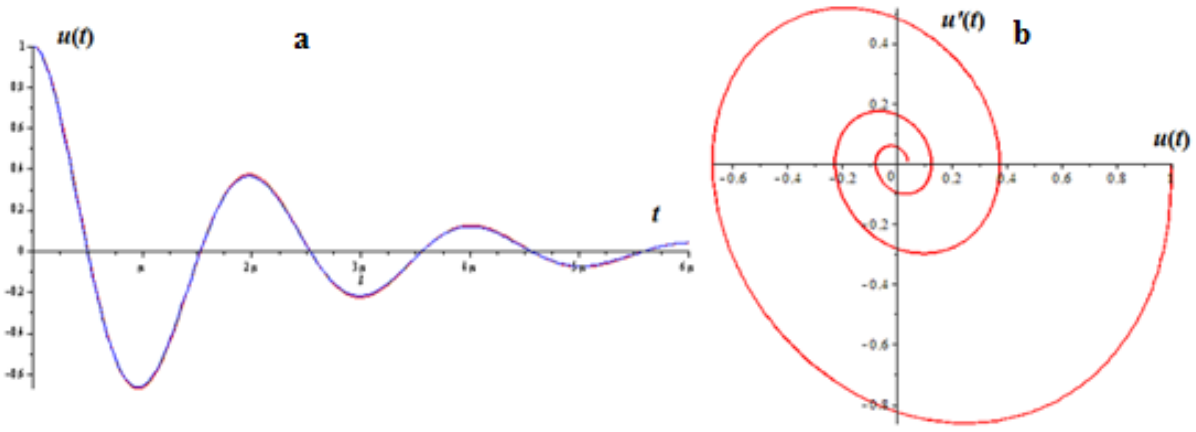

Fig. 1. a) simulations calculated by the formula (3) (red line) and exact solution – (blue line) for parameter values $A = 1, \alpha = 1.8, t \in [0, 6\pi]$. b) phase trajectory

It is clear from Fig. 1a that the scheme of (3) approximates well the exact solution of (4), and the oscillations attenuate. It is confirmed by the phase trajectory which has a stable focus (Fig. 1b).

2. **Fractal oscillator with the variable parameter α.** Consider the case when in the solution of (3) $\alpha(t) = \dfrac{(1-\varepsilon-\delta)\cos(t\cdot m)+\varepsilon-\delta+3}{2}$ and $A(t) = 1$, where δ and ε determine the range for parameter $\alpha(t)$ change: $1+\varepsilon < \alpha < 2-\delta$, and $\delta+\varepsilon < 1, \delta, \varepsilon \geq 0$, m is the arbitrary number [5].

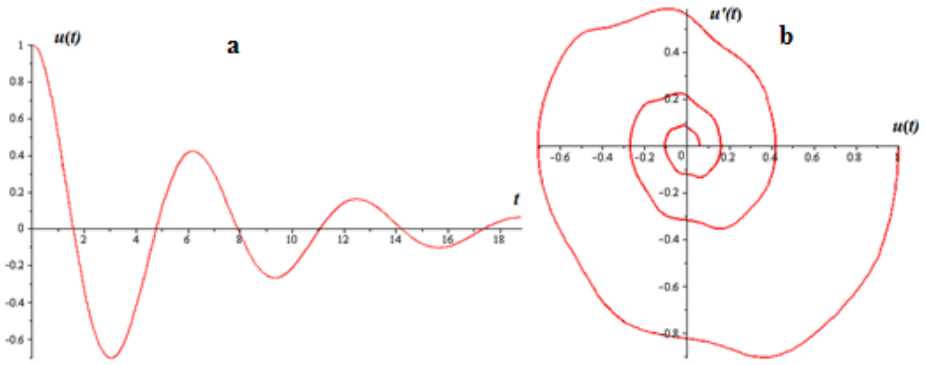

Fig. 2. a) simulation of the equation (1) solution when $\alpha(t) = \dfrac{(1-\varepsilon-\delta)\cos(t\cdot m)+\varepsilon-\delta+3}{2}$; b) phase trajectory

It is clear from Fig. 2a that the oscillation process attenuates, but in comparison to the previous case (Fig. 1b), phase trajectories are deformed (Fig. 2b). This fact indicates that the process attenuates slower in this case.

3. **Airy fractal oscillator.** Consider the case when

$$\alpha(t) = \frac{(1-\varepsilon-\delta)\cos(t\cdot m)+\varepsilon-\delta+3}{2}, A(t) = t.$$

The following parameters were chosen for the problem: $m = 7$, $\varepsilon = 0.69$, $\delta = 0.003$, $a = 1.8$, $\omega = 3$.

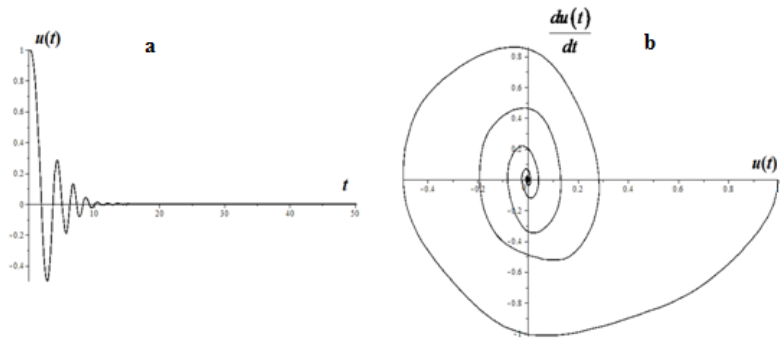

Fig. 3. a) simulation b) phase trajectory

It is clear in Fig. 3a that the oscillation process attenuates fast, and the phase trajectory (Fig. 3b) is bent, but close to a stable focus. Such a behavior of the solution agrees well with the results obtained earlier [7].

When hereditarity properties are taken into the account in the model equation (1), it results in fast dissipation of oscillating system energy and time decrease to its full relaxation.

4. **Fractal parametric oscillator.** Consider the case when $\alpha(t) = \frac{(1-\varepsilon-\delta)\cos(t\cdot m)+\varepsilon-\delta+3}{2}$ and $A(t) = a + b\cos(\omega t)$. The following parameters were chosen for the problem: $m = 7, \quad \varepsilon = 0.69,\ \delta = 0.003,\ a = 1.8,\ \omega = 3.$

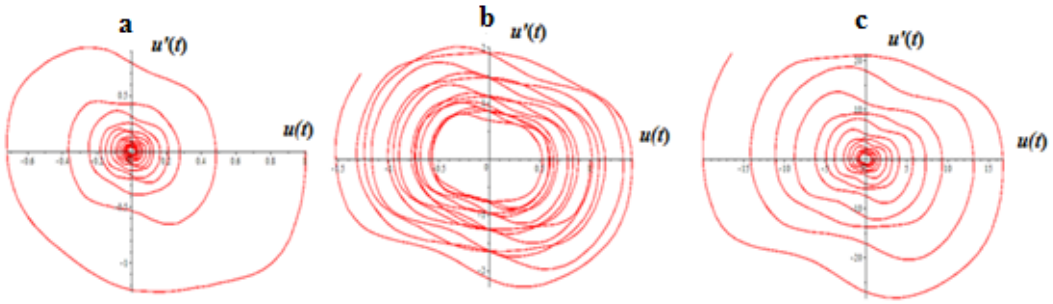

Fig. 4. Phase trajectories a) - $b = 0.9$; b) - $b = 1$; c) - $b = 1.2$

We should note that phase trajectories in Fig. 4 confirm the possibility of application of fractional calculus in the description of non-linear effects. Actually, the phase trajectory in Fig. 4a twists clockwise, and a singular point is a stable focus.

In Fig. 4b, phase pattern changes; first, the trajectory twists clockwise, and then it untwists from some moment of time. Culmination of such a transition is the phase trajectory in Fig. 4c, on which it is clear that the phase trajectory untwists, i.e. it is an unstable focus.

5. **Generalized fractal parametric oscillator.** Consider the case when $\alpha(t) = \frac{(1-\varepsilon-\delta)\cos(t\cdot m)+\varepsilon-\delta+3}{2}$ and $A(t) = a + b\cos_\beta(\omega t),\ \cos_\beta(\omega t) = E_{\beta,1}\left[-(\omega t)^\beta\right] = \sum_{k=0}^{\infty} \frac{(-1)^k (t\omega)^{\beta k}}{\Gamma(\beta k+1)}$ is Mittag-Leffler type function. The following parameters were chosen for the problem: $m = 7, \quad \varepsilon = 0.69,\ \delta = 0.003,\ a = 1.8,\ \omega = 3,\ \beta = 1.2.$

It is clear in Fig. 5 how the phase pattern changes in comparison to other cases. Besides the non-linear effects as in case 4, phase trajectory compresses significantly.

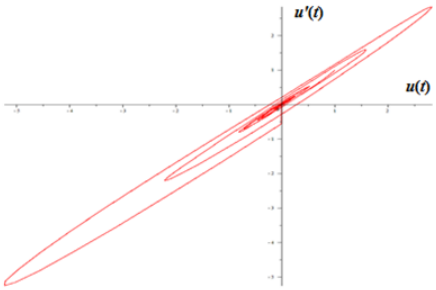

Fig. 5. Phase trajectory (case 5)

Conclusions

We should note, that in contrast to the paper [5], phase trajectories in this paper are built in plane $[u(t), u'(t)]$, not in plane $[u(t), \partial_{0t}^{\alpha-1} u(\eta)]$. That is why we do not observe here the effects associated with multiple reversal point in the center of phase plane.

The paper was carried out within the Project №12-I-OFN-16 "Fundamental problems of powerful radio wave effect on the Earth atmosphere and plasmasphere" and the Program of strategic development of V.Bering Kamchatka State University for 2012-2016 supported by the Ministry of Education and Science of the Russian Federation.

References

1. Nahushev A.M. *Drobnoe ischislenie i ego prilozhenie* [Fractional calculus and its application]. Moscow, Fizmatlit Publ., 2003. 272 p.

2. Shogenov V.H., Ahkubekov A.A., Ahkubekov R.A. Metod drobnogo differencirovaniya v teorii brounovskogo dvizheniya [The method of fractional differentiation in the theory of Brownian motion]. *Izvestie vuzov Severo-Kavkazskij region. Estestvennye nauki – Proceedings of the universities of the North Caucasus region. Natural sciences*, 2004, no. 1, pp. 46-50.

3. Shen S., Liu F. Error analysis of an explicit difference approximation for the fractional diffusion equation with insulated ends. ANZIAM J., 2005, 46(E), pp. 871-887.

4. Mainardi F. Fractional relaxation-oscillation and fractional diffusion-wave phenomena. Chaos, Solitons and Fractals, 9(7), 1996, pp. 1461-1477. Mejlanov R.P., Yanpolov M.S. Osobennosti fazovoj traektorii fraktal'nogo oscillyatora [Features of the phase trajectory of fractal oscillator]. *Pis'ma ZhTF – Letters to JTP*, 2002, vol. 28, no. 1, pp. 67-73.

5. Parovik R.I. Zadacha Koshi dlya nelokal'nogo uravneniya Mat'e [The Cauchy problem for the nonlocal Mathieu equation]. *Doklady Adygskoj (Cherkesskoj) Mezhdunarodnoj Akademii Nauk – Reports Adyghe (Circassian) International Academy of Sciences*, 2011, vol. 13, no. 2, pp. 90-98.

6. Parovik R.I. Fractal Parametric Oscillator as a Model of a Nonlinear Oscillation System in Natural Mediums. Int. J. Communications, Network and System Sciences, 2013, vol. 6, pp. 134-138.

7. Parovik R.I. Zadachi Koshi dlya obobschennogo uravneniya 'Ejri [Cauchy problem for generalized Airy equation], *Doklady Adygskoj (Cherkesskoj) Mezhdunarodnoj Akademii Nauk – Reports Adyghe (Circassian) International Academy of Sciences*, 2014, vol. 16, no. 3, pp.64-69.

Original article submitted: 23.06.2014

Bulletin KRASEC. Phys. & Math. Sci, 2014, vol. , no. 2, pp. 39-47. ISSN 2313-0156

MSC 86A10

POSSIBLE EFECTS OF THE LIGHTNING CENTERS IN WHISTLER RATES IN KAMCHATKA

G.M. Vodinchar[1, 2], V.P. Sivokon'[1], N.V. Cherneva[1], B.M. Shevtsov[1], E.A. Malysh[2]

[1] Institute of Cosmophysical Researches and Radio Wave Propagation Far-Eastern Branch, Russian Academy of Sciences, 684034, Kamchatskiy Krai, Paratunka, Mirnaya st., 7, Russia

[2] Vitus Bering Kamchatka State University, 683031, Petropavlovsk-Kamchatsky, Pogranichnaya st., 4, Russia

E-mail: gvodinchar@gmail.com

The paper investigates possible sources of Kamchatka whistlers in March and September 2013. Applying the data from WWLLN and AWDANet worldwide networks, it is shown that statistically significant sources may be located in the global lightning centers.

Key words: Whistlers, VLF radiation, magnetosphere.

Introduction

Every lightning discharge occurring in the Earth atmosphere forms an electromagnetic pulse distributed in a wide frequency range. In particular, this pulse appears in the very low frequency range (VLF) where it is called an atmospheric [1]. Besides the atmospherics, signals having a characteristic saber-like form in spectral-time diagram also appear in VLF range radio signals. An example of such a signal is shown in Fig.1.

An acoustic analogue of a signal with such a spectrum is whistle, so they are called whistling atmospherics or whistlers. Just like atmospherics, whistlers are associated directly with lightning discharges.

Vodinchar Gleb Mikhailovich – Ph.D. (Phys. & Math.), Head of Lab. Modeling of physical processes, Institute of Cosmophysical Researches and Radio Wave Propagation FEB RAS, Associate Professor, Dept. Mathematics & Physics, Vitus Bering Kamchatka State University. *Sivokon' Vladimir Pavlovich* – Dr. Sci. (Tech.), Chief Researcher of the Lab. of Electromagnetic Radiation of the Institute of Cosmophysical Research and Radio Wave Propagation FEB RAS. *Cherneva Nina Volodarovna* – Ph.D. (Phys. & Math.), Leading Research Scientist of Lab. of Electromagnetic Radiation of the Institute of Cosmophysical Research and Radio Wave Propagation FEB RAS. *Shevtsov Boris Mikhailovich* – Dr. Sci (Phys. & Math.), Director, Institute of Cosmophysical Research and Radio Wave Propagation FEB RAS. *Malysh Ekaterina Alexandrovna* – Assistent of Dept. Informatics, Vitus Bering Kamchatka State University.

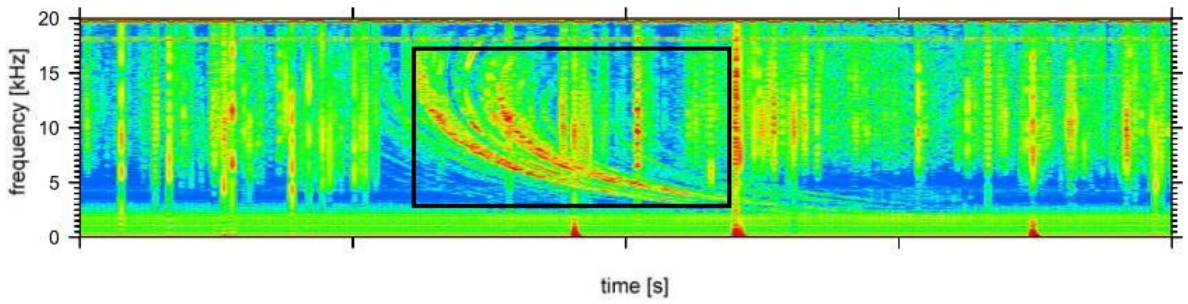

Fig. 1. Whistler typical imaging in spectral-time diagram of VLF signal.

The mechanism for whistler generation was suggested in the classical paper by Storey [2]. According to this theory, an atmospheric with the power of ∽ 20 GV initiated by a lightning discharge propagates in the Earth-ionosphere waveguide. It almost does not dissipate, and may pass considerable distances with slight deviation of ∽ 1 dB/Mm. However, some part of the atmospheric energy may penetrate through the ionosphere and enter the magnetosphere. In irregular anisotropic magnetospheric plasma, the electromagnetic wave undergoes frequency dispersion. As a result, pulse is transformed into a complicated signal with saber-like frequency-time characteristic determined by field line strength and plasma density along the trajectory in the magnetosphere. The fact that the whistler form depends on plasma distribution and field intensity makes it a natural marker of the Earth plasmasphere state and an interesting object in cosmic weather system.

According to the described mechanism, the most possible lightning source of a whistler may be located either in the vicinity of the point of its registration or in the vicinity of a magnetically conjugate point. In the first case, a whistler which passed the magnetospheric channel an even number of times is recorded; in the second case, a recorded whistler passes the channel uneven number of times. Nevertheless, whistler drift in the magnetosphere between different waveguides and registration of "outside"whistlers are theoretically possible [1].

The favorable conditions for VLF signal penetration into the magnetospheric channel are in high latitudes where field lines are almost vertical and field intensity is higher [3]. We should also note that whistler drift between the tubes is possible if a wavelength is comparable with a duct width. [4, 5]. Thus, in spite of the fact, that most of the lightning occur in the low latitude regions (tropics and subtropics), whistler sources are mostly located higher along the geomagnetic latitude. We may even suppose that there is a cutoff latitude for whistlers at the level of about ±16° of the latitude [6, 7].

While the mechanism for whistler generation does not arouse a discord among the specialists, lightning source region parameters and geometry are debatable problems. It is the most natural to suppose that the source must be symmetrical relative to the entry point into the magnetosphere, and the penetration efficiency must decrease with distance from this point. Nevertheless, it has been stated in a number of papers that the penetration efficiency is shifted relative to the entry point in the direction of the geomagnetic pole [8, 9]. Also, there is no one opinion about the region dimensions.

The present paper investigates the question, if "outside"whistlers are recorded in Kamchatka.

Initial data

The detailed information on the distribution of lightning discharges occurring on the Earth is contained in the databases of the World Wide Lightning Location Network (WWLLN). This network was founded and developed by the specialists of Washington University, Seattle, USA (http://webflash.ess.washington.edu/).

The network gives quite an accurate display of global lightning activity. It records discharges with heavy currents and registers the first stroke in a multi-flash. For every stroke, time and geographical coordinates are recorded, where time and space distributions are about 3×10^{-5} s and 10 km, correspondingly [10]. The network includes about 80 receiving stations determining lightning location all over the globe, located at paired distances from several meters to 10,000 km. Distribution of the world wide network stations is shown in Fig. 2.

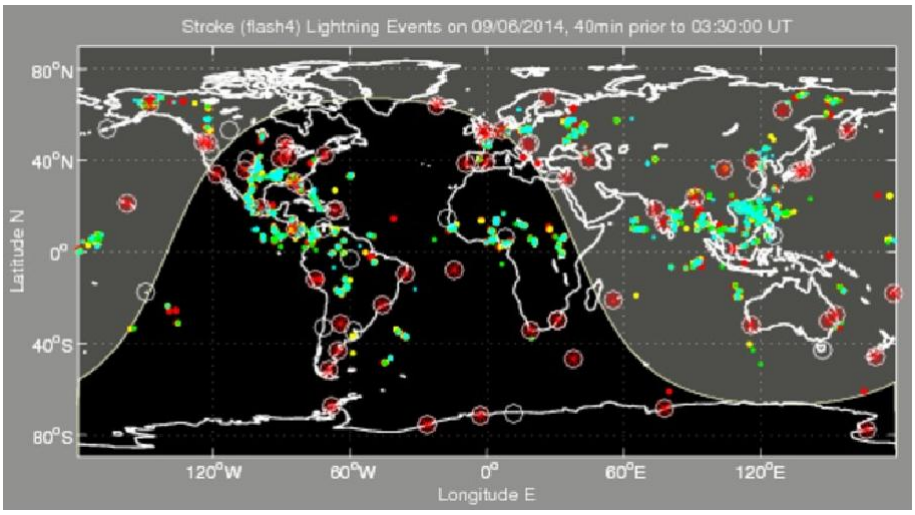

Fig. 2. Distribution of WWLLN network receiving stations. The image is taken from the site http://webflash.ess.washington.edu/

WWLLN identifies cloud-ground (CG), cloud-cloud (CC), and inter-cloud (IC) lightning discharges, but does not distinguish them [10]. Comparison of discharge detection efficiency by WWLLN and by a number of regional networks showed that WWLLN allows us to obtain representative information on lightning activity in planetary scale [11, 12].

The receiving stations register radiation arriving via the Earth-ionosphere waveguide with the maximum at the frequency of 10 kHz (30 km wavelength). To locate a lightning, three stations surrounding this lighting are enough. Spectrograms are updated every 10 minutes on the page http://webflash.ess.washington.edu/spectra.html. One of the stations of this network is installed at the Institute of Cosmophysical Research and Radio Wave Propagation (IKIR) FEB RAS in Kamchatka. WWLLN data allow us to make a time sequence, an ascending sequence of lightning stroke random moments, for a chosen geographical region.

Automatic Whistler Detector and Analyzer systems' Network (AWDANet) was developed for global whistler detection on the Earth. This network was founded and developed within several international projects under the direction of the specialists from Eotvos University, Budapest, Hungary [13]. AWDANet has been recently extended by a far-eastern Karymshina station, Kamchatka, Russia (LAT 52.83, LON 158.13, L=2.13). The

activity of whistlers recorded in Kamchatka is unusually high. During the first five months of the operation, more than 200,000 whistlers were recorded. AWDANet system was completed by PLASMON automatic analyzer (http://plasmon.elte.hu). It is based on the recently developed model for whistler inversion [14], that allowed us to make the process of whistler analysis automatic not only for events with a single whistler arrival but also for complex analysis of multiple path propagating whistler groups. Distribution of AWDANet stations is shown in Fig. 3.

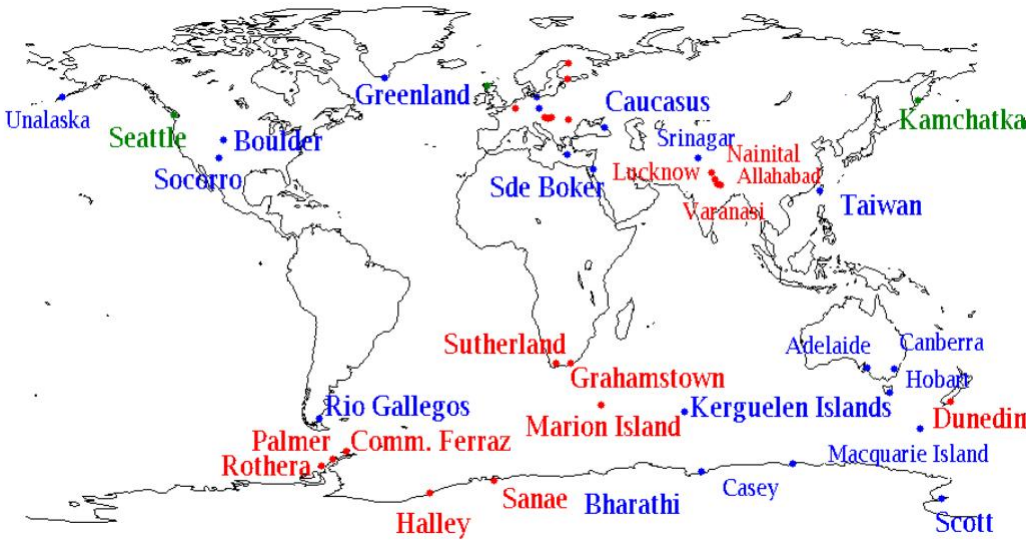

Fig. 3. Distribution of AWDANet receiving stations. Red and green dots correspond to active stations. Blue dots are the stations planned to be installed. The image is taken from the site http://plasmon.elte.hu

To detect whistlers automatically considering regional peculiarities of their dispersion curve, a detection algorithm was developed at IKIR FEB RAS [15, 16], the basis of which is a method of two-dimensional correlation of an initial signal spectrum and a model signal spectrum. The system based on this method consists of a detector and a determining factor, an adaptive threshold. The detector performs the two-dimensional correlation of signal fragment spectrum in a 4-second time window. The adaptive threshold is some average value. If its «normal level» is exceeded, a preliminary conclusion is formed that the signal contains a whistler. The detection algorithm is realized in the neural network operating automatically.

Analysis technique

The statistical relation between Kamchatka whistlers and lightning discharges from a given geographical region was analyzed by the correlation method.

Whistler time series W_t was composed, it is a number of whistlers registered per a period of time $[t;t+\Delta t]$. For the given geographical region, lighting discharge time series L_t, registered in this region for the same period of time, was composed from WWLLN network database. The sampling interval Δt was 1 min and 15 min for two variants of comparison. Since the sampling interval was larger than the time of signal propagation from the lightning source to the point of whistler registration even for the

case of multiple propagation in the magnetosphere, cross-correlation between the series was calculated only for the time zero shift.

The characteristic peculiarity of the analyzed time series is the presence of large spikes, the number of events may sharply change in neighbor time samples from zero to hundreds. It is known that the usually applied Pearson correlation coefficient is very sensitive to such spikes, just like any other characteristic based on average values. Moreover, if the correlation coefficient is small, then it is possible to conclude that series are independent only in the case of Gaussian statistics that is not correct for the analyzed series due to the presence of large spikes. In the case of strong but considerably nonlinear relation, the correlation coefficient may be small and even equal to zero.

To repress the effect of large spikes in the investigation of the relation between whistlers and lightning, data are sometimes roughened to Boolean values. In this case, if the interval contains discharges or whistlers, the time series sample is assigned the value 1; in other cases, it is 0 [17, 18].

Another way to obtain robust estimations is the application of real, not Boolean, values of time series with calculation of Spearman rank correlation coefficient. It is the correlation between value ranks in data series and it is stable to its monotonous transformations [19]. In particular, sharp spikes do not affect it. It is supposed that application of rank correlation allows us to obtain reliable statistical conclusions, from one side, and not to loose the information in Boolean roughening, from the other.

Analysis results

Two time intervals were under the analysis: 1-11 March 2013, and 1-30 September 2013. In the first case, rank correlation was estimated; in the second case, series were roughened to Boolean values.

Consider the analysis results for each case in detail.

In the first case, we carried out lightning sampling to make a series L_t for large geographical regions: Kamchatka (LAT 43N-63N LON 150E-170E), Australia (LAT 25S-45S LON 140E-160E), American (LAT 0N-45N LON 40W-110W), African (LAT 10S-20N LON 15W-45E), Indonesian (LAT10S-30N LON 100E-130E) lightning centers. Sampling interval is 15 min.

Fig. 4-5 show intensity rate series of whistlers and lightning discharges, normalized to the maximal number of events for the analyzed period for magnetically conjugate points.

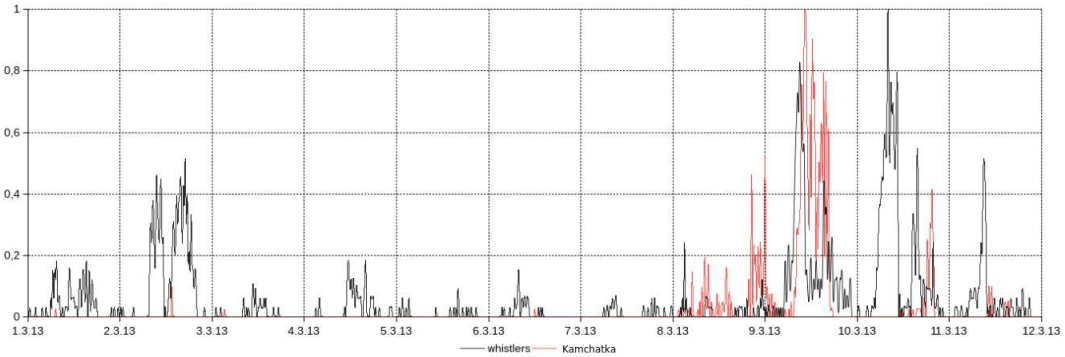

Fig. 4. Intensities of whistlers in Kamchatka and lightning discharges in Kamchatka.

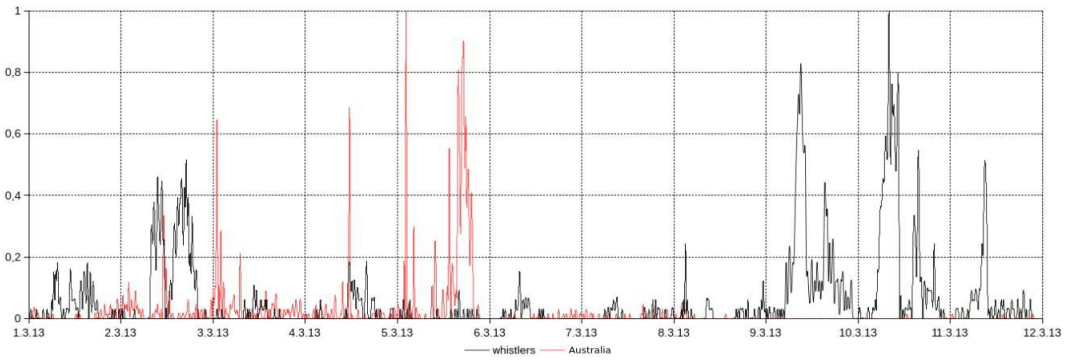

Fig. 5. Intensities of whistlers in Kamchatka and lightning discharges in Australia.

Visual comparison of these series shows a certain relation between the rates. For example, there is a clear relation of the sharp increase in whistler intensity on 9 March with Kamchatka lightning. Further correlation analysis determined an spike of whistler number on March 2 which coincides with the increase in discharge intensity in America, Africa, and Indonesia. It is difficult to separate them visually. Consider the results of calculation of rank correlation shown in Table.

Table

Rank correlation between whistler and lightning discharge rates

Date, time	Kamchatka	America	Africa	Indonesia	Australia
01.03.13 5:45-9:15	0.25	**0.37/0.2**	-0.44	-0.35	-0.16
01.03.13 9:45-13:00	–	-0.64	**0.42/0.15**	0.06	-0.19
01.03.13 13:15-19:00	–	-0.31	-0.23	-0.38	-0.38
02.03.13 7:30-12:15	–	-0.54	-0.34	-0.34	-0.34
02.03.13 12:30-21:00	-0.06	0.24	**0.62/0.0001**	**0.43/0.01**	-0.28
03.03.13 8:00-15:00	–	0.06	0.06	-0.37	-0.05
04.03.13 10:45-20:30	–	-0.26	-0.61	0.18	**0.35/0.03**
05.03.13 14:30-22:00	–	-0.21	-0.05	0.23	0.34/0.1
06.03.13 5:30-14:00	-0.17	**0.2/0.25**	-0.08	-0.26	-0.3
08.03.13 2:15-5:15	0.05	-0.04	**0.46/0.15**	-0.62	0.11
09.03.13 4:45-13:45	0.08	-0.57	0.14	-0.65	–
09.03.13 14:15-23:15	**0.57/0.0005**	0.005	-0.34	0.26	0.06
10.03.13 4:00-13:00	-0.25	-0.47	0.29	-0.29	-0.17
10.03.13 13:15-22:15	**0.42/0.01**	0.02	0.14	0.09	–
11.03.13 5:00-11:30	-0.59	-0.36	**0.56/0.005**	0.09	–

The first column contains time intervals with increases in whistler rates, and the following ones contain the correlation coefficient values between the whistlers and lightning discharges during these intervals. The significant levels of positive correlation are marked by bold type and splashes separate the significance levels on which the hypothesis on non-correlatedness is rejected.

It is clear that there were significant positive correlations of whistler rates with lightning discharges in Kamchatka (9 and 10 March), in Australia (4 and 5 March), in the American source (1 and 6 March), in African source (1, 2, 8, and 11 March). It is

difficult to attribute the spikes on 3, 9 and 10 March to one of the given sources; their sources are likely to be located in other regions.

Now, consider the analysis results for the second time interval on 1-31 September 2013.

The analysis was carried out according to the method described in the paper [17]. The Earth surface was separated into the regions of 3×3 degrees, and a time series L_t of lightning discharge number per 1 min was formed for every region. The same time series W_t was composed for Kamchatka whistlers. Then correlation coefficient between the series, roughened to Boolean values, was calculated.

The hypothesis on zero correlation for the considered series with the significance level $\gamma = 0.05$ is rejected for the correlation sample value of 0.011. Fig. 6 illustrates the correlation coefficient distribution for those elements of the grade grid, where its value exceeds the significance limit.

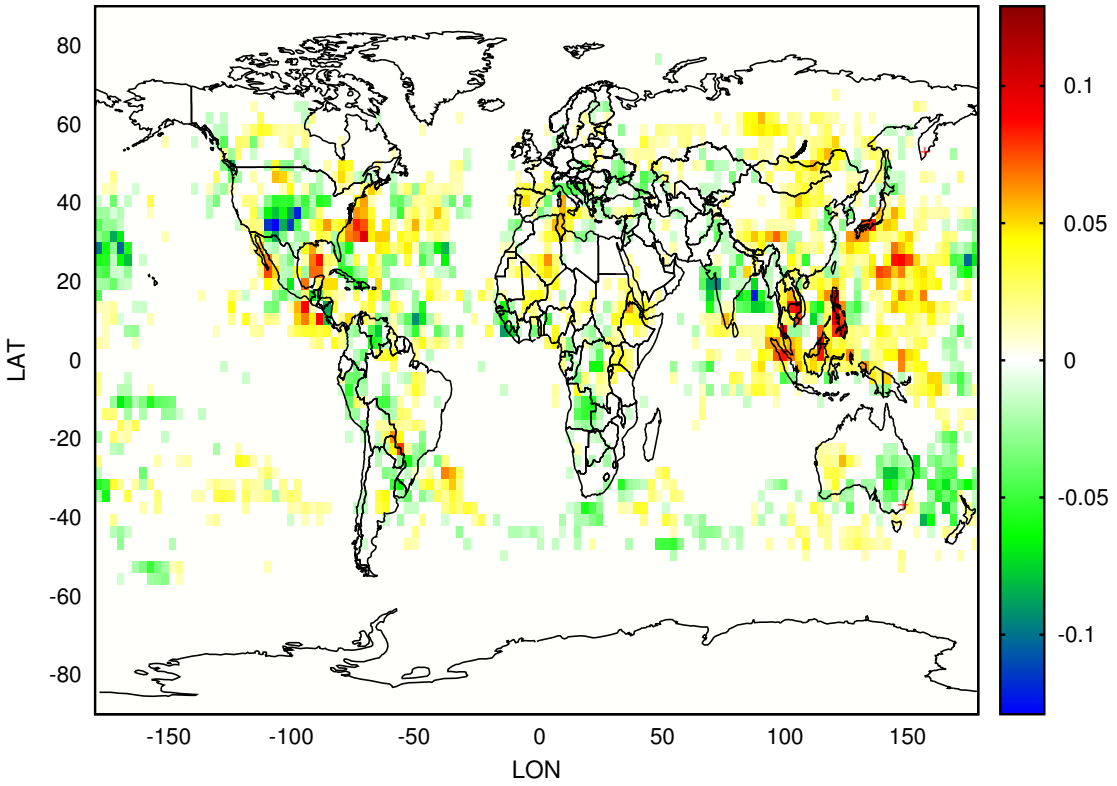

Fig. 6. Distribution of correlation coefficient between the series of Kamchatka whistlers and lightning discharges on the grade greed of 3×3. Red rhombs indicate the location of Kamchatka observatory (LAT 52.97N LON 158.25E) and the magnetically conjugate point in Australia (LAT 36.77S LON 149.40E). The cell color corresponds to correlation coefficient values. In white colored cells, the correlation is insignificant.

It is clear from this distribution that during the considered time interval, correlation between the Kamchatka whistlers and lightning in the Australian conjugate point was not observed. Nevertheless, there is correlation between the whistlers and the activity of Indonesian and American lightning centers.

Conclusions

Analysis of whistler intensity series for the periods 1-13 March 2013, and 1-30 September 2013, recorded in Kamchatka, showed that the registered signals may have lightning sources both from "Kamchatka"magnetic field tube and from other regions. Kamchatka and Australia lightning did not dominate as it might be expected. The possible explanation of this fact is that lightning intensity in American, African, and Indonesian sources was significantly higher during the considered periods than that in Australia and, especially, in Kamchatka.

References

1. Gershman B.N., Ugarov V.A. Rasprostranenie i generaciya nizkochastotnyh 'elektromagnitnyh voln v verhnej atmosfere [Distribution and generation of low-frequency electromagnetic waves in the upper atmosphere]. *Uspehi fizicheskih nauk – Successes of physical sciences*, 1960, vol. 72, no. 2, pp. 235-271.

2. Storey L. R. O. An investigation of whistling atmospherics. *Philos. Trans. R. Soc. London A*. 1953, vol. 246(908), pp. 113–141. doi:10.1098/rsta.1953.0011.

3. Helliwell R.A. Whistlers and Related Ionospheric Phenomena, Stanford Univ. Press, Stanford, Calif, 1965.

4. Strangeways H.J., Rycroft M.J. Trapping of whistler-waves through the side of ducts. *J. Atmos. Terr. Phys.*, 1980, 42(11-12), pp. 983-994. doi: 10.1016/0021-9169(80)90112-9.

5. Strangeways H.J. Whistlers leakage from narrow ducts. *J. Atmos. Terr. Phys.*, 1986, 48(5), pp. 455-462. doi: 10.1016/0021-9169(86)90122-4.

6. Rao M., Somayajulu V.V., Dikshit S.K., Tantry A.P. Low-latitude cutoff for whistlers observed on the ground. *J. Geophys. Res.*, 1974, 79(25), pp. 3867-3869.

7. Throne R.M., Horne R.B. Landau damping of magnetosphericalle reflected whistlers. *J. Geophys. Res.*, 1994, 99(A9), pp. 249-258.

8. Yoshino T. Low-latitude whistlers and cloud distributions in the conjugate area. *J. Geophys. Res.*, 1976, 81(A25), pp. 4793-4796.

9. Collier A.B., Hughes A.R.W., Lichtenberger J., Steinbach P. Seasonal and diurnal variation of lighthning activity over Southern Africa and correlation with European whistlers observations. *Ann. Geophys.*, 2006, 24(2), pp. 529-542.

10. Rodger C.J., Werner S., Brundell J.B., Lay E.H., Thomson N.R., Holzworth R.H., Dowden R.L. Detection efficiency of the VLF World-wide Lightning Location Network (WWLLN): Initial case study. *Ann. Geophys.*, 2006, 24(12), pp. 3197–3214.

11. Dowden R.L. et al. World-wide lightning location using VLF propagation in the Earth-ionosphere waveguide. I*EEE Antennas Propag. Mag.*, 2008, 50(5), pp. 40-60. doi:10.1109/MAP.2008.4674710.

12. Abarca S.F., Corbosiero K.L., Galarneau Jr. T.J. An evaluation of the Worldwide Lightning Location Network (WWLLN) using the National Lightning Detection Network (NLDN) as ground truth. *J. Geophys. Res.*, 2010, vol. 115, D18206. doi:10.1029/2009JD013411.

13. Lichtenberger J., Ferencz C., Bodnár L., Hamar D., Steinbach P. Automatic Whistler Detector and Analyzer system: Automatic Whistler Detector. *J. Geophys. Res.*, 2008, vol. 113, A12201. doi:10.1029/2008JA013467.

14. Lichtenberger J. A new whistler inversion method. J. Geophys. Res., 2009, vol. 114, A07222. doi:10.1029/2008JA013799.

15. Cherneva N. V., Agranat I.V. Avtomaticheskoe detektirovanie svistyaschih atmosferikov i ih sopostavlenie s grozovoj aktivnost'yu [Automatic detection of whistlers and their comparison with thunderstorm activity]. *Trudy VII Vserossijskoy konferencii po atmosfernomu 'elektrichestvu. Kn. 2.*[Proc. 7th All-Russian Conference on Atmospheric Electricity]. Saint Petersburg, 2012, pp. 45-46.

16. Cherneva N.V., Vodinchar G.M., Sivokon' V.P., Mel'nikov A.N., Sannikov D.V., Agranat I.V. Korrelyacionnyj analiz potokov svistyaschih atmosferikov i grozovyh razryadov [Correlation analysis flows whistlers and lightning]. *Vestnik KRAUNC. Fiziko-matematicheskie nauki–Bulletin of the Kamchatka Regional Association «Education-Scientific Center». Physical & Mathematical Sciences*, 2013, vol. 7, no. 2, pp. 59-67.

17. Collier A.B., Delport B., Hughes A.R.W., Lichtenberger J., Steinbach P., Oster J., Rodger C.J. Correlation between global lightning and whistlers observed at Tihany, Hungary. *J. Geophys. Res.*, 2009, vol. 114, A07210. doi: 10.1029/2008JA013863.

18. Collier A.B., Bremner S., Lichtenberger J., Downs J.R., Rodger C.J., Steinbach P. Global lightning distribution and whistlers observed at Dunedin, New Zealand. *Ann. Geophys.*, 2010, 28(2), pp. 499-513.

19. Ajvazyan S.A., Yunyukov I.S., Meshalkin L.D. *Prikladnaya statistika. Issledovanie zavisimostej* [Applied Statistics. Study of dependencies]. Moscow, Finansy i statistika Publ., 1985.

Original article submitted: 15.10.2014

Bulletin KRASEC. Phys. & Math. Sci, 2014, vol. , no. 2, pp. 48-55. ISSN 2313-0156

MSC 86A25

LOCATION OF THE SOURCE OF THE GEOMAGNETIC FIELD GENERATION

V.V. Kuznetsov

Institute of Cosmophysical Researches and Radio Wave Propagation Far-Eastern Branch, Russian Academy of Sciences, 684034, Kamchatskiy Kray, Paratunka, Mirnaya st., 7, Russia

E-mail: vvkuz38@mail.ru

Using well-known data on the structure of the geomagnetic field it is shown that its generation source is located at the boundary between the Earth inner and outer cores, most likely, in the F-layer.

Key words: geomagnetic field, generation source location

Introduction

As generally accepted in geodynamo model the geomagnetic field dipole source is located in the outer core, closer to the boundary with mantle or at the boundary itself. As a rule, the question on the location of the generation source is not usually discussed in Geomagnetism, nevertheless, some attempts to determine the source size (depth of is location in Earth radius fractions R) are known. It is possible to estimate it on the basis of available data on geomagnetic field structure. Several methods to estimate the size of geomagnetic field generation source are considered and compared with the results of similar estimates obtained by different authors.

Computer model

Computer modeling of the geomagnetic field by a set of current loops was carried out in a number of papers by L.R. Alldridge [1]-[4], as well as in the paper [5]. The optimal number of loops and the radius of their arrangement were obtained. In all these investigations the unequivocal result that the source of the geomagnetic field is located at the radius $a = 0.2\ R$, where R is the Earth radius was obtained.

Kuznetsov Vladimir Valeryevich – Dr. Sci. (Tech.), Leading Researcher comprehensive geophysical observatory «Paratunka», Institute of Cosmophysical Researches and Radio Wave Propagation FEB RAS.

Estimation based on the dipole size

The size of the Earth magnetic field generation region was estimated by Zhizhimov O.L. [6] on the basis of spherical coefficient analysis. Here the author supposed that the expansion of the field by the spherical functions on the Earth surface and the expansion of this field on the small-parameter such as the ratio of the source size to the distance to it are equivalent. Knowing the value of the small parameter, it is possible to estimate the source characteristic size if one assumes that the source generates only the lowest multipoles in the form of magnetic charges, dipoles, and quadrupoles.In modeling on even and uneven harmonics of the geomagnetic field expansion, the unequivocal result that the depth of magnetic field generation turned out to be equal to $x = a/R = 0.2R$ (R is the Earth radius) was obtained. This approach is considered in detail below.

The simplest model for a source with a dipole moment is a system of two opposite charges arranged symmetrically relatively the Earth center. The potential of the dipole with the finite size (distance between the charges is 2) is: Рассмотрим этот подход немного подробнее.

$$V(\vec{R}) = \sum_{lm} A_{lm} l_{em}(\vec{R}), \tag{1}$$

where coefficients A_{lm} are linearly related to the standard harmonic coefficients by:

$$(-1)^m \frac{R}{2}\sqrt{\frac{2\pi}{2l+1}}\,(g_l^m + ih_l^m), \quad A_{l0} = R\sqrt{\frac{2\pi}{2l+1}}\,g_l^0, \; A_{l-m} = (-1)^m A_{lm}. \tag{2}$$

Model dipole parameters lead to the following expression:

$$x = \left\{ \frac{A_3^+ C_3 + C_3^+ A_3}{2C_3^+ C_3} \right\}^{1/2}, \tag{3}$$

that is the estimation of dipole eigen size. Here, composed of A_3 and C_3 coefficients the column matrixes are implied under A_{3m}, C_{3m}. Значок "+" sign means Hermitean conjugation. Numerical values of x are shown in Fig. 1.

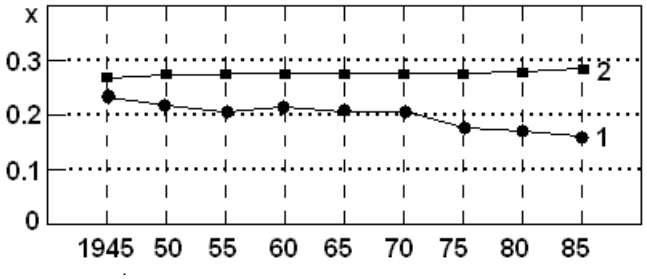

Fig. 1. Model source size for dipole (1) and quadrupole (2)

Estimation by the distance between virtual magnetic poles (VMP)

Estimating the non-dipolarity degree of geomagnetic field source Kuznetsov V.V. [7]investigated the relation of the distance between two different VMP and this between

the points of their observation. If all VMP are at the same point, then the geomagnetic field is dipole. If the distance between two VMP is equal to this between the points where the poles were determined, it would show the absence of dipole character of the field and the inclination of a line in Fig. 2-a would be equal to 45°.

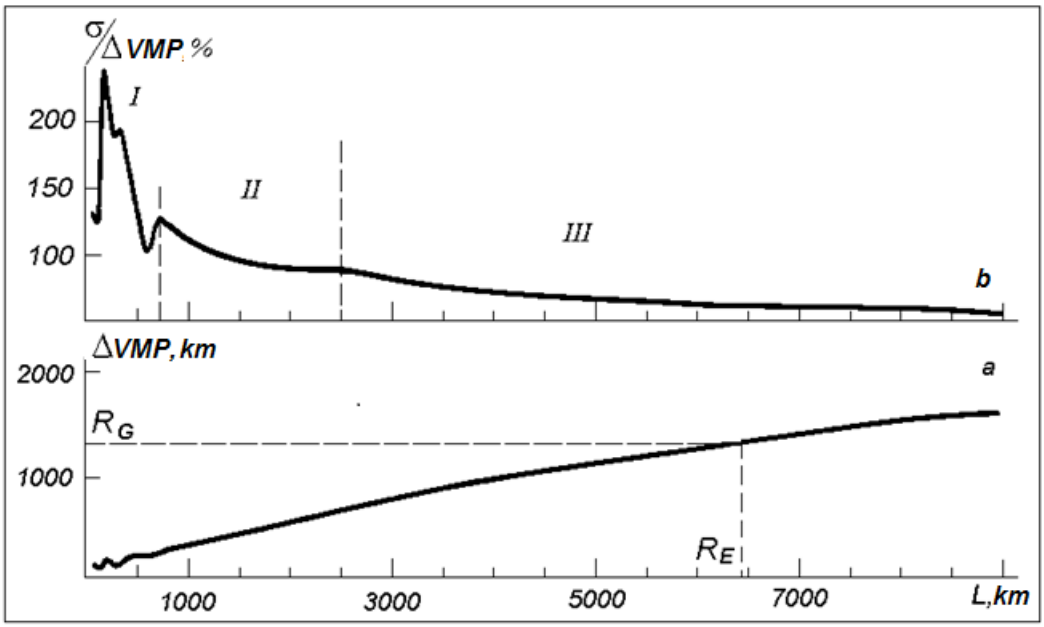

Fig. 2. The distance between virtual magnetic poles, determined at the observatories and the distance between these observatories L – *a*; *b* - the relative root-mean-square deviation s from the VMF average coordinates related to L.

In fact, this angle is significantly less, which indicates the dipole character of geomagnetic field. Taking the distance L between two observatories, i.e. points of VMP determination, to be equal to the Earth radius R_E, then the distance between VMP is 0.2 R_E, that is equal to the inner core radius R_G (Fig. 2-a). It confirms once more the validity of former estimations.

Fig. 2-b illustrates the variation of relative root-mean-square deviation σ from VMP average value (σ/ΔVMP) with the distance L. The curve in Fig. 2-b consists of three parts, marked by *I, II, III*. In part *I* the sharp changes of σ/ΔVMP are observed. Most likely, it is explained by the fact that when the distance between the observatories is short ($L < 700$ km), magnetic anomalies, natural for the Earth crust, have their impact. In part *II*, the decrease of σ/ΔVMP is due to the increase of depth factors effects over the crust ones. In part *III* ($L > 2500$ км) a smooth decrease of σ/ΔVMP associated with the decrease of depth source effect during the increase of an averaging interval (the last point on the curve $L \approx 9000$ was obtained by averaging of 16110 values) is observed.

Estimation by spatial dimension of anomaly

In our model global magnetic anomalies (GMA) are presented by magnetic dipoles. It is known that if it is a central dipole (its center is on the Earth rotation axis), then its components are:

$$Z = (2m/4\pi) \times \cos\left(\theta/r^3\right), H = (m/4\pi) \times \sin\left(\theta/r^3\right) \quad , \qquad (4)$$

where m is the dipole moment, and θ is the angle between a vector, directed to the point on the Earth surface where the dipole is pointing at and $Z = \max$, and a vector, directed to the point where one intends to determine the dipole field values (Fig. 3).

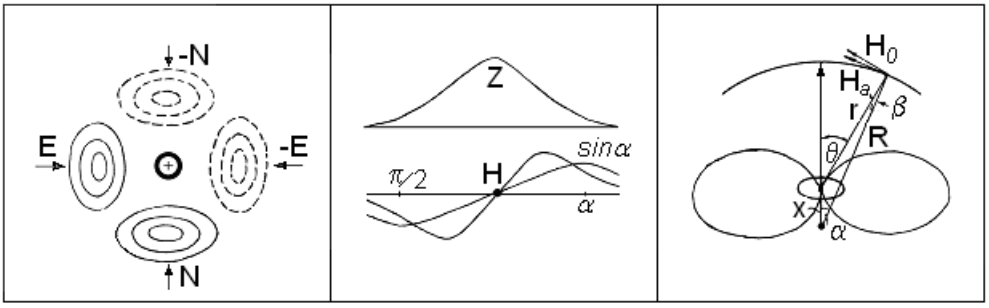

Fig. 3. Estimation of the Earth radius part appropriate to the region of the source of the magnetic anomaly field generation

It follows from the figure that on the maps of geomagnetic field E- and N-components, we observe their maxima and minima distant from the dipole center (we should note, that there are such maxima and minima on maps indeed). If we succeeded to estimate the distances (in geographic degrees) from the dipole center to these component maxima, we would be able to estimate the depth where GMA generation takes place. We are interested in angle, but to estimate x value (Fig. 3) we use the values of θ and α angles (in geographic degrees). Note that GMA dipole field coordinates do not coincide with the central dipole form. Equating the Earth radius to a unit ($R = 1$), supposing that:

$$H_\theta = \sin\left(\theta / r^3\right) = \max.$$

and taking the obvious relation: $\sin(\theta) = \sin(\alpha/r)$, we obtain:

$$H_\theta = \sin\left(\theta / r^4\right).$$

If $\beta\,(\beta = \theta - \alpha)$ is the angle between H_α and H_θ vectors , then H_θ value should be multiplied by: $\cos(\beta) = (1 - x\cos(\alpha))/r$.

It results in:

$$H_\alpha = \sin(\alpha)(1 - x\cos(\alpha))\Big/ r^5, r = \left(1 + x^2 - 2x\cos(\alpha)\right)^{1/2}. \quad (5)$$

Having determined α values for GMA and for secular variation current focuses from the maps of the Earth magnetic field E- and N-components, x average value equal to $x = 0.2\,(\pm 0.1)R$. is obtained.

Estimation of the source location by geomagnetic spectrum

Geomagnetic field spectrum was studied in the papers [8]-[10]. Geomagnetic field spectrum is the variation of geomagnetic field root-mean-square intensity R_n, estimated on the Earth surface (R_n dimension is given in $(\mathrm{nTl})^2$) as a sum of n-th power harmonics from the harmonic number:

$$R_n = (n+1)\sum_{m=0}^{n}\left[(g_n^m)^2 + (h_n^m)^2\right]. \quad (6)$$

In the paper [9], a set of Rn values is presented in a table from which it is clear that the main part of the field intensity (95%) is concentrated in the region of geomagnetic field generation (dipole field) with $n = 1$ harmonic. The spectrum pattern is a declining curve for the harmonics with the power from 1 to $n = 13$. For the harmonics of the higher order, the curve is horizontal.

$$R_n = 1.349 \times 10^9 (0.270)^n (nT)^2. \quad (7)$$

Estimating the shape of geomagnetic field spectrum relative to the core-mantle boundary, it was shown [8]-[9] that R_n coefficients decrease smoothly to a certain n value corresponding to that boundary and then they begin to increase. The nature of Rn increase is not quite clear. This increase (dots on Fig. 4-b) does not fit the formula (7).

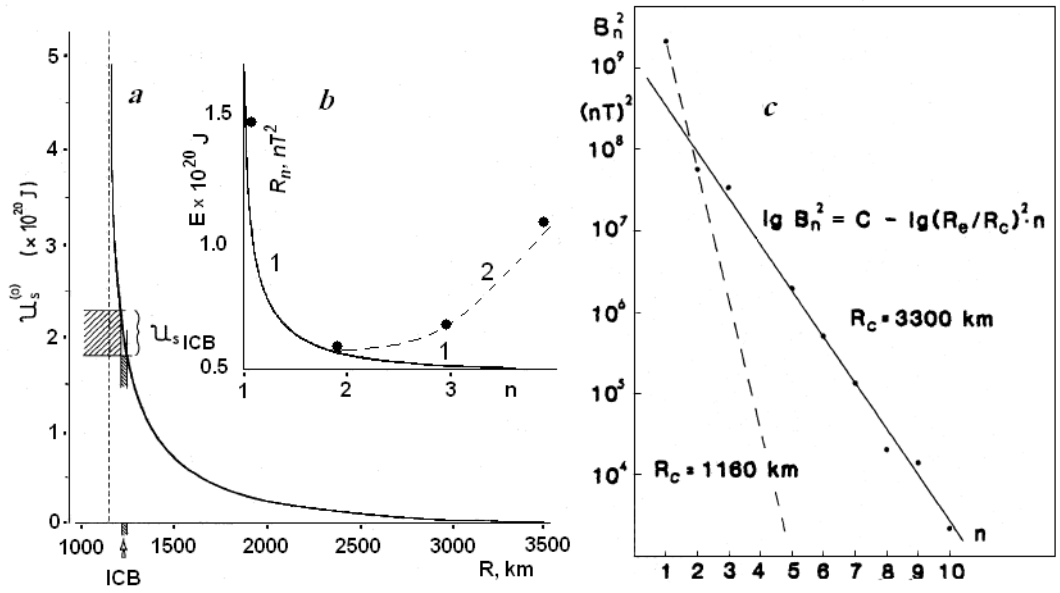

Fig. 4. Estimation of geomagnetic field energy value depending on the Earth radius (*a*) [9], on the number of spherical harmonic (*b*) for the inner core surface, geomagnetic field spectrum () for two spheres with R_c radius [10]

The authors [9]) try to explain this phenomenon by a possible effect of the crust and mantle magnetic fields. Most likely, the spectrum steepening determined in some papers is associated with a computational algorithm which does not take into account the fact that determined for the Earth surface Gauss coefficients g_n^m and h_n^m were applied to estimate the spectrum on inner spheres. It is equivalent to the situation when, for example, some function limited by a defined interval would be expanded in a series of polynoms and then the expansion final level would be transferred into the interval defined for this function. Here similarly the coefficients for the harmonics series which does not fit a new interval will increase as the harmonic number grows, whereas they decreased within the limited interval discussed earlier.

R_n is the total root-mean-square contribution into the vector range of all harmonics with n power. R_n calculated according to IGRF 1980 data applying equation 6 ([10]) is shown in Fig. 4-c. The regression line decline (solid line) yields the core boundary radius of 3300 km. The dashed line passing through the first two harmonic coefficients is a spatial spectrum of magnetic field source located in the inner core.

Modeling by magnetic dipoles and current loops

In modeling an iterative damped Newton-Gauss method was applied to minimize an efficiency function. Square of an averaged over the Earth surface residual field, that is the difference between the model and the observed ones, was used as the efficiency function [11].

It was shown that the most optimal generator is a differential current system with a short distance between circular loops. By the search of current loop dimensions and arrangement, and values of magnetic dipoles on the Earth inner spheres, it was determined that the main (prevailing) part of the Earth magnetic moment is generated in the volume adjacently surrounding the inner core ($R_G = 0.2\ R_E$). The most optimal number of current loops additional to the central axial dipole is four, as well as four global magnetic anomalies are observed. The geomagnetic field configuration of the central dipole and four dipoles (current loops) as most corresponding to the observable one (Fig. 5) is obtained if the calculated geographic coordinates of dipoles do not coincide with the coordinates of GMA dipoles which vectors are at some angle to the inner core surface.

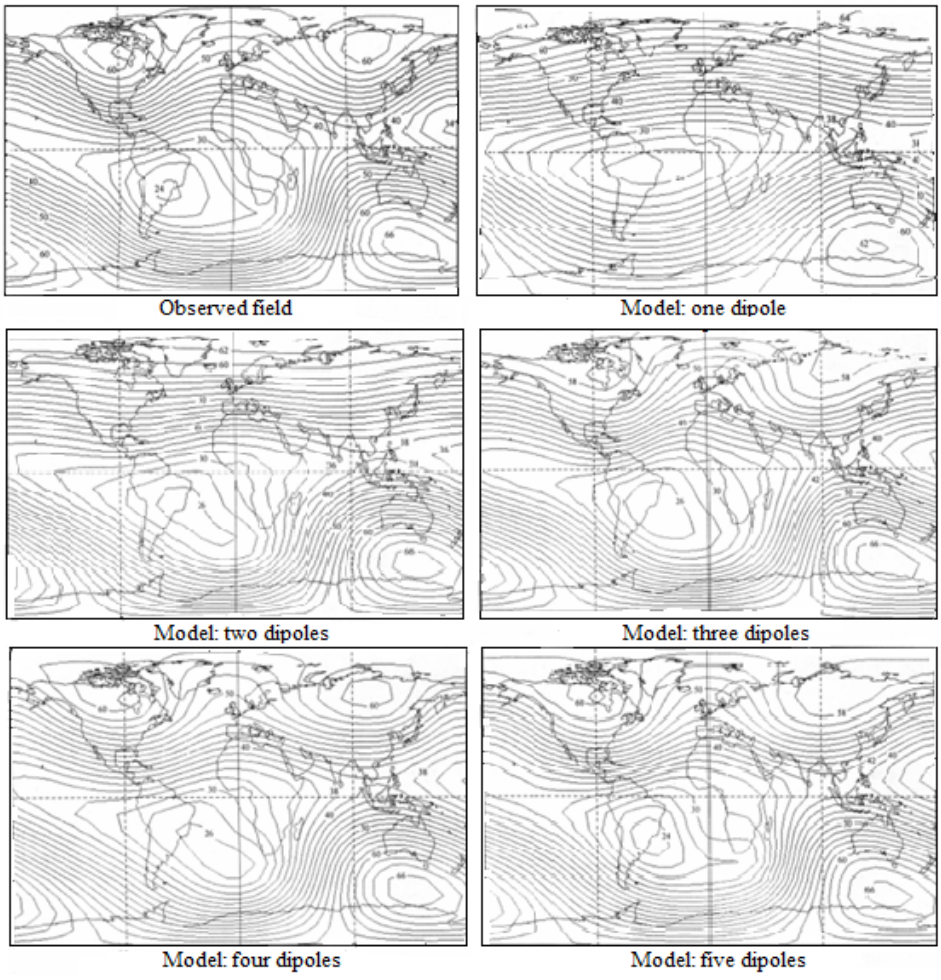

Fig. 5. Geomagnetic field structure for different number of dipoles located on the sphere of the radius $= 0.2\ R$

In the table the dipole directions are indicated by errors, and the dipole field moduli (Md) are given in Tesla per volume ($^3 \times 10^{15}$).

Table

Dipole	Central	Canadian	Siberian	Brazilian	Southern
Coordinates	78.3 °S106 °E	60 °N 90 °W	60 °N 120 °E	15 °S 90 °W	70 °S 150 °E
Calc. coord.	63.3 S25.3 °E	24 N 62.8 W	45 N 66.8 °E	69.1 S9.9 °W	72.5 S133 °E
M.d.$\times 10^{15}$Тм^3	7.8	1.8	2.4	4.3	2,5
Dip. direct.	↓	↓	↓	↑	↓

As clear from the table the moduli of the central dipole and GMA are comparable-sized, and the moduli of three anomalies enhance the main field, whereas the modulus of the Brazil anomaly decreases it.

Conclusion

All well-known methods for estimation of the source location result in: the geomagnetic field is generated at the boundary of the inner core. This fundamental result contradicts the geodynamo classical model. The boundary between the inner (G) and the outer (E) cores is easily detected by seismological methods. With real thickness of about 100 km the boundary is called the F-layer.

The distribution of P-waves velocities in the F-layer allows to suppose that the first-order phase transition takes place here. It means that electric charges may be generated in the layer with their separation during mass transfer and double electric layer appears. Taking into account these conditions, it is real that the geomagnetic field is generated just in this layer.

References

1. Alldredge L.R., Hurwitz L. Radial dipoles as the sources of the Earth's main magnetic field. *J. Geophys. Res.*, 1964, vol. 69, pp. 2631-2636.

2. Alldridge L.R., Stearns C.O. Dipole model of the sources of the Earth's magnetic field. *J. Geophys. Res.*, 1969, vol. 74, pp. 6583-6593.

3. Alldridge L.R. Circular current loops, magnetic dipoles and spherical harmonic analyses. *J. Geomag. Geoelectr.*, 1980, vol. 32, pp. 357-364.

4. Alldridge L.R. Current loops fitted to geomagnetic model spherical harmonic coefficients. *J. Geomag. Geoelectr.*, 1987, vol. 39, pp. 271-296.

5. Peddie N.W., Zunde A.K. A model of geomagnetic secular variation for 1980-1983. *Phys. Earth Planet. Inter.*, 1987, vol. 48, pp. 324-329.

6. Zhizhimov O.L. Ocenka razmera oblasti generacii magnitnogo polya Zemli [Estimating the size of the region of generation of the magnetic field of the Earth]. Novosibirsk, Preprint IGiG Publ., 1988, no. 13, 12 p.

7. Kuznecov V.V., Pavlova I.V., Semakov N.N. Ocenka stepeni nedipol'nosti glavnogo magnitnogo polya Zemli [Estimating the size of the main points in non-dipolarity Earth's magnetic field]. *Doklady Akademii Nauk – Reports of the Academy of Sciences of the USSR*, 1987, vol. 296, no. 4, pp. 819-821.

8. Langel R.A., Estes R.H. A geomagnetic field spectrum. *Geophys. Res. Lett.*, 1982, vol. 9, no. 4, pp. 250-253.

9. Gregori G.R., Dong W-J., Gao X-Q., Gizzi F.T. The separation of the geomagnetic field originated in the core, in the asthenosphere, and in the crust. *Ann. Geoph.*, 1999, vol. 42, no. 2, pp. 191-209.

10. Nevanlinna H. Notes on global mean-square values of the geomagnetic field and secular variation. *J. Geomagn. Geoelectr.*, 1987, vol. 39, no. 3, pp. 165-174.

11. Botvinovskij V.V. *Modelirovanie generatora glavnogo magnitnogo polya Zemli s pomosch'yu magnitnyh dipolej i tokovyh konturov.* Diss. kand. fiz.-mat. nauk [Modeling generator main geomagnetic field using magnetic dipoles and current loops. PhD. phys. and math. sci. diss.]. Novosibirsk, 2000.

Original article submitted: 09.12.2014

Bulletin KRASEC. Phys. & Math. Sci, 2014, vol. , no. 2, pp. 56-61. ISSN 2313-0156

MSC 35C05

PASSAGE THROUGH X-RAY PROTECTION HAVING THE STRUCTURE OF HOMOGENEOUS FRACTALS

V.A. Churikov

Tomsk Polytechnic University, Tomsk, 634050, Tomsk, pr. Lenina 30, Russia
E-mail: vachurikov@list.ru

In this paper we generalize the law of Bouguer-Lambert in the case of a homogeneous fractal. With detailed analysis in terms of d-output operator generalized law of Bouguer-Lambert-Beer law, which in particular includes the classical law of optics Bouguer-Lambert-Beer.

Key words: d-operator, homogeneous fractal, fractal dimension, the law of Bouguer-Lambert-Beer

Introduction

Suppose, there is a fractal x_α in a three-dimensional Euclidean space, it has fractional dimension Euclidean space, it has fractional dimension α for which the equations $0 \leq \alpha \leq 1$ are true, along the x axis. The fractal is assumed to be isotropic and homogeneous, i.e. its dimension is constant $\alpha = const$ and does not depend on space coordinates and time. Moreover, the topological properties are assumed to be independent on space and time.

Fractal x_α points lie on the transversal axis. Axis x points, not belonging to the fractal, belong to a conjugate fractal $x_{1-\alpha}$, with the dimension $1-\alpha = const$, $0 \leq 1-\alpha \leq 1$, which is also a homogeneous fractal. In its turn, the fractal x_α is a conjugate one relative to its conjugate fractal $x_{1-\alpha}$. On x coordinate, the points of the fractal and the conjugate fractal are related as

$$x_\alpha \cup x_{1-\alpha} = x; x_\alpha \cap x_{1-\alpha} = \emptyset.$$

The second relation will be further called the property of fractal orthogonality, from which it follows that most of the physical processes occurring in the fractal and in the conjugate fractal may be independent, not affecting each other. In particular, interaction of electromagnetic radiation with the fractal and the conjugate fractal may refer to such processes.

Churikov Viktor Anatolyevich – Ph.D. (Phys. & Math.), Associate Professor Dep. of Mathematics, Tomsk Polytechnic University.

Definition of the problem

Damping of electromagnetic radiation beam in a continuum is described by the differential equation which describes absorption of a light beam in a medium propagating along the axis x [1]

$$dI = -kIdx.$$

Here I is the intensity of the radiation along the space coordinate ; k is the coefficient of beam attenuation in a medium.

If the continuum is composed of the combination of the fractal and the conjugate fractal, which have different physical-chemical properties, the processes of photon interaction will be different, and the corresponding differential equation describing photon beam attenuation may be written in the form of the ratio

$$dI \propto (-\tau_\alpha k_\alpha I dx_\alpha) \cup (-\tau_{1-\alpha} k_{1-\alpha} I dx_{1-\alpha}). \quad (1)$$

Here dx_α $dx_{1-\alpha}$ and are differentials on the points of the fractal x_α and the conjugate fractal which lie on the axis x; k_α is the attenuation linear coefficient in the fractal which may be represented as the sum $k_\alpha = k_{\alpha|A}(\lambda) + k_{\alpha|D}(\tau_\alpha) + k_{\alpha|S}(\tau_\alpha)$, $k_{\alpha|A}(\lambda)$, is the absorption coefficient which depends on the wave lengths of photons λ and on other factors, $k_{\alpha|D}(\tau_\alpha)$ is the inner diffraction coefficient which describes diffraction on fractal inner structures and depends on geometric and topological features of the fractal, i.e. on τ_α, $k_{\alpha|S}(\tau_\alpha)$, is the inner scattering coefficient on the fractal irregularities which also depends on τ_α ; τ_α is the topological coefficient of the fractal space for the considered process [2], $0 \le \tau_\alpha \le 1$; $k_{1-\alpha}$ is the attenuation linear coefficient in the conjugate fractal, which, just like in the fractal, may be presented as the sum $k_{1-\alpha} = k_{1-\alpha|A}(\lambda) + k_{1-\alpha|D}(\tau_{1-\alpha}) + k_{1-\alpha|S}(\tau_{1-\alpha})$; $k_{1-\alpha|A}(\lambda)$; $k_{1-\alpha|A}(\lambda)$ is the absorption coefficient in the conjugate fractal, $k_{1-\alpha|D}(\tau_{1-\alpha})$ is the inner diffraction coefficient in the conjugate fractal, $k_{1-\alpha|S}(\tau_{1-\alpha})$ is the inner scattering coefficient on the conjugate fractal irregularities; $\tau_{1-\alpha}$ is the topological coefficient of the conjugate fractal, $0 \le \tau_{1-\alpha} \le 1$.

The topological coefficients τ_α , and $\tau_{1-\alpha}$ depend on the definite topological and geometric properties of the fractal and the conjugate fractal.

When the considered process is impossible due to the topological properties, the process is topologically forbidden, then $\tau_\alpha = \tau_{1-\alpha} = 0$. The considered process is realized only through the fractals which topological coefficients are nonzero. Thus, if the topological coefficient of at least one the fractals is nonzero, the considered process is topologically allowed in this medium.

For the inner diffraction coefficients of the fractal and the conjugate fractal, the equality $k_{\alpha|D}(\tau_\alpha) = k_{1-\alpha|D}(\tau_{1-\alpha})$. must hold.

This equality holds since the fractal and the conjugate fractal share the boundary on which inner diffraction takes place. Thus, any of these two coefficients may be put into the relations, which contain them.

Strictly speaking, we may not put the sign of equality into the relation (1), since the physical dimensions of the left and the right parts are not the same in the equation during such a change

$$[dx_\alpha] = L^\alpha; [dx_{1-\alpha}] = L^{1-\alpha}; [dx] = L.$$

Due to the same reason, the term values in the right part may not be added. That is why, the sign of proportion $\propto$ is put instead of the one of equality, and the sign of union $\cup$ is put instead of the addition.

For the differentials on the fractals, $dx = dx_\alpha \cup dx_{1-\alpha}$ will be true.

Due to the orthogonality of the fractal and the conjugate fractal, the orthogonality property will be also true for the differentials

$$dx_\alpha \cap dx_{1-\alpha} = \emptyset.$$

Obtaining the solution

At first, to obtain the solution we divide the variables and put them under the integral.

$$\int \frac{dI}{I} \propto (-\tau_\alpha k_\alpha \int dx_\alpha) \cup (-\tau_{1-\alpha} k_{1-\alpha} \int dx_{1-\alpha}). \quad (2)$$

Transform the right part so that the both terms are consistent qualitatively and quantitatively between each other and are consistent with the lift part.

In order to do that, the right part should be brought to the same scale and to the same physical dimension with the left part. The first term in the right part should be multiplied by the dimension transformation coefficient $x^{1-\alpha}$, and the second term should be multiplied by the dimension transformation coefficient x^α , which brings the dimension of the right part to Euclidean space dimension where the fractal and the conjugate fractal are. Physically, it corresponds to the situation when we consider photon beam propagation along all the points on the axis x, some part of which belong to the fractal, and the rest belong to the conjugate fractal.

Then the first term in the right part should be multiplied by the fractal scale coefficient $\alpha^2\Gamma(\alpha)$, and the second term should be multiplied by scale coefficient of the conjugate fractal $(1-\alpha)^2\Gamma(1-\alpha)$. These coefficients bring the beam propagation length to the fractal effective thickness and to the conjugate fractal effective thickness $(1-\alpha)x$ which in the one-dimensional case are αx and $(1-\alpha)x$, correspondingly.

In the result, the transition from integration by the fractal of dimension α to the integral of fractional order α on the basis of d-operator is reduced to the change

$$\int dx_\alpha \to \alpha^2\Gamma(\alpha)x^{1-\alpha} \int d^\alpha x,$$

$$\int dx_{1-\alpha} \to (1-\alpha)^2\Gamma(1-\alpha)x^\alpha \int d^{1-\alpha} x.$$

Here $\int d^\alpha x$ and $\int d^{1-\alpha} x$ are the integrals of fractional orders α and $\alpha - 1$; $\Gamma(...)$ is the Euler gamma function.

After the transformations, the both terms in the right part may be added and equated with the lift part. In the result, the equation is obtained in which the variables are divided

$$\int \frac{dI}{I} = -\tau_\alpha k_\alpha \alpha^2\Gamma(\alpha)x^{1-\alpha} \int d^\alpha x - \tau_{1-\alpha} k_{1-\alpha}(1-\alpha)^2\Gamma(1-\alpha)x^\alpha \int d^{1-\alpha} x.$$

Integrating the left part, we obtain

$$\int \frac{dI}{I} = \ln(I) - \ln(C).$$

Here C is the integration constant. Integrating the right part by d-operator [3], for the first term we obtain

$$-\tau_\alpha k_\alpha \alpha^2 \Gamma(\alpha) x^{1-\alpha} \int d^\alpha x = -\frac{\tau_\alpha k_\alpha \alpha^2 \Gamma(\alpha) x^{1-\alpha}}{\alpha(\alpha)} x^\alpha + \alpha^2 \Gamma(\alpha) x^{1-\alpha} C_\alpha(x).$$

Integrating the second term, we obtain

$$-\tau_{1-\alpha} k_{1-\alpha} (1-\alpha)^2 \Gamma(1-\alpha) x^\alpha \int d^\alpha x =$$

$$= -\frac{\tau_{1-\alpha} k_{1-\alpha} (1-\alpha)^2 \Gamma(1-\alpha) x^{1-\alpha}}{(1-\alpha)(1-\alpha)} x^\alpha + (1-\alpha)^2 \Gamma(1-\alpha) x^\alpha C_{1-\alpha}(x).$$

Here $C_\alpha(x)$ and $C_{1-\alpha}(x)$ are the integration polynomials of the orders α and $1-\alpha$, which are generalization of integration constants within d-analysis [3].

De to the randomness of the second terms, they are equated to zero

$$\alpha^2 \Gamma(\alpha) x^{1-\alpha} C_\alpha(x) = 0,$$

$$(1-\alpha)^2 \Gamma(1-\alpha) x^\alpha C_{1-\alpha}(x) = 0.$$

Finally, for the sum in the right part we obtain

$$-\tau_\alpha k_\alpha \alpha^2 \Gamma(\alpha) x^{1-\alpha} \int d^\alpha x = -\tau_\alpha k_\alpha \alpha x,$$

$$-\tau_{1-\alpha} k_{1-\alpha} (1-\alpha)^2 \Gamma(1-\alpha) x^\alpha \int d^\alpha x = -\tau_{1-\alpha} k_{1-\alpha} (1-\alpha) x.$$

Equating the both parts, we obtain the solution

$$\ln(I) = -\tau_\alpha k_\alpha \alpha x - \tau_{1-\alpha} k_{1-\alpha} (1-\alpha) x + \ln(C).$$

Potentiating this expression, we obtain general explicit solution

$$I = C \exp(-\{\tau_\alpha k_\alpha \alpha + \tau_{1-\alpha} k_{1-\alpha} (1-\alpha)\} x).$$

Find a particular solution for Cauchy problem with the initial conditions x_0 and $I_0 = I(x_0)$. Expressing the integration constant in terms of the initial conditions, we obtain: $C = \exp(-\{\tau_\alpha k_\alpha \alpha + \tau_{1-\alpha} k_{1-\alpha} (1-\alpha)\} x_0 + \ln(I_0))$.

Substituting the value C into the general solution, we find the particular solution for the defined initial conditions which is the generalization of Bouguer-Lambert-Beer law for the case of light beam propagation in the medium which is the combination of the fractal and the conjugate fractal.

$$I = I_0 \exp[-\{\tau_\alpha \alpha k_\alpha + \tau_{1-\alpha} (1-\alpha) k_{1-\alpha}\}(x - x_0)]. \tag{3}$$

Here $x - x_0 \geq 0$ is the medium thickness through which the photon beam propagates, $\alpha(x - x_0)$ is the fractal effective thickness, and $(1-\alpha)(x - x_0)$ is the conjugate fractal effective thickness for which the equation $(x - x_0) = \alpha(x - x_0) + (1-\alpha)(x - x_0)$ always holds.

In particular, when $\alpha = 1$, (or $\alpha = 0$)), the effective thickness of the fractal (or the conjugate fractal) becomes equal to zero and the topological coefficient will be $\tau_\alpha = 1$ (or $\tau_{1-\alpha} = 1$)) which corresponds to the absence of the fractal (or the conjugate fractal). In these extreme cases, medium becomes continuous, and the relation (3) transforms into the classical Bouguer-Lambert-Beer law, $I = I_0 \exp[-k(x - x_0)]$ [1].

In the case, when $\tau_\alpha k_\alpha \alpha >> \tau_{1-\alpha} k_{1-\alpha}(1-\alpha)$ or $\tau_\alpha k_\alpha \alpha << \tau_{1-\alpha} k_{1-\alpha}(1-\alpha)$, beam attenuation may be neglected in the conjugate fractal or in the fractal. Then the relation will transfer to the Bouguer-Lambert-Beer law for one homogeneous fractal. Such approximation is called single-beam approximation [4].

Assume that the fractal consists of one element atoms, and the conjugate fractal consists of atoms of another element. Suppose that a beam of hard X-radiation with the wave length of less than one angstrom propagates through the medium in a second. In this case the inner diffraction may be neglected. Then attenuation coefficients for the X-radiation propagation through the fractal and the conjugate fractal will be [5]

$$k_\alpha = k_{\alpha|A}(\lambda) + k_{\alpha|S}(\tau) \approx \frac{\eta_\alpha N_A}{A_\alpha}\left(B_\alpha Z_\alpha^4 \lambda^3 + \frac{8\pi e^4 Z_\alpha}{3m^2c^4}\right),$$

$$k_{1-\alpha} = k_{1-\alpha|A}(\lambda) + k_{1-\alpha|S}(\tau) \approx \frac{\eta_{1-\alpha} N_A}{A_{1-\alpha}}\left(B_{1-\alpha} Z_{1-\alpha}^4 \lambda^3 + \frac{8\pi e^4 Z_{1-\alpha}}{3m^2c^4}\right).$$

Here $k_{\alpha|A}(\lambda)$ and $k_{1-\alpha|A}(\lambda)$ are absorption coefficients associated with the interaction of X-radiation with the atom shell inner electrons of the fractal and the conjugate fractal (inner photo effect); $k_{\alpha|S}(\tau)$ and $k_{1-\alpha|S}(\tau)$ are scattering coefficients for the fractal and the conjugate fractal material; B_α and $B_{1-\alpha}$ are semi-empirical coefficients depending on photon wave length and on atom structure of the fractal and the conjugate fractal material [3]; Z_α and $Z_{1-\alpha}$ are nuclear charges of the elements which compose the fractal and the conjugate fractal; η_α and $\eta_{1-\alpha}$ are densities of the fractal and the conjugate fractal material; N_A is the Avogadro number; A_α and $A_{1-\alpha}$ are weights of one gamma atom (atomic weight) of the fractal and the conjugate fractal material; e is the electron charge; m is the electron mass; is light velocity.

Substituting the obtained expressions for the coefficients k_α and $k_{1-\alpha}$ into (2), we obtain the Bouguer-Lambert-Beer law describing the propagation of the hard X-radiation through the medium composed of two homogeneous and orthogonal fractals

$$I = I_0 \exp\left[-\left\{\tau_\alpha \alpha\left(\frac{\eta_\alpha N_A}{A_\alpha}\left(B_\alpha Z_\alpha^4 \lambda^3 + \frac{8\pi e^4 Z_\alpha}{3m^2c^4}\right)\right) + \right.\right.$$

$$\left.\left. + \tau_{1-\alpha}(1-\alpha)\frac{\eta_{1-\alpha} N_A}{A_{1-\alpha}}\left(B_{1-\alpha} Z_{1-\alpha}^4 \lambda^3 + \frac{8\pi e^4 Z_{1-\alpha}}{3m^2c^4}\right)\right\}(x - x_0)\right].$$

For the problem under consideration, it is possible to accept to a high accuracy $\tau_{1-\alpha} = \tau_\alpha = 1$.

References

1. Ahmanov S.A., Nikitin S. Yu. *Fizicheskaya optika*[Physical optics]. Moscow, Nauka Publ., 2004. 656 p.

2. Churikov V.A. Zamechaniya po povodu drobnoj razmernosti pri opisanii processov vo fraktalah [Comments on the fractional dimension in describing processes in fractals]. *Trudy 7 Vserossijskoj molodezhnoj*

nauchno-innovacionnoj shkoly "Matematika i matematicheskoe modelirovanie" [Proc. 7th All-Russian Youth Research and Innovation School "Mathematics and Mathematical Modeling"]. Sarov, 2013, pp. 59.

3. Churikov V.A. Kratkoe vvedenie v drobnyj analiz celochislennyh poryadkov [A brief introduction to the detailed analysis of integer orders]. Tomsk, TPU Publ., 2011. 72 p.

4. Churikov V.A. Zamechaniya o metode razdeleniya potokov bez obmena pri opisanii fizicheskih processov na fraktalah [Note the method of separation of flows without sharing in the description of physical processes on fractals].*Trudy 7 Vserossijskoj molodezhnoj nauchno-innovacionnoj shkoly "Matematika i matematicheskoe modelirovanie"* [Proc. 7th All-Russian Youth Research and Innovation School "Mathematics and Mathematical Modeling"]. Sarov, 2013. pp. 54–55.

5. Blohin M.A. *Fizika rentgenovskih luchej* [X-ray physics]. Moscow, GITTL Publ., 1957. 518 p.

Original article submitted: 03.12.2014

Bulletin KRASEC. Phys. & Math. Sci, 2014, vol. , no. 2, pp. 62-69. ISSN 2313-0156

MSC 65C20

THE USE OF PARALLEL PROGRAMMING METHODS FOR TIME-FREQUENCY ANALYSIS OF GEOACOUSTIC EMISSION SIGNALS

A.A. Kim[1, 2]

[1] Institute of Cosmophysical Researches and Radio Wave Propagation Far-Eastern Branch, Russian Academy of Sciences, 684034, Kamchatskiy Kray, Paratunka, Mirnaya st., 7, Russia

[2] Vitus Bering Kamchatka State University, 683031, Petropavlovsk-Kamchatsky, Pogranichnaya st., 4, Russia

E-mail: a.a.afanaseva@yandex.ru

It has been shown in previous studies that the sparse approximation methods with combined dictionary and refining have been used for this purpose. The main disadvantage of this method is its computational expensive. The realization of parallel matching pursuit algorithm has been considered in this article. It has been shown that using of parallel algorithm speeds up the processing and enables signal analysis in real time.

Key words: sparse approximation, geoacoustic emission, matching pursuit, parallel programming

Введение

Acoustic emissions in solid bodies are elastic oscillations generating in the result of dislocation changes in a medium. Characteristics of the excited pulse radiation are intermediately associated with the peculiarities of plastic processes that determines the interest to the investigation of the emission to develop methods for acoustic diagnostics of a medium. Researches in Kamchatka showed the efficiency of application of acoustic methods for diagnostics of natural environments on the scales, corresponding to sound oscillation wavelengths [1],[2]. The relation between intensification of deformation processes and the behavior of acoustic emission was detected, in particular, during earthquake preparation [1]-[4].

An acoustic signal consists of a series of relaxation oscillations (geoacoustic pulses) with shock excitation, amplitude of 0.1 – 1 Pa, duration of not more than 200 ms, filling frequency of the first units and first tens of kilohertz [2]. Pulse repetition frequency is determined by rock deformations and may change within a wide range, from single signals on a time interval of several seconds during calm periods to tens and even hundreds per a second during anomalies before earthquakes. The most informative pulse

Kim Alina Alexandrovna – Assistent of Dept. Informatics, Vitus Bering Kamchatka State University, Postgraduate Student, Institute of Cosmophysical Research and Radio Wave Propagation FEB RAS.

sections are the front and the beginning of the drop with the duration up to 25 ms and the signal/noise relation up to 30 times which allow us to determine the direction to a source; and the filling frequency contains information on its dimensions and dynamics [2]. Thus, time-frequency analysis of geoacoustic signals is very important for the investigation of emission sources, and, finally, for the diagnostics of plastic process features.

Sparse approximation methods

Application of classical methods for time-frequency analysis (Fourier transform, wavelet-transform, wavelet package and so on) do not give the desired results and do not allow us to determine the inner structure of acoustic signals. In 2011 application of sparse approximation methods to analyze and to detect the structure of acoustic emission signals was suggested at the Laboratory of Acoustic Research of IKIR FEB RAS [5],[6].

Under the signal approximation, we assume a problem of signal presentation in the form of a superposition of some function set from a preassigned dictionary (classes of functions):

$$\begin{array}{l} f(t) = \sum\limits_{m=0}^{N-1} a_m g_m(t) + R_N \\ \|R_N\| \to \min \end{array},$$

where $f(t)$ is the investigated signal, $g_m(t)$ is the element (atom) of the dictionary $D = \{g_m(t), \quad \|g_m\| = 1\}$, $a_m$are the decomposition coefficients, N is the number of expansion elements, R_N is the approximation error.

Sparse approximation assumes the construction of a signal model containing the least number of elements, i.e.

$$\begin{array}{l} f(t) = \sum\limits_{m=0}^{N-1} a_m g_m(t) + R_N \\ \|R_N\| \to \min \\ \|a_m\|_0 \to \min \end{array},$$

where $\|\cdot\|_0$ is the pseudonorm which is equal to the number of nonvanishing terms of a vector.

As a rule, sparse approximation methods are applied for signal decomposition into redundant dictionaries (the number of dictionary atoms is much more than the initial signal dimension) that gives a wide set of tools for the analysis of signal structure. However, this problem is very complicated for computation, and there is no algorithm to solve it during polynomial time.

Pursuit algorithms, searching for effective but not optimal approximations, decrease the computation complexity of the given problem. One of such algorithms is the matching pursuit [7], [8], suggested by Mallat S. snd Zhang Z. The essence of the algorithm comes to the irrational process of the search for dictionary elements minimizing

the approximation error at every step:

$$\begin{cases} R^0 f = f \\ R^n f = \left\langle R^n f, g_{\gamma_n} \right\rangle g_{\gamma_n} + R^{n+1} f \\ g_{\gamma_n} = \arg \left[\max_{g_{\gamma_i} \in D} \left| \left\langle R^n f, g_{\gamma_i} \right\rangle \right| \right] \end{cases}.$$

The choice of the basic dictionary is the important task and it significantly affects the approximation quality. The paper [9] suggested applying a combined dictionary which is composed from:

- scaled, modulated and time shifted Gaussian functions

$$g(t) = Ae^{-Bt^2} \sin(2\pi f t);$$

- scaled, modulated and time shifted Berlage functions

$$g(t) = At^n e^{-Bt} \cos\left(2\pi f t + \frac{\pi}{2}\right).$$

It was shown [10] that Berlage functions have the same structure as the geoacoustic emission (GAE) elementary pulses, that is why, the sections containing a pulse approximate better. In contrast with that, it is better to apply Gaussian functions for approximation of noise sections of a signal. Thus, application of a combined dictionary is an optimal solution for approximation of GAE signals by matching pursuit method [9].

To increase the quality of signal approximation, a modified method of matching pursuit with refinement was suggested. When the dictionary element, minimizing the approximation error at this step, is determined, an additional dictionary is constructed in its vicinity, where the search for the more significant atom for decomposition is carried out.

The research has shown that application of the modified method of matching pursuit applying combined dictionaries and the refinement algorithm improves the quality of approximation and gives the possibility of analysis of GAE signal inner structure [9]. However, the considerable disadvantage of the proposed method is its computation complexity, the time of signal analysis was tens of times the signal duration.

The most complex procedure of the method is the determination of a covariance matrix. Assume that there is a signal S with count length L and a dictionary D, composed of N atoms with count length M. Then the covariance matrix C has the dimension $N \times (L+M-1)$ and is calculated by the formula

$$_{i,j} = \sum_{k=\max(1,j+1-M)}^{\min(j,1)} D_{i,k} \cdot S_{M-j+k}.$$

The time for matrix computation is more than 90%from the total time of execution of iteration 1 (Table 1).

Table 1

Time for computation of a covariance matrix

Signal length L, counts	Execution time for iteration 1, ms	Computation time for covariance matrix, ms
1000	291	274
2500	717	695
5000	1434	1396
10000	2859	2796

To speed up the algorithm, in particular, covariance matrix computation, it is appropriate to apply methods of parallel computation. Development of a parallel algorithm implies several stages [4]:

1) decomposition;

2) detection of information dependences;

3) scaling and distribution of sub-problems between the processors.

Decomposition suggests partition of the algorithm or its part into the finite number of sub-problems. The most complex procedure of the method performs a homogeneous processing of large volume of data; each element of a covariance matrix is computed independently from other ones by the same formula. The homogeneous processing of a large volume of information allows us to use parallelism at data level. Let every sub-problem calculate one element of the covariance matrix $_{i,j}$, then the number of sub-problems k is equal to the number of elements in the matrix C: $k = N \times (L + M - 1)$. All the determined sub-problems depend only on initial data and do not depend on each other that indicates inner parallelism in the considered procedure and total information independence of sub-problems.

To realize the developed parallel algorithm, it was decided to apply CUDA technology based on SIMD (Single Instruction stream/Multiple Data stream) conception. CUDA is a software-hardware platform which is used to organize parallel computations on graphic processing units (GPU) [3]. The basic notion of CUDA software model is a Thread. Threads are joint into blocks, and the block, in their turn, are joint into nets. Net and blocks may be one-, two-, and three-dimensional. The number and dimensionality of net components are determined by video card class and version. Application of such grouping allows us to run millions of threads, and it saves the programmer from the necessity of scaling of computational blocks. If a GPU does not have enough resources, bocks will be executed sequentially. It is only necessary to define the dimension of the running net. Let the number of threads n_t , running in every block, be equal to 256. This number gives an optimum relationship of the used memory and delays [13]. Consequently, the number of blocks n_b, required to calculate the covariance matrix, will be determined as follows: $n_b = k/256$.

To realize the parallel algorithm of the matching pursuit method, MS Visual Studio 2010 programming environment and CUDA 5.0 package were used.

It should be noted that the major part of the method is executed on the central processing unit (CPU), but the most complex process of covariance matrix computation is sent to the video card (GPU), where a net, consisting of n_b blocks with n_t threads each, is run. One thread calculates one element of a covariance matrix. After execution of all the threads from all the blocks, the output matrix C is transferred into CPU memory, and the algorithm is executed on the central processor again.

Testing of the parallel algorithm operability was carried out on real geoacoustic signals with sampling frequency of 48 KHz. A notebook with Intel Core i3-2330M central processor (2.2 GHz) and NVIDIA GeForce 410M video card (48 CUDA cores, performance 73 Gflops) was used in the experiment. Execution times for standard and parallel algorithms of the matching pursuit were measured for signal sections of different lengths and different number of iterations (Table 2).

Table 2

Speedup of signal approximation when applying parallel algorithm

Iteration number	Standard method, ms	Parallel algorithm, ms	Speedup, times
Signal length = 100 counts			
1	249	47	5,3
5	1285	235	5,5
10	2391	449	5,3
20	4912	884	5,6
Signal length = 250 counts			
1	568	55	10,3
5	2781	279	10
10	5584	557	10
20	11440	1100	10,4
Signal length = 500 counts			
1	1135	72	15,8
5	5032	362	13,9
10	10743	721	14,9
20	20580	1404	14,7
Signal length = 1000 counts			
1	2307	101	22,8
5	10696	506	21,1
10	19296	1010	19,1
20	41908	2017	20,8

We should note, that the combined dictionary composed of 1040 atoms (640 Berlage functions and 400 Gaussian functions) was applied. The refinement algorithm for dictionary atoms was also used; at every algorithm iteration, a distinguished atom was refined five times.

The developed parallel algorithm of matching pursuit applying the combined dictionary and refinement algorithms was introduced as a software module of the system for

automatic detection and analysis of GAE pulses at the Laboratory of Acoustic Research of IKIR FEB RAS where it showed high speed of operation in comparison to standard (nonparallel) method. The system was implemented in a PC with Intel(R) Pentium(R) CPU G2120 (3.10 GHz) and NVIDIA GeForce GTX 760 video card (1152 CUDA cores, performance 2258 Gflops).

GAE signals in the form of 15-minute wav-files are fed to the input of the system. The system detects possible pulses from a signal according to a certain algorithm and transfers them sequentially for the processing by the matching pursuit method. The obtained pulse decomposition is saved into a file.

Application of a standard (nonparallel) algorithm of matching pursuit allowed us to process a 15-minute signal with sampling frequency of 48 KHz for 65 minutes on the average. Implementation of the method parallel algorithm applying the combined dictionary and the refinement algorithm reduced the time for processing of such files to 50 seconds.

Figure shows an example of application of the matching pursuit parallel method on a section of acoustic emission signal with the length of 289 counts.

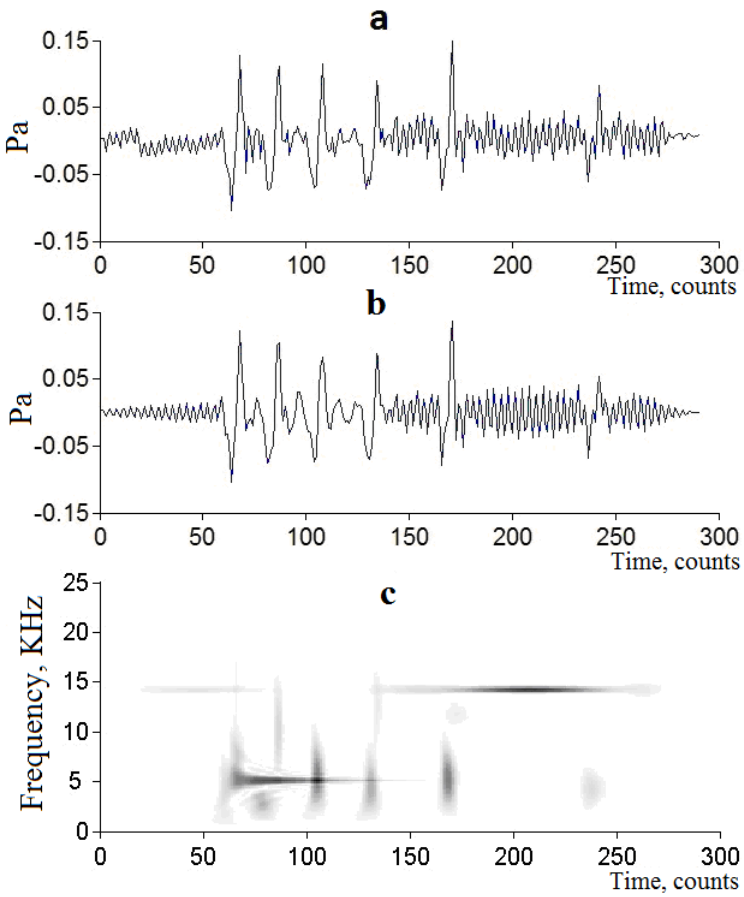

Figure. Analysis of geoacoustic signal applying the parallel algorithm of matching pursuit method (*a* – the initial signal, *b* – the reconstructed signal, *c* – signal frequency-time structure)

Conclusion

Testing on real data showed that application of the parallel algorithm of matching pursuit method applying the combined dictionary and the refinement algorithm speeded up significantly the processing of GAE signals. Application of the obtained algorithm as a system module for automatic detection and analysis of GAE pulses allowed us to process the data in real time mode.

References

1. Kupcov A. V., Larionov I.A., Shevcov B.M. Osobennosti geoakusticheskoj 'emissii pri podgotovke kamchatskih zemletryasenij [Features geoacoustic emission during preparation Kamchatka earthquakes]. *Vulkanologiya i sejsmologiya – Volcanology and Seismology*, 2005, no. 5, pp. 45-59.

2. Marapulec Yu.V. Shevcov B.M. *Mezomasshtabnaya akusticheskaya 'emissiya* [Mesoscale acoustic emission]. Vladivostok, Dal'nauka Publ., 2012.

3. Gordienko V.A., Gordienko T.V., Kupcov A.V., Marapulec Yu.V., Shevcov B.M., Rutenko A.N. Geoakusticheskaya lokaciya oblastej podgotovki zemletryasenij [Geoacoustic location of earthquake preparation areas]. *Doklady Akademii Nauk – Reports of the Academy of Sciences*, 2006, vol. 407, no. 5, pp. 669-672.

4. Dolgih G.I., Kupcov A.V., Larionov I.A., Marapulec Yu.V., Shvec V.A., Shevcov B.M., Shirokov O.N., Chupin V.A., Yakovenko S.V. Deformacionnye i akusticheskie predvestniki zemletryasenij [Deformation and acoustic earthquake precursors]. *Doklady Akademii Nauk – Reports of the Academy of Sciences*, 2007, vol. 413, no. 1., pp. 96-100.

5. Marapulec Yu.V., Tristanov A.B. Primenenie metoda razrezhennoj approksimacii v zadachah analiza signalov geoakusticheskoj 'emissii [Application of the sparse approximation for the analysis of signals geoacoustical emission]. *Cifrovaya obrabotka signalov – Digital signal processing*, 2011, no. 2, pp. 13-17.

6. Afanas'eva A.A., Lukovenkova O.O. Metody obnaruzheniya impul'sov geoakusticheskoj 'emissii na osnove algoritmov razrezhennoj approksimacii i klasterizacii [Methods of detection pulses geoacoustical emission based on sparse approximation algorithms and clustering]. *Vestnik KRAUNC. Fiziko-matematicheskie nauki – Bulletin of the Kamchatka Regional Association «Education-Scientific Center». Physical & Mathematical Sciences*, 2013, vol. 7, no. 2, pp. 68-73.

7. Mallat S., Zhang Z. Matching pursuits with time-frequency dictionaries. *IEEE Transactions on Signal Processing*, 41(12), pp. 3397-3415.

8. Mallat S. *A Wavelets Tour of Signal Processing.*. New York, Academic Press, 1999. (Russ. ed.: Malla S. Vejvlety v obrabotke signalov. Moscow, Mir Publ., 2005. 672 p.)

9. Lukovenkova O.O., Tristanov A.B. Adaptivnyj algoritm soglasovannogo presledovaniya s utochneniem na smeshannyh slovaryah v analize signalov geoakusticheskoj 'emissii [Adaptive algorithm prosecution agreed with the specification for mixed signal analysis in dictionaries geoacoustical emission]. *Cifrovaya obrabotka signalov – Digital signal processing*, 2014, no. 2, pp. 54-57.

10. Afanas'eva A.A., Lukovenkova O.O., Marapulec Yu.V., Tristanov A.B. Primenenie razrezhennoj approksimacii i metodov klasterizacii dlya opisaniya struktury vremennyh ryadov akusticheskoj 'emissii [Application of sparse approximation and clustering methods for describing the structure of the time series of acoustic emission]. *Cifrovaya obrabotka signalov – Digital signal processing*, 2013, no. 2, pp. 30-34.

11. Voevodin V.V., Voevodin Vl.V. *Parallel'nye vychisleniya* [Parallel Computing]. Saint Petersburg, BVH-Peterburg Publ., 2002. 608 p.

12. Boreskov A.V., Harlamov A.A. *Osnovy raboty s tehnologiej CUDA* [Basics of CUDA technology]. Moscow, DMK Press Publ., 2010. 232 p.

13. Sanders D., K'endrot 'E. *Tehnologiya Cuda v primerah. Vvedenie v programmirovanie graficheskih processorov* [CUDA technology in the examples. Introduction to Programming GPUs]. Moscow, DMK Press Publ., 2011. 232 p.

Original article submitted: 25.11.2014

Bulletin KRASEC. Phys. & Math. Sci, 2014, vol. , no. 2, pp. 70-78. ISSN 2313-0156

MSC 65C20

COMPARISON OF THE SPARSE APPROXIMATION METHODS BASED ON ITS USE TO GEOACOUSTIC EMISSION SIGNALS

O.O. Lukovenkova[1, 2]

[1] Institute of Cosmophysical Researches and Radio Wave Propagation Far-Eastern Branch, Russian Academy of Sciences, 684034, Kamchatskiy Kray, Paratunka, Mirnaya st., 7, Russia

[2] Vitus Bering Kamchatka State University, 683031, Petropavlovsk-Kamchatsky, Pogranichnaya st., 4, Russia

E-mail: o.o.lukovenkova@yandex.ru

The paper is devoted to the comparative analysis of some sparse approximation methods. The first part of the paper describes general sparse approximation problem and two main approaches solved it. Classification of testing pursuit algorithm is illustrated. Features of the methods application to geoacoustic emission signals are considered in the second part. The sparseness, accuracy and runtime of described pursuit algorithms are compared.

Key words: matching pursuit, basis pursuit, geoacoustic emission

Introduction

Since 1999, investigation of geoacoustic emission (GAE) signals has been carried out at different stages of seismic activity at the Institute of Cosmophysical Research and Radio Wave Propagation (IKIR) FEB RAS. A typical GAE signal is a series of relaxation pulses with shock excitation, amplitude of 0.1 – 1 Pa, filling frequency from the units to the first tens of kHz (Fig. 1) [1].

Signal registration is carried out continuously with the sampling frequency of 48 kHz which does not allow manual processing. As a rule, classical methods of frequency-time analysis are applied for the analysis of pulse nature signals. However, during the last years, methods of sparse approximation become more popular. The paper compares sparse approximation algorithms in accuracy, sparseness of the obtained solution and time of execution on the example of GAE signals.

Lukovenkova Olga Olegovna – Assistent of Dept. Informatics, Vitus Bering Kamchatka State University, Postgraduate Student, Institute of Cosmophysical Research and Radio Wave Propagation FEB RAS.

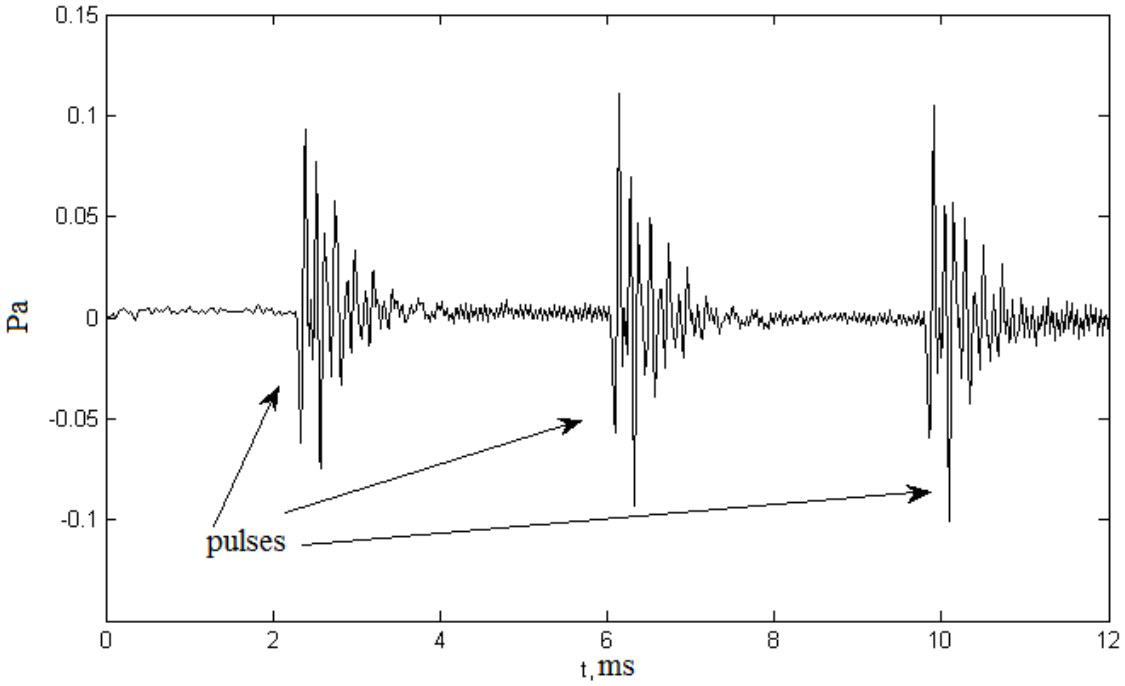

Fig. 1. GAE signal

Sparse approximation

Signal approximation is a problem of signal decomposition in some function set (function dictionary):

$$f(t) = \sum_{m=0}^{N-1} a_m g_m(t) + R_N, \|R_N\| \to \min,$$

where $f(t)$ is the signal under the investigation, $g_m(t)$ is the element (atom) of the dictionary $D = \{g_m(t), \quad \|g_m\| = 1\}$, a_m – are the decomposition coefficients, N is the number of decomposition elements, R_N is the approximation error.

Sparse approximation assumes building of a signal model, containing the least number of elements, i.e.

$$f(t) = \sum_{m=0}^{N-1} a_m g_m(t) + R_N, \|R_N\| \to \min, \|a\|_0 \to \min,$$

where $\|\cdot\|_0$ is the pseudonorm (L_0-norm), equal to the number of nonvanishing terms of a vector.

One of the main advantages of sparse approximation is the possibility to build signal decomposition simultaneously containing the least number of elements and minimizing the error in redundant unorthogonal dictionary, in general case. A redundant dictionary contains the number of atoms which significantly exceeds the dimensionality of the initial signal. However, such type of problems of search for an optimum basis of decomposition is very complicated for computation and may not be solved for the polynomial time.

There are two different approaches to the sparse approximation of signals. The both make the computation of the given problem not so complicated and find an effective but not an optimum solution:

1) Basis Pursuit (BP). The essence of this approach, suggested by Chen S.S. and Donoho D.L. [2], comes to the change of the computationally complicated problem of L_0-approximation by an easier problem of L_1-approximation.

$$D \cdot a = f, \|a\|_1 \to \min,$$

where

$$\|a\|_1 = \sum_{m=0}^{N-1} |a_m|.$$

Minimization of L_1-norm eliminates energy f dissipation in dictionary D atoms, thus, reducing the number of elements of the desired decomposition.

The basis pursuit problem may be simplified by the change of L_1-norm minimization by its limitation [2].

$$f(t) = \sum_{m=0}^{N-1} a_m g_m(t) + R_N, \|R_N\| \to \min, \|a\|_1 < \lambda.$$

We should note that basis pursuit is an optimization principle rather than a concrete algorithm for solution of a problem. The basis pursuit problem may be solved by the reduction to the problem of linear programming [2] or by one of optimization methods [3],[4] refining the given initial approximation at each iteration.

1) Matching Pursuit (MP) was suggested by Mallat S. and Zhang Z. [5]. The essence of the algorithm comes to the iterative process of search for dictionary elements minimizing the approximation error at every step.

$$\begin{cases} R^0 f = f \\ s = \arg\left[\min_m \left|\langle g_m, R^N f\rangle\right|\right] \\ R^{N+1} f = R^N f - \langle g_s, R^N f\rangle g_s \end{cases}.$$

On the basis of the matching pursuit method, an orthogonal matching pursuit (OMP) method was developed. The main difference of it from the classical realization is the orthogonal basis, minimizing the approximation error [6].

$$\begin{cases} R^0 f = f, \qquad U = \emptyset \\ s = \arg\left[\min_{m \notin U} \left|\langle g_m, R^N f\rangle\right|\right] \\ U = U \cup s \\ a^N = D_U^+ f \\ R^{N+1} f = f - D \cdot a^N \end{cases}.$$

Classification of approximation algorithms for signals, tested on GAE signals, is illustrated in Fig. 2.

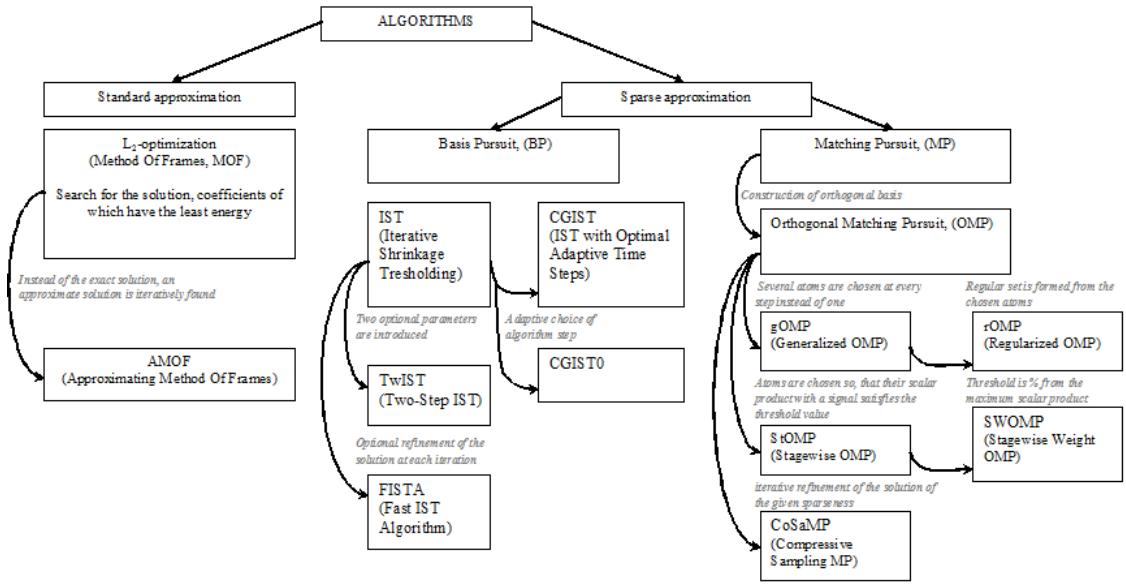

Fig. 2. Classification of signal approximation algorithms

Comparison of sparse approximation methods on GAE signals

To compare the algorithms of sparse approximation, a sample was formed which contained 100 clear pulses, distinguished from GAE signals, with the amplitude of 0.02 – 0.05 Pa, filling frequency of 5-10 kHz (Fig. 3), and duration of 8 ms. Preliminary processing of signals included filtration in the frequency range of 1-24 kHz and amplitude normalizing.

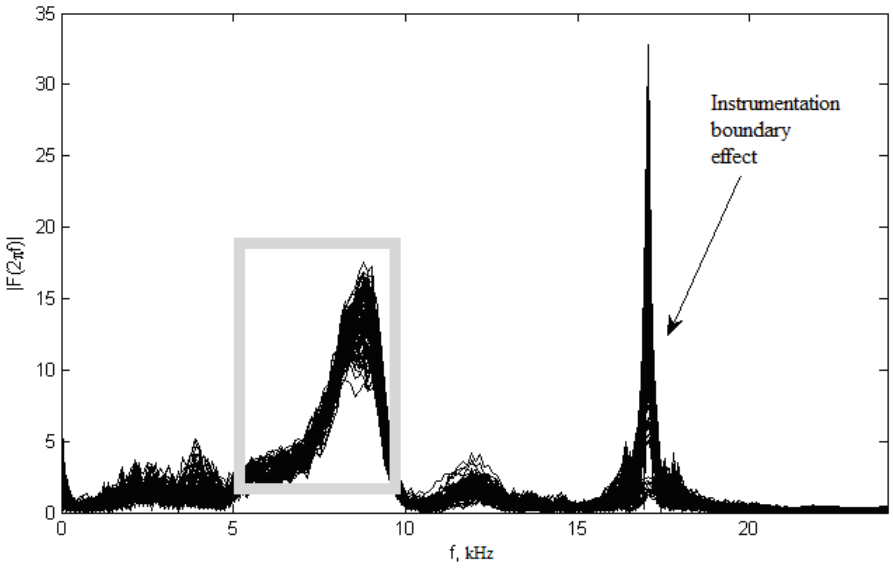

Fig. 3. Spectrum of the chosen pulses

Choice of the dictionary D is an important problem which determines the quality of further analysis. The previous papers showed that the most effective dictionary for geoacoustic signal approximation is the dictionary formed from Berlage modulated

functions, since Berlage pulses have similar structure with geoacoustic emission elementary pulses [7]-[9]. In the course of the experiments, a dictionary was chosen which gave an appropriate accuracy of approximation. The dictionary, applied in the experiment, contained 2460 Berlage functions with the following parameters: duration of 3.8 ms, envelope maximum at 152 – 0.95 ms from the pulse beginning, filling sinusoid frequency from 4,5 to 10,5 kHz (Fig. 4).

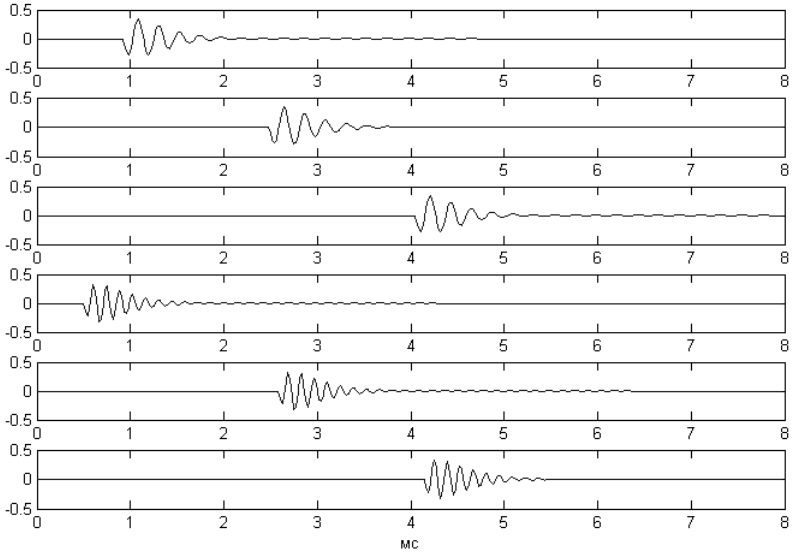

Fig. 4. Examples of dictionary atoms

For each signal under the investigation, a classical approximation (all dictionary atoms were included into signal decomposition) was constructed obtained by solving the L_2-optimization problem. In the result of the analysis of the obtained decomposition coefficient vectors, it was determined that in every of the 100 solutions, all the 2460 coefficients were nonvanishing. However, in average, only 991 coefficients in the decomposition had values exceeding 1% from the maximum, and only 294 coefficients exceeded the threshold of 5% (Fig. 5).

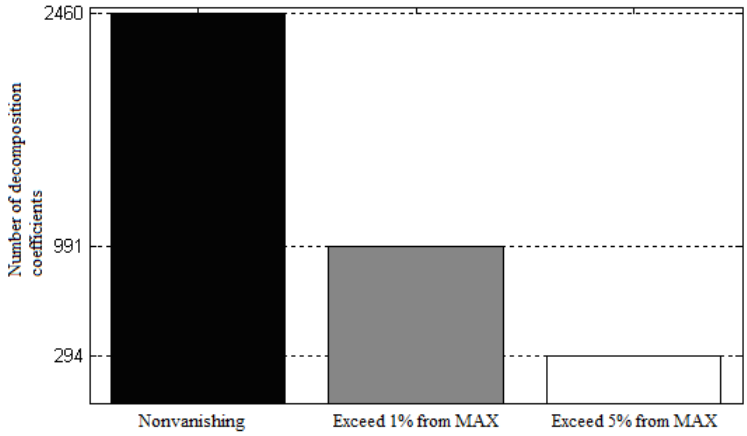

Fig. 5. Results of L_2-optimization

Thus, the correlation of more than a half of the dictionary atoms with the signal was insignificant, so the obtained decomposition was redundant. Redundancy of the presentation may be avoided if sparse approximation of the given data is executed on the defined dictionary.

Applying the sparse approximation method, one should remember, that in comparison to matching pursuit, it is impossible in the basis pursuit algorithms to define the exact limitation on L_0-norm of the desired coefficient vector and sparseness degree is regulated by a control parameter μ, the higher its value is, the less is the L_0-norm of decomposition coefficients and larger the error [4].

$$\mu \|a\|_1 + \frac{1}{2} \left\| R^N f \right\|^2 \to \min .$$

The choice of the proper values for the control parameter and algorithm step, which ensure the required relation «sparseness-error», is a complicated problem solved only by experimental selection (Fig. 6).

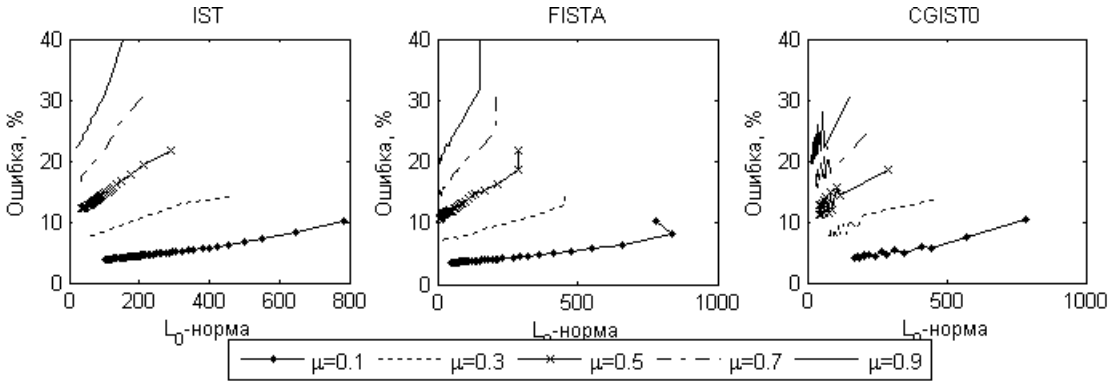

Fig. 6. Influence of parameter μ on the solution of basis pursuit problem

In most of the matching pursuit algorithms, except for StOMP and SWOMP, L_0-norm of coefficient vectors either depends on the number of iterations (it coincide in the case with MP and OMP) or is directly indicated as an input parameter of the algorithm (CoSaMP) that is more convenient for the researcher, if the priority is given to the solution sparseness.

Fig. 7 shows the graphs of the dependence for average approximation error of the investigated signals on the mean value of coefficient vector L_0-norm for different algorithms of sparse approximation. The values 0.5 and 0.7 were experimentally selected as the control parameters μ for basis pursuit algorithms. They gave the proper error level and solution sparseness. TwIST pursuit algorithm is applied for the dictionaries satisfying the condition $0 < k \le \lambda_{\min}(D^T D) \le 1$, for the defined dictionary $\lambda_{\min}(D^T D) < 0$, so this algorithm was excluded from the list of tested ones.

From the graphs in Fig. 7(a) and 7(b), the differences in the dynamics of error decrease for matching and basis pursuit methods are clear. In the first case, the error gradually decreases with the increase of the number of decomposition elements, in the second case it decreases with the decrease of element number.

If every algorithm is presented as an ellipse with semiaxes, corresponding to confidence intervals of resultant L_0-norm and error average values, then the efficiency of application

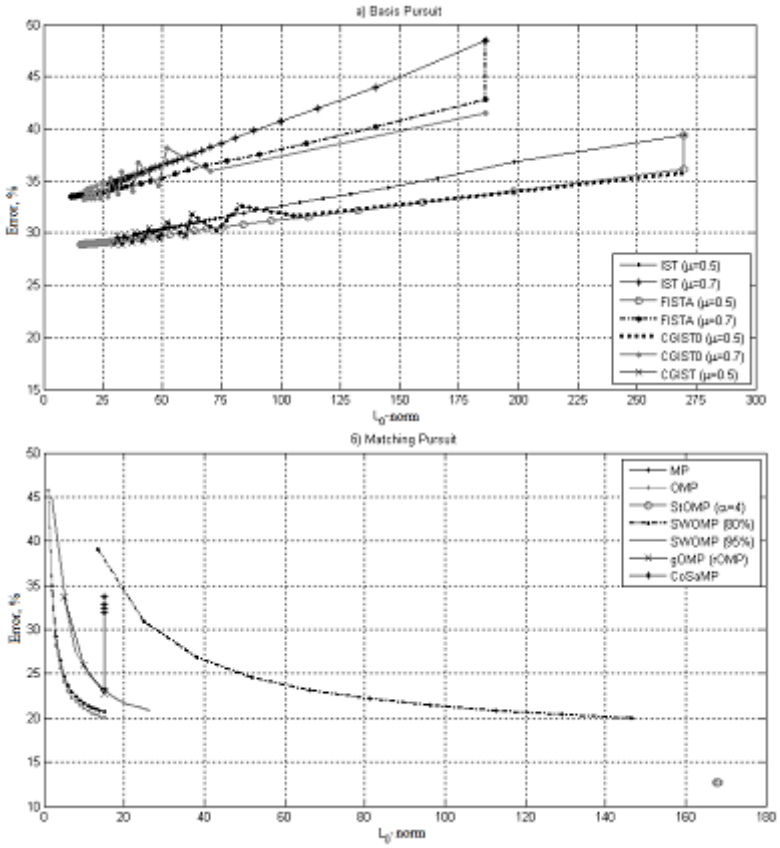

Fig. 7. Dependence of error decrease on solution sparseness

of the algorithm for the investigated signals and the defined dictionary may be evaluated by the arrangement of this ellipse on the coordinate plate (Fig. 8).

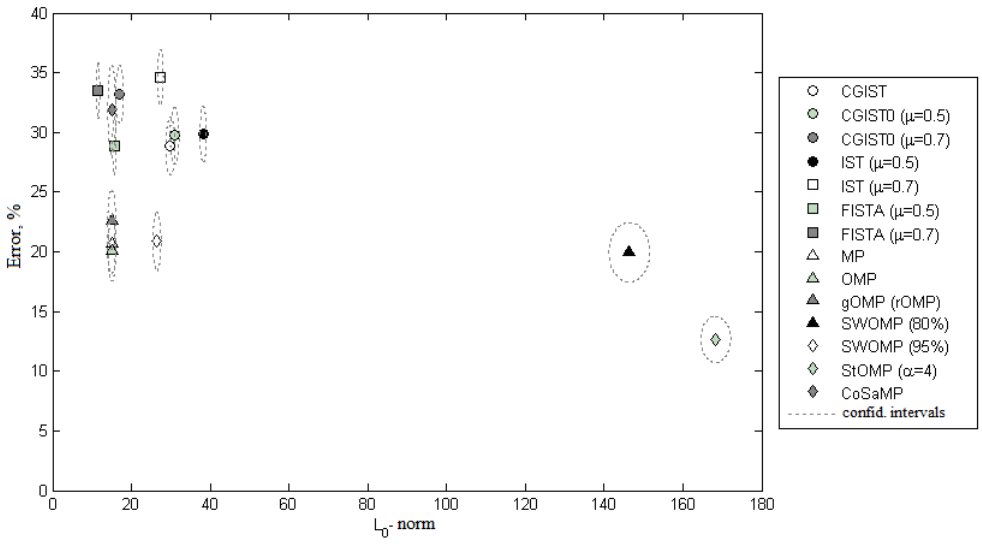

Fig. 8. The relation «sparseness-error» for sparse approximation algorithms

Table shows the time for execution of 20 algorithm iterations, sparseness and error averaged for 100 pulses. The computations were carried out on a PC with the following characteristics: Intel Core i5-3210M processor (2.50 GHz), main memory size 4 Gb.

Table

Pursuit algorithm characteristics

Method	**Execution time for 20 iter., sec**	**Res. L_0**	**Res. error**
OMP	0.8644	15	20%
MP	0.7927	15	21%
gOMP (rOMP)	time depends on the parameters 10 it. with 2 atoms: 0.4693 (0.5191) 4 it. with 5 atoms 0.2423 (0.2832) 2 it. with 10 atoms: 0.1651 (0.2119)	15	23%
FISTA (μ=0.5)	1.3582	16	29%
SWOMP (95%)	0.9770	26	21%
CoSaMP	0.1310	15	32%
FISTA (μ=0.7)	1.3582	12	33%
CGIST0 (μ=0.7)	15.6585	17	33%
CGIST (μ=0.5)	27.8995	30	29%
CGIST0 (μ=0.5)	15.6585	31	30%
IST (μ=0.7)	1.3509	27	35%
IST (μ=0.5)	1.3509	38	30%
SWOMP (80%)	2.0469	146	20%
StOMP (α=4)	1.3351	168	13%

According to the graph, shown in Fig. 8, and Table data, MP, OMP, gOMP matching pursuit methods are the most effective for the relation «sparseness-error». In the course of testing of rOMP, it was determined that for the investigated signals, a set of atoms, chosen for each iteration, is already regular, so approximation solutions, obtained by rOMP and gOMP, are identical. From the basis pursuit methods, FISTA gave the best results. Comparison of execution times for the algorithms showed that matching pursuit algorithms are faster than the basis pursuit ones, as long as, in practice, 15-20 iterations of matching pursuit algorithms and 50-70 iterations of basic pursuit algorithms are needed to achieve an optimum result.

Conclusion

In the result of the study, we may conclude that the solutions obtained by matching pursuit algorithms, MP, OMP, and gOMP, have better sparseness and higher accuracy in comparison to the solutions obtained by other considered algorithms. The algorithms are less complicated and, consequently, their application in GAE signal analysis is reasonable and effective. The choice between the three algorithms is determined by the requirements of a researcher: the fastest one is gOMP, the most accurate one is OMP, MP is the «golden mean».

References

1. Marapulec Yu.V. Shevcov B.M. *Mezomasshtabnaya akusticheskaya 'emissiya* [Mesoscale acoustic emission]. Vladivostok, Dal'nauka Publ., 2012.

2. Chen S. S., Donoho D. L., Saunders M. A. Atomic decomposition by basis pursuit. *SIAM Journal on Scientic Computing*, 1998, vol. 20, no. 1, pp. 33–61.

3. Beck A. and Teboulle M. A Fast Iterative Shrinkage-Thresholding Algorithm for Linear Inverse Problems. *Siam J. Imaging Sciences*, 2009, vol. 2, no. 1, pp. 183–202.

4. Goldstein T., Setzer S. High-order methods for basis pursuit. Los Angeles, Preprint University of California, 2010.

5. Mallat S., Zhang Z. Matching pursuits with time-frequency dictionaries. *IEEE Transactions on Signal Processing*, 1993, 41(12), pp. 3397-3415.

6. Tropp J. A. and Gilbert A. C. Signal recovery from random measurements via orthogonal matching pursuit. *IEEE Transactions Information Theory*, 2007, vol. 53, no. 12, pp. 4655–4666.

7. Marapulec Yu.V., Tristanov A.B. Primenenie metoda razrezhennoj approksimacii v zadachah analiza signalov geoakusticheskoj 'emissii [Application of the sparse approximation for the analysis of signals geoacoustical emission]. *Cifrovaya obrabotka signalov – Digital signal processing*, 2011, no. 2, pp. 13-17.

8. Marapulec Yu.V., Tristanov A.B. Razrezhennaya approksimaciya akusticheskih vremennyh ryadov s ispol'zovaniem chastotno-vremennogo slovarya Berlage [Sparse approximation of the acoustic time series with time-frequency vocabulary Berlage]. Trudy Rossijskogo nauchno-tehnicheskogo obschestva radiotehniki, 'elektroniki i svyazi im. A.S. Popova. Seriya: Cifrovaya obrabotka signalov i ee primenenie [Proc. of the Russian Scientific and Technical Society of Radio Engineering, Electronics and Communication named after AS Popova]. Moscow, 2012, vol. 1, pp. 91-94.

9. Afanas'eva A.A., Lukovenkova O.O. Metody obnaruzheniya impul'sov geoakusticheskoj 'emissii na osnove algoritmov razrezhennoj approksimacii i klasterizacii [Methods of detection pulses geoacoustical emission based on sparse approximation algorithms and clustering]. *Vestnik KRAUNC. Fiziko-matematicheskie nauki – Bulletin of the Kamchatka Regional Association «Education-Scientific Center». Physical & Mathematical Sciences*, 2013, vol. 7, no. 2, pp. 68-73.

Original article submitted: 29.11.2014

Bulletin KRASEC. Phys. & Math. Sci, 2014, vol. , no. 2, pp. 79-84. ISSN 2313-0156

MSC 68T10

THE TECHNIQUE OF INCREASE THE EFFICIENCY OF LEARNING NEURAL KOHONEN MAPS FOR RECOGNITION OF PERTURBATIONS GEOACOUSTIC EMISSION

A.V. Shadrin

Institute of Cosmophysical Researches and Radio Wave Propagation Far-Eastern Branch, Russian Academy of Sciences, 684034, Kamchatskiy Kray, Paratunka, Mirnaya st., 7, Russia

E-mail: SugerMas@yandex.ru

This work is dedicated to technique of training Kohonen maps on the example of geoacoustical signal in the subrange 1500-6000 Hz. Describes the parameters of learning the Kohonen maps to classify anomalies in geoacoustical signal on different types.

Key words: geoacoustical emission, geoacoustic signal, disturbance, neural Kohonen maps, learning

Introduction

Scientists from many countries have studied natural catastrophic phenomena for many years. One of the main aims of these researches is the forecast of such events, which would help to reduce human and economic losses. Science predicts hurricanes, floods and other disasters, and only earthquakes are unpredictable, killing people at home where they feel the most safe [1]. Though earthquakes occur suddenly, it has been scientifically proved that it takes some finite time to accumulate energy in a source for rock breaking [2],[3].

One of the perspective directions of investigations to detect anomalies preceding the earthquakes is registration and analysis of geoacoustic emission disturbances. This phenomenon is determined by deformation processes from the sources of future earthquakes. Investigations of geoacoutstic emission are carried out by hydrophones oriented according to the cardinal points and installed in small reservoirs in Kamchatka [4], [5]. The frequency range under study is from 0.1 Hz to 10 kHz (the subranges are: 0.1–10 Hz, 10–50 Hz, 50–200 Hz, 200–700 Hz, 700–1500 Hz, 1500–6000 Hz, 6000–10000 Hz). Signals are stored for every 4 seconds on a PC hard disc. Data analysis showed that for the period 2001-2003, 34 from 74 earthquakes with the magnitude $M>4$, occurred

Shadrin Alexander Vitalyevich – Junior Researcher of Lab. Acoucstic Research, Institute of Cosmophysical Research and Radio Wave Propagation FEB RAS.

at the epicentral distance up to 250 km from observation points, were preceded by a high increase of geoacoustic emission level in kilohertz range within a day [4], [5].

It was ascertained that emission disturbance amplitude depends on earthquake magnitude and epicenter location. Besides the disturbances of geoacoustic nature, the systems register signals determined by bad weather conditions, by precipitation and strong wind, first of all. The frequency range of such effects is also from hundreds of hertz to units of kilohertz, and it is close to the range of disturbances before earthquakes. For the more detailed investigation of geoacoustic emission behavior before seismic events and for its recognition at the background of weather anomalies, there was a necessity to classify signals into the main types: rain, wind, anomalies of deformation nature. Due to the peculiarities of signal registration, application of standard frequency methods for processing is not effective. For this reason, the author applied one of neural network variants, Kohonen maps, the bases of which are data classification and clusterization.

The paper considers a method for Kohonen maps training on the example of a geoacoustic signal, and describes the techniques to solve the problems which arose during the training. To test the method, the subrange of 1500-6000 Hz was taken, since all the major events which need to be classified appear there the most clearly. Network training was carried out on the signal for 2007. The criteria, determining the choice, were the following: starting the operation of the digital system for data registration in this year, and high activity of the signal.

Choice of initial parameters for network training

At the first stage, the training sample was formed from elementary effects of anomalies of different nature with the duration of 80 sec (20 stored for 4 s samples). Then the network was trained by MATLAB program. There are no recommendations how to train Kohonen maps, thus, default training parameters suggested by the program were used. The dimensionality of the network was chosen to be two-dimensional.

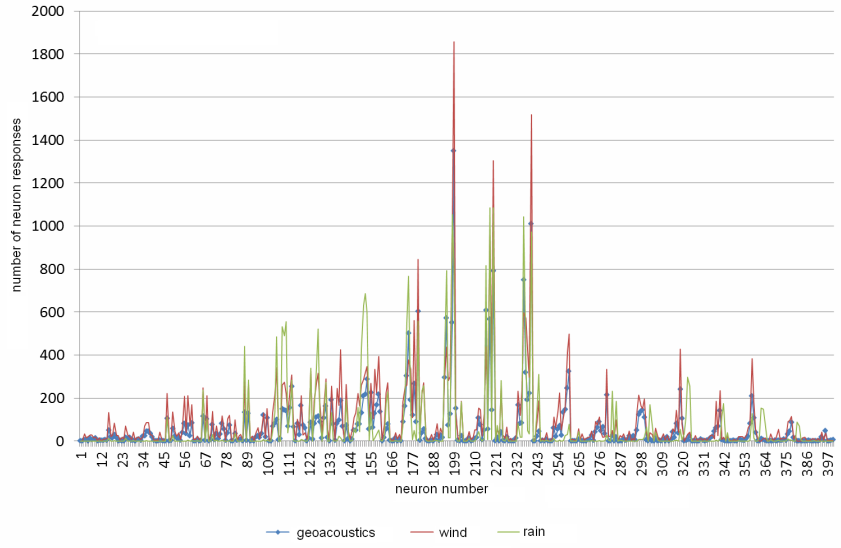

Fig. 1. Neuron distribution of events applying the recommended parameters for network training

After network training, neuron distribution of events was studied, which showed that the network distributed events evenly but could not classify anomalies of different types by separate neurons. It is clear that the same number of responses for signals of different types fall on the same neurons (Fig. 1).

Method for improvement of training efficiency of Kohonen maps

After having analyzed the neural network functioning, a method was developed allowing us to train the network and to separate the signal into different classes.

Due to the large dimensionality of the training sample, the following algorithm for data choice was used. Signal mathematical expectation (ME), its root-mean square deviation (RSD), and their relation to each other were calculated. Only signals which had a unique relation of ME and RSD fitted the training sample. In connection with the fact that it is impossible to determine the definite dependence of network neuron on the type of input signal, every neuron of the network was presented in the form of a ratio of anomaly distribution falling on it. It is considered on the example of estimation of disturbance distributions. Five responses of deformation nature anomalies, 1 response from wind, and 0 responses from rain fall on neuron 1. Processing the result, the estimation is be presented in the following form: 1 anomaly of deformation nature, 0 anomalies from wind, and 0 anomalies from rain. If event distribution on a neuron is even (5 responses of deformation nature anomalies, 5 from wind, and 5 from rain), the estimation is 0.3 0.3 0.3. If two events have the same number of responses, then 0.5 0.5 0 or 0 0.5 0.5 or 0.5 0 0.5. It is necessary to choose the network parameters so, that after the network training, the number of neurons with the result 0.3 0.3 0.3 is minimal, and with 0 0 1, 0 1 0 and 1 0 0 is maximal.

During the network training, it is very important to choose the appropriate number of training epochs that prevents from the lack of training and retraining of the map. There is a set of tools in MATLAB system allowing us to monitor the process of network training. One of them is the graphic representation of arrangement of network weight coefficients in vector space of the training sample during network training. Unfortunately, the tools allow us to see how the trained network covers the input data in space only on two first coordinates. The network frequently covers the whole data cloud unevenly, it is vary clear and noticeable. The training epoch, for which weight coefficients «covered» the input data, is taken as the datum point. Fig. 2 shows the uneven change of the arrangement of map weight coefficients.

After the network training, the total number of neuron responses for deformation nature anomalies is estimated. The network is trained with the step increase of epoch number relative to the datum point so long as the maximal number of neuron responses reaches the maximal level and stops growing. If we continue to increase the number of epochs further, the total number of responses will begin to decrease, and the network becomes retrained, as the consequence.

There may be a situation, when a network with the same number of responses but with different number of training epochs may be obtained. To evaluate the quality of the network, methods for estimation of neural networks, suggested in [6]-[8], may be used. It is qualitative (average quantization error) and quantitative (topographic error) assessment. The qualitative assessment shows the capability of a neural network to reveal the hidden structure and to cluster the data. Such assessment may be applied as

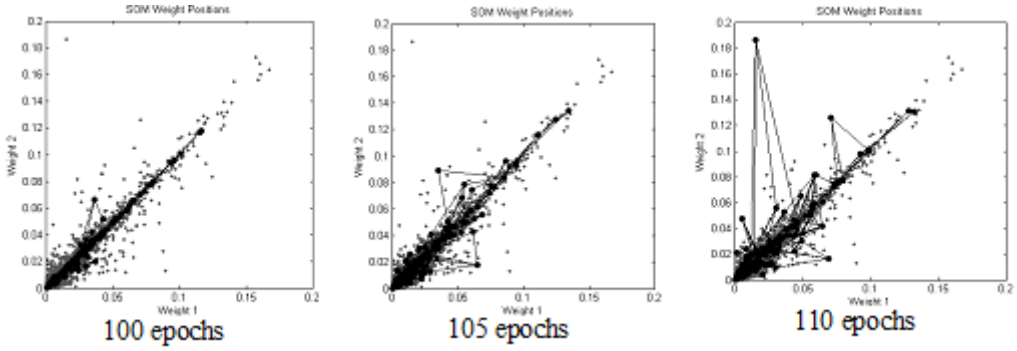

Fig. 2. Uneven change of arrangement of map weight coefficients at different stages of training. Small dots indicate the training sample; large dots, connected by lines, indicate weight coefficients

a map resolution measure. The average quantization error is estimated according to the formula:

$$eq = \frac{1}{N}\sum_{i=1}^{N} d(X, W_w),$$

where N is the total number of input vectors, participating in the assessment of the map; X is the current vector from the input sample; W_w is the vector of neuron winner weights on the current input effect.

The quantitative assessment determines the uninterrupted reflections of input vectors on the map space [6]-[8]. It measures the proportion of all data vectors, for which the first and the second neuron winners are non-adjacent. The less this error is, the better the map keeps its topology. The topographic error is estimated as follows

$$et = \frac{1}{N}\sum_{i=1}^{N} u(X),$$

where X is the current vector from the input sample; $u(X)$ is the function, possessing the value 0 if the first and the second neuron winners of the network are adjacent, and 1 in the contrary case.

Training results

After training the network with best characteristics, neuron distribution of events was re-investigated. It showed that the network could classify the larger part of anomalies of different types by separate neurons (Fig. 3).

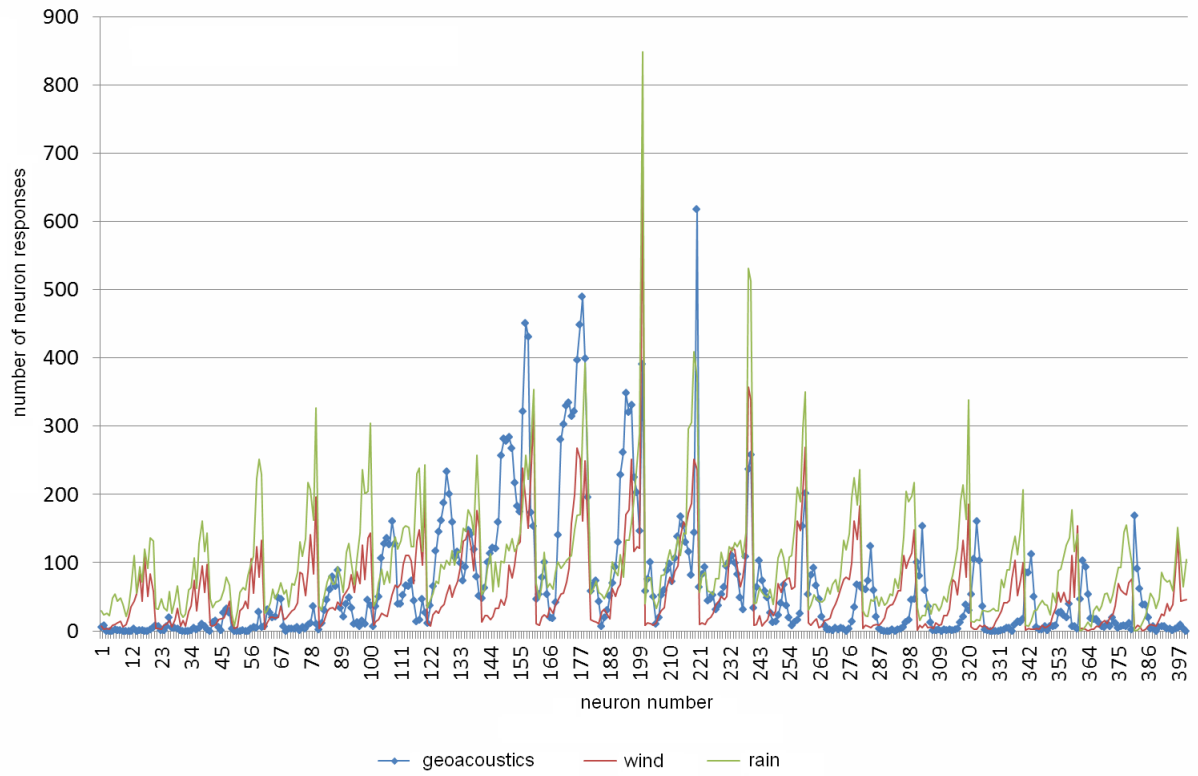

Fig. 3. Neuron distribution of events applying the best parameters of network training

Having chosen the network with best characteristics, the signal for 2007 was analyzed. The obtained assessment of the network was compared with earthquake catalogue [9]. After the comparison, the accuracy of network classification was estimated (Table)

Table

Percentage of signals for 2007 classified correctly

	February	March	April	May	June	July	August	September	October	November	December
Deformation nature anomalies	35	10	4	7	1	4	3	3	4	12	17
Weather anomalies	92	94	96	97	99	98	98	98	98	96	91

As it is clear from the table that the network handled well weather anomalies, and poorly the deformation nature anomalies. It is due to the fact that a great many of anomalies are similar in properties with the signal determined by weather anomalies. For this reason, to improve the recognition results, it is necessary to make additional study on the improvement of network training. Moreover, many experiments showed that it is necessary to perform complex analysis of all the signal subranges to achieve more exact results.

Conclusions

Thus, the developed method allows us to apply Kohonen maps to classify weather anomalies in geoacoustic signal. To improve the accuracy of recognition of deformation nature anomalies, additional investigations are required.

References

1. M. Rodkin. Prognoz nepredskazuemyh katastrof [Forecast unpredictable disasters]. *Vokrug sveta – Round the world*, 2008, no. 6, pp. 88-100.

2. A. G. Sobolev, A. V. Ponomarev. Fizika zemletryasenij i predvestniki [Physics and forerunners of earthquakes]. Moscow, Nauka Publ., 2003. 270 p.

3. Dobrovol'skij I.P., Zubkov S.I., Myachkin V.I. *Ob ocenke razmerov zony proyavleniya predvestnikov zemletryasenij. Modelirovanie predvestnikov zemletryasenij* [On the estimation of the size of the zone display of earthquake precursors. Simulation of earthquake precursors]. Moscow, Nauka Publ., 1980. pp. 7–44.

4. A. V. Kupcov, Yu. V. Marapulec, B. M. Shevcov. Analiz izmenenij geoakusticheskoj 'emissii v processe podgotovki sil'nyh zemletryasenij na Kamchatke []. *Issledovano v Rossii – Investigated in Russia*, 2004, vol. 262, pp. 2809-2818. URL: http://zhurnal.ape.relarn.ru/articles/2004/262.pdf.

5. Kupcov A. V., Larionov I.A., Shevcov B.M. Osobennosti geoakusticheskoj 'emissii pri podgotovke kamchatskih zemletryasenij [Features geoacoustic emission during preparation Kamchatka earthquakes]. *Vulkanologiya i sejsmologiya – Volcanology and Seismology*, 2005, no. 5, pp. 45-59.

6. J. Schatzmann. Using Self-Organizing Maps to Visualise Clusters and Trends in Multidimensional Datasets BEng thesis, Imperial College. June 19. 2003. URL: http://mi.eng.cam.ac.uk/~js532/papers/schatzmann03soms.pdf)

7. Vesanto J. Data Exploration Process Based on the Self-Organizing Map, Acta Polytechnica Scandinavica. *Mathematics and Computing Series*, 2002, no. 115, pp. 96.

8. Arsuaga Uriarte, F. Diaz Martin. Topology Preservation in SOM. *PWASET*, 2006, vol. 15, pp. 187-191.

9. Mischenko M.A. Statisticheskij analiz vozmuschenij geoakusticheskoj 'emissii, predshestvuyuschih sil'nym zemletryaseniyam na Kamchatke [Statistical analysis of the perturbation geoacoustical emission prior to strong earthquakes in Kamchatka]. *Vestnik KRAUNC. Fiziko-matematicheskie nauki – Bulletin of the Kamchatka Regional Association «Education-Scientific Center». Physical & Mathematical Sciences*, 2011, vol. 2, no. 1, pp. 56–64.

Original article submitted: 15.11.2014

ABOUT THE AUTHORS

Vodinchar Gleb Mikhailovich – Ph.D. (Phys. & Math.), Head of Lab. Modeling of physical processes, Institute of Cosmophysical Researches and Radio Wave Propagation FEB RAS, Associate Professor, Dept. Mathematics & Physics, Vitus Bering Kamchatka State University.

Godomskaya Anna Nikolaevna – Postgraduate Student, Institute of Cosmophysical Researches and Radio Wave Propagation FEB RAS.

Goryshkin Alexander Petrovich – Ph.D. (Phys. & Math.), Professor Dept. of Mathematics & Physics, Vitus Bering Kamchatka State University.

Kuznetsov Vladimir Valeryevich – Dr. Sci. (Tech.), Leading Researcher comprehensive geophysical observatory «Paratunka», Institute of Cosmophysical Researches and Radio Wave Propagation FEB RAS.

Kim Alina Alexandrovna – Assistent of Dept. Informatics, Vitus Bering Kamchatka State University, Postgraduate Student, Institute of Cosmophysical Research and Radio Wave Propagation FEB RAS.

Lukovenkova Olga Olegovna – Assistent of Dept. Informatics, Vitus Bering Kamchatka State University, Postgraduate Student, Institute of Cosmophysical Research and Radio Wave Propagation FEB RAS.

Malysh Ekaterina Alexandrovna – Assistent of Dept. Informatics, Vitus Bering Kamchatka State University.

Nishonboev Azizbek Solizhonovich – Lecturer, of Dep. Mathematical Analysis and Differential Equations, Fergana State University, Republic of Uzbekistan.

Parovik Roman Ivanovich – Ph.D. (Phys. & Math.), Head of the Dep. Mathematics and Physics, Vitus Bering Kamchatka State University, Senior Researcher of Lab. Modeling of Physical Processes, Institute of Cosmophysical Researches and Radio Wave Propagation FEB RAS.

Sivokon' Vladimir Pavlovich – Dr. Sci. (Tech.), Chief Researcher of the Lab. of Electromagnetic Radiation of the Institute of Cosmophysical Research and Radio Wave Propagation FEB RAS.

Cherneva Nina Volodarovna – Ph.D. (Phys. & Math.), Leading Research Scientist of Lab. of Electromagnetic Radiation of the Institute of Cosmophysical Research and Radio Wave Propagation FEB RAS.

Churikov Viktor Anatolyevich – Ph.D. (Phys. & Math.), Associate Professor Dep. of Mathematics, Tomsk Polytechnic University.

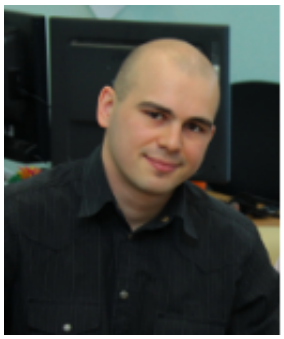

Shadrin Alexander Vitalyevich – Junior Researcher of Lab. Acoucstic Research, Institute of Cosmophysical Research and Radio Wave Propagation FEB RAS.

Shevtsov Boris Mikhailovich – Dr. Sci (Phys. & Math.), Director, Institute of Cosmophysical Research and Radio Wave Propagation FEB RAS.

Sheremetyeva Olga Vladimirovna – Ph.D. (Tech.), Researcher of Lab. Modeling of physical processes, Institute of Cosmophysical Researches and Radio Wave Propagation FEB RAS., Associate Professor, Dept. of Mathematics and Physics, Vitus Bering Kamchatka State University.

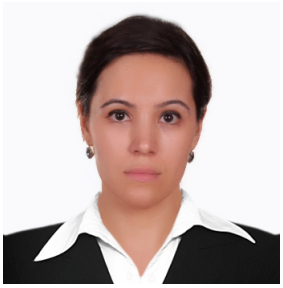

Yuldasheva Asal Victorovna – Ph.D. (Phys. & Math.), Lecturer of the Dep. Differential Equations and Mathematical Physics, of the National University of Uzbekistan, Tashkent.

TOPICS OF THE JOURNAL AND RULES FOR AUTHORS

The journal publishes results of fundamental and applied research in physics and mathematics (mathematical modeling of physical processes, mathematical physics, information and computing technology, mathematics). The journal is a peer-reviewed. Publication of manuscripts is free. The editors asked the authors of the journal follow the rules set out below:

1. Articles must be accompanied by a letter and an act of expertise, which was accomplished. At the end of the article put the signatures of all authors. For the article, sent to the editor, must be attached on a separate page the author's background in Russian and English languages: surname, name, degree, title, position, place of employment, exact postal address, phone, fax, e-mail (if any) of each author. You must specify the name of the author responsible for the passage of articles in the editorial.

2. The paper should not exceed (including figures, tables and references) 10 printed pages.

3. Articles submitted to the editor printed in the form of the manuscript in Russian language in two copies on one-sided sheet of A4. The text of the manuscript is typed in the LaTeX according to the rules below and print out a pdf-file created by the system after the final assembly of the document. Printout of the manuscript should be clear, the contrast and easily readable. In the paper version of the manuscript, you must provide an electronic version of an article in a separate file whose name must match the name of the first author. This file should contain files with extensions article tex, pdf, as well as drawings.

4. In Russian and English languages attached page with the article title, author, abstract (200-300 characters) and keywords. In electronic form in the file of the manuscript that the page is placed at the end.

5. Materials are sent to the address: 683032, Russia, Kamchatka krai, Petropavlovsk-Kamchatsky, Pogranichnaya, st. 4, Kamchatka State University by Vitus Bering, Department of Applied Mathematics. The electronic version of the manuscript should be sent by e-mail: fmit@mail.ru.

All journal published on the website of the Institute of Space Physics Research and Radio Wave Propagation FEB RAS, `http://www.ikir.ru/ru/krasec/journal/index.html`.

6. The editors asked the authors carefully prepared texts of articles and illustrations.

7. The Editors reserve the right to shorten the article and expose them, if necessary literary revision.

8. In the event of a return to the author of article to further refine the date of receipt is the receipt of the final edited text.

9. The manuscripts which, without these rules, shall be returned to authors without review.